

---

# Generative Adversarial Network for Photoplethysmography Reconstruction

---

Master of Science Thesis  
University of Turku  
Department of Computing  
Health Technology  
2022  
Yuning Wang

Supervisors:  
Ph.D. Iman Azimi  
Ph.D. Pasi Liljeberg

---

# 用于光电容积脉搏波重建的生成对抗网络

---

理学硕士论文  
图尔库大学  
电子计算学系  
卫生技术  
2022  
王玉宁

主管：  
博士伊曼·阿兹米  
博士帕西·利耶贝格

UNIVERSITY OF TURKU

Department of Computing

YUNING WANG: Generative Adversarial Network for Photoplethysmography Reconstruction

Master of Science Thesis, 53 p.

Health Technology

June 2022

---

Photoplethysmography (PPG) is an optical measurement method for blood pulse wave monitoring. The method has been widely applied in both clinical and wearable devices to collect physiological parameters, such as heart rate (HR) and heart rate variability (HRV). Unfortunately, the PPG signals are very vulnerable to motion artifacts, caused by inevitable movements of human users. To obtain reliable results from PPG-based monitoring, methods to denoise the PPG signals are necessary. Methods proposed in the literature, including signal decomposition, time-series analysis, and deep-learning based methods, reduce the effect of noise in PPG signals. However, their performance is insufficient for low signal-to-noise ratio PPG signals, or limited to noise from certain types of activities. Therefore, the aim of this study is to develop a method to remove the motion artifacts and reconstruct noisy PPG signals without any prior knowledge about the noise.

In this thesis, a deep convolutional generative adversarial network (DC-GAN) based method is proposed to reconstruct the PPG signals corrupted by real-world motion artifacts. The proposed method leverages the temporal information from the distorted signal and its preceding data points to obtain the clean PPG signal. A GAN-based model is trained to generate succeeding clean PPG signals by previous data points. A sliding window moving at a fixed step on the noisy signal is used to select and update the input for the trained model by the information within the noisy signal. A PPG dataset collected by smartwatches in a health monitoring study is used to train, validate, and test the method in this study. A noisy dataset generated with real-world motion artifacts of different noise levels and lengths is used to evaluate the proposed and baseline methods. Three state-of-the-art PPG reconstruction methods are compared with our method. Two metrics, including maximum peak-to-peak error and RMSSD error, are extracted from the original and reconstructed signals to estimate the reconstruction error for HR and HRV.

Our method outperforms state-of-the-art methods with the lowest values of the two evaluation matrices at all noise levels and lengths. The proposed method achieves 0.689, 1.352 and 1.821 seconds of maximum peak-to-peak errors for 5-second, 10-second, and 15-second noise at the highest noise level, respectively, and achieves 0.021, 0.048 and 0.067 seconds of RMSSD errors for the same noise cases.

Consequently, our method performs the best in reconstructing distorted PPG signals and provides reliable estimation for both HR and HRV.

Keywords: Motion artifacts removal, Photoplethysmography reconstruction, Generative Adversarial Network

图尔库大学  
电子计算学系

王宇宁：用于光电容积脉搏波重建的生成对抗网络

理学硕士论文，53页。健康技术  
2022年6月

---

光电容积描记法 (PPG) 是一种用于监测脉搏波的光学测量方法。该方法已广泛应用于临床和可穿戴设备中，以收集生理参数，例如心率 (HR) 和心率变异性 (HRV)。不幸的是，PPG信号非常容易受到由人类用户的不可避免的运动引起的运动伪影的影响。为了从基于PPG的监测中获得可靠的结果，对PPG信号进行降噪的方法是必要的。文献中提出的方法，包括信号分解、时间序列分析和基于深度学习的方法，减少了PPG信号中噪声的影响。然而，它们的性能对于低信噪比PPG信号是不够的，或者限于来自某些类型的活动的噪声。因此，本研究的目的是开发一种方法来消除运动伪影和重建噪声PPG信号没有任何先验知识的噪声。

在这篇论文中，提出了一种基于深度卷积生成对抗网络 (DC-GAN) 的方法来重建被真实世界运动伪影破坏的PPG信号。所提出的方法利用来自失真信号及其先前数据点的时间信息来获得干净的PPG信号。基于GAN的模型被训练以通过先前的数据点生成后续的干净PPG信号。在噪声信号上以固定步长移动的滑动窗口用于通过噪声信号内的信息来选择和更新用于训练模型的输入。智能手表在健康监测研究中收集的PPG数据集用于训练，验证和测试本研究中的方法。使用不同噪声水平和长度的真实运动伪影生成的噪声数据集来评估所提出的方法和基线方法。三个国家的最先进的PPG重建方法与我们的方法进行了比较。从原始信号和重建信号中提取两个度量，包括最大峰-峰误差和RMSSD误差，以估计HR和HRV的重建误差。我们的方法优于最先进的方法，在所有噪声水平和长度的两个评估矩阵的最低值。该方法实现了0.689, 1.352 和1.821秒的最大峰-峰误差为5秒，10秒，15秒的噪声在最高的噪声水平，分别为0.021, 0.048 和0.067秒的RMSSD误差为相同的噪声情况下。

因此，我们的方法在重建失真的PPG信号方面表现最好，并为HR和HRV提供可靠的估计。

关键词：运动伪影去除，光电容积脉搏波重建，生成对抗网络

# Contents

<b>1</b>	<b>Introduction</b>	<b>1</b>
1.1	Research questions . . . . .	3
1.2	Contributions . . . . .	3
1.3	Thesis content summary . . . . .	4
<b>2</b>	<b>Background</b>	<b>5</b>
2.1	Photoplethysmography . . . . .	5
2.1.1	Noise in Photoplethysmography . . . . .	6
2.1.2	Heart rate variability . . . . .	7
2.2	Generative adversarial network . . . . .	9
2.2.1	Deep Convolutional Generative Adversarial Network . . . . .	9
<b>3</b>	<b>Related work</b>	<b>11</b>
3.1	Quality assessment methods . . . . .	11
3.2	Noise removal methods . . . . .	12
3.2.1	Reference-signal-based method . . . . .	12
3.2.2	Signal-component-analysis methods . . . . .	13
3.2.3	Time-series methods . . . . .	13
3.2.4	Deep-learning-based methods . . . . .	14
<b>4</b>	<b>Dataset</b>	<b>15</b>

# 内容

<b>1 介绍</b>	<b>1</b>
1.1 研究问题	3
1.2 贡献	3
1.3 论文内容摘要	4
<b>2 背景</b>	<b>5</b>
2.1 光电体积描记法	5
2.1.1 光电体积描记术中的噪声	6
2.1.2 心率变异性	7
2.2 生成对抗网络	9
2.2.1 深度卷积生成对抗网络	9
<b>3 相关工作</b>	<b>11</b>
3.1 质量评价方法	11
3.2 噪声消除方法	12
3.2.1 参考信号法	12
3.2.2 信号成分分析法	13
3.2.3 时间序列方法	13
3.2.4 深度学习方法	14
<b>4 数据集</b>	<b>15</b>

<b>5 Proposed method</b>	<b>18</b>
5.1 Proposed model architecture . . . . .	18
5.1.1 Loss functions . . . . .	20
5.1.2 Reconstruction method . . . . .	21
5.2 Model training . . . . .	22
5.2.1 Training and validation data preparation . . . . .	23
5.2.2 Segmentation and filtering . . . . .	23
5.2.3 Signal quality assessment . . . . .	25
5.3 Test data preparation . . . . .	27
5.3.1 Noisy signal generation . . . . .	27
<b>6 State-of-the-art methods</b>	<b>31</b>
6.1 Kalman filter and Auto regression model . . . . .	32
6.2 Empirical Mode Decomposition and Discrete Wavelet Transform . . .	32
6.3 Bidirectional Long Short-Term Memory Auto-encoder . . . . .	33
<b>7 Results and discussion</b>	<b>38</b>
7.1 Setup . . . . .	38
7.2 Performance evaluation . . . . .	39
7.2.1 Maximum peak-to-peak error . . . . .	39
7.2.2 RMSSD error . . . . .	39
7.3 Reconstruction results . . . . .	40
7.3.1 5-second noise . . . . .	40
7.3.2 10-second noise . . . . .	44
7.3.3 15-second noise . . . . .	48
7.4 Impact of Noise Duration . . . . .	51
<b>8 Conclusion</b>	<b>52</b>

<b>5 建议方法</b>	<b>18</b>
5.1 拟议模型架构	18
5.1.1 损失函数	20
5.1.2 重建方法	21
5.2 模型训练	22
5.2.1 培训和验证数据准备	23
5.2.2 分割和滤波	23
5.2.3 信号质量评估	25
5.3 测试数据准备	27
5.3.1 噪声信号产生	27
<b>6 最先进的方法</b>	<b>31</b>
6.1 卡尔曼滤波和自回归模型	32
6.2 经验模态分解与离散小波变换。 . .	32
6.3 双向长短期记忆自动编码器	33
<b>7 结果和讨论</b>	<b>38</b>
7.1 设置	38
7.2 绩效评价	39
7.2.1 最大峰间误差	39
7.2.2 RMSSD 错误	39
7.3 重建结果	40
7.3.1 5- 第二噪声	40
7.3.2 10- 第二噪声	44
7.3.3 15- 第二噪声	48
7.4 噪音持续时间的影响	51
<b>8 结论</b>	<b>52</b>





# List of Figures

2.1	Typical waveform of PPG signals. . . . .	6
2.2	Waveform and power spectral density from 10-second PPG segment and artifact. The clean PPG and artifacts are in blue and green. (a) Clean PPG waveform, (b) clean PPG PSD, (c) motion artifact waveform, and (d) motion artifact PSD. . . . .	8
2.3	The architecture of Generative Adversarial Network . . . . .	9
5.1	The architecture of proposed model. K, S, and P represent the kernel size, stride and padding parameters in convolutional layers respectively	19
5.2	The reconstruction process of proposed method . . . . .	22
5.3	Block diagram of training data preparation . . . . .	24
5.4	PPG signal (a) before filtering, and (b) after filtering . . . . .	25
5.5	PPG signal classified as (a) clean segment, and (b) noisy segment by SVM. . . . .	26
5.6	Block diagram of test data preparation . . . . .	28
6.1	The architecture of Bidirectional LSTM method . . . . .	34
6.2	An example of synthesized PPG signal with white noise (orange) and ground truth (blue) . . . . .	36
6.3	An example of synthesized PPG signal with slope noise (orange) and ground truth (blue) . . . . .	36

# 图目录

2.1	Typical waveform of PPG signals	6
2.2	Waveform and power spectral density from 10-second PPG segment	6
	and artifact. The clean PPG and artifacts are in blue and green.	
	波形 和 (d) 运动伪影PSD	8
	(a) Clean PPG waveform, (b) clean PPG PSD, (c) motion artifact	
2.3	生成式对抗网络的体系结构	9
5.1	提出的模型的架构。K、S和P代表内核 分别在卷积层中的大小、步幅和填充参数	19
5.2	所提出的方法的重建过程	22
5.3	训练数据准备框图	24
5.4	PPG信号 (a) 滤波前, 和 (b) 滤波后	25
5.5	PPG信号分类为 (a) 干净段和 (B) 噪声段, SVM	26
5.6	试验数据准备框图	28
6.1	双向LSTM方法的架构	34
6.2	具有白色噪声 (橙子) 的合成PPG信号的示例, 以及 ground truth (blue)	36
6.3	具有斜率噪声 (橙子) 的合成PPG信号的示例, 地面实况 (蓝色)	36

6.4 An example of synthesized PPG signal with saturation noise (orange) and ground truth (blue) . . . . .	37
7.1 Reconstruction results from proposed method and baseline methods (SNR=-8.09 dB). Blue dotted line is the clean ground truth.(a) Synthesized signal, (b) Proposed method, (c) Bidirectional LSTM, (d) EMD and DWT, and (e) Kalman and AR. . . . .	41
7.2 Reconstruction errors from all methods with 5-second noise. (a) Maximum peak-to-peak error, and (b) RMSSD error. . . . .	43
7.3 Reconstruction errors from all methods with 10-second noise. (a) Maximum peak-to-peak error, and (b) RMSSD error. . . . .	46
7.4 Reconstruction errors from all methods with 15-second noise. (a) Maximum peak-to-peak error, and (b) RMSSD error. . . . .	49

6.4 An example of synthesized PPG signal with saturation noise (orange) and ground truth  
(blue)  

37

7.1 Reconstruction results from proposed method and baseline methods



(SNR = 8.09 dB)。蓝色虚线是干净的地面真相。(a) 同-  
(B) 提出的方法, (c) 双向LSTM, (d)  
EMD和DWT, 以及 (e) Kalman 和AR

41

7.2 具有5秒噪声的所有方法的重建误差。(a)麦克斯

最大峰- 峰误差和 (B) RMSSD误差

43

7.3 Reconstruction errors from all methods with 10- second noise . (a)    
最大峰间误差, 和 (B) RMSSD误差

46

7.4 所有方法的重建误差均为15秒噪声。 (一)

Maximum peak - to- peak error , and (b) RMSSD error



49

# List of Tables

4.1	Background information of participants . . . . .	16
7.1	Performance of all methods on 5-second noise . . . . .	42
7.2	Performance of all methods on 10-second noise . . . . .	45
7.3	Performance of all methods on 15-second noise . . . . .	48

# 表的列表

4.1	与会者的背景资料	16
7.1	所有方法对5秒噪声的性能	42
7.2	所有方法在10秒噪声下的性能	45
7.3	所有方法对15秒噪声的性能	48

# List of acronyms

**ADC** Analog-to-Digital Conversion

**ANS** Autonomic Nervous System

**AR** Auto-regressive

**BRDAE** Bidirectional Recurrent Denoising Auto-encoder

**CNN** Convolutional Neural Network

**CycleGAN** Cycle Generative Adversarial Network

**DC-GAN** Deep Convolutional Generative Adversarial Network

**DWT** Discrete Wavelet Transform

**ECG** Electrocardiogram

**EMD** Empirical Mode Decomposition

**HR** Heart Rate

**HRV** Heart Rate Variability

**IMF** Intrinsic Mode Function

**LED** Light emitting diode

**LSTM** Long Short-Term Memory

# 缩略语表

ADC模数转换

自主神经系统

AR自回归

双向递归去噪自动编码器

CNN卷积神经网络

CycleGAN循环生成对抗网络

DC- GAN深度卷积生成对抗网络

离散小波变换

ECG心电图

经验模态分解

HR Heart Rate  

HRV Heart Rate Variability  

IMF Intrinsic Mode Function  

LED发光二极管

LSTM长短期记忆

**MA** Motion Artifact

**PPG** Photoplethysmography

**PSD** Power Spectral Density

**RAM** Random-Access Memory

**ReLU** Rectified Linear Units

**RMSSD** Root Mean Square of Successive Differences between Heart Beat Interval

**RNN** Recurrent Neural Network

**ROM** Read-Only Memory

**SNR** Signal-to-Noise Ratio

**SVM** Support Vector Machine

MA Motion

PPG光电体积描记术

PSD功率谱密度

RAM随机存取存储器

ReLU校正线性单元

心搏间期连续差值的均方根

RNN递归神经网络

只读存储器

SNR信噪比

SVM支持向量机

# 1 Introduction

Photoplethysmography (PPG) is a non-invasive measuring method to reflect the blood volume change of the pulse wave. The method uses a light emitting diode (LED) to send light to a tissue and a light detector to receive the changing amount of light transmission from tissue such as the surface of wrist, finger, forehead and earlobe caused by blood flow [1]. Smartwatches apply the technique to collect PPG signals from the wrist of the watch users. Various healthcare applications using PPG signals have been proposed, focusing on sleep monitoring, blood pressure monitoring, and cardiovascular diseases. [2]–[4].

However, the PPG signals can be easily affected by noise during data collection. Such noises caused by the external environment and user's motion artifacts are commonly seen in PPG signals. The external environment may distort the collected PPG. For example, the ambient light from a room light with variable frequency causes saturation noise to PPG signals [5]. The motion artifacts caused by the daily activities of the subject may also be collected together with PPG by a wearable device. PPG signals with these noises may result in unreliable decision making.

The quality of the PPG signal is indicated by the signal-to-noise ratio (SNR), which is the ratio between signal power and noise power. The larger the SNR value is, the less the PPG signal is distorted. Although spectral analysis and different filtering methods can reduce the effect of most of the noises in PPG signals, the motion artifacts, which have overlapped frequency-domain features with clean PPG signals,

## 15 | 言

Photoplethysmography (PPG) is a non-invasive measuring method to reflect the



?

blood volume change of the pulse wave. The method uses a light emitting diode



?

(LED) to send light to a tissue and a light detector to receive the changing amount



?

of light transmission from tissue such as the surface of wrist, finger, forehead and



?

earlobe caused by blood flow [1]. Smartwatches apply the technique to collect PPG and cardiovascular diseases . [2]–[4].



?

However , the PPG signals can be easily affected by noise during data collection . signals from the wrist of the watch users . Various healthcare applications using

ECG noises ? caused by the external environment and user's motion artifacts are

signals ? have been proposed , focusing on sleep monitoring , blood pressure

commonly seen in PPG signals . The external environment may distort the collected



?

PPG. For example , the ambient light from a room light with variable frequency



?

causes saturation noise to PPG signals [5]. The motion artifacts caused by the device . PPG signals with these noises may result in unreliable decision making . daily



?

The quality of the PPG signal is indicated by the signal - to- noise ratio (SNR) , activities of the subject may also be collected together with PPG by a wearable which is the ratio between signal power and noise power . The larger the SNR value is ,



?

the less the PPG signal is distorted . Although spectral analysis and different

filtering



?

methods can reduce the effect of most of the noises in PPG signals , the motion



?

artifacts , which have overlapped frequency - domain features with clean PPG

signals ,



?

are especially difficult to remove. Therefore, an accurate PPG signal reconstruction method to eliminate the effect of motion artifacts is necessarily required for studies working with PPG signals.

Many studies have been proposed to detect the motion artifacts in PPG signals. Various time and frequency-domain features are extracted to classify whether the signal is clean or not. The noisy segment is then excluded from further analysis [6]. However, these methods can not produce continuous PPG signals or provide reliable estimation for certain health-related parameters, such as heart rate variability.

Signal components analysis methods are proposed to improve the PPG signal quality. These methods decompose the noisy PPG signals into noise components and clean components based on mathematical algorithms. Then, the noise components are removed, and the methods reconstruct the PPG with only clean components provided by the algorithms to improve the signal quality [7]–[11].

Time-series based methods are also applied for PPG signal reconstruction. These methods regard the PPG signal as time-series data, and train the model with the clean signal before the distorted PPG signal. Then, the trained model predicts the succeeding data points based on the previous clean PPG signals to perform the reconstruction for PPG signal [12]. However, these methods fail to reconstruct signals with low SNR values. The reconstruction results from these methods are also highly dependent on the quality of proceeding signals.

In addition, deep-learning based methods are recently applied to reconstruct the signals. These models are trained to produce the clean PPG signals as output [13], [14]. However, the models are only developed for certain types of noises.

As a result, we believe that a robust PPG signal reconstruction method is required to regenerate the distorted PPG signals without prior knowledge about the noise such as type, noise level, or length of noise.

尤其难以去除。因此，准确的PPG信号重建  
研究中需要一种消除运动伪影影响的方法

### 用PPG信号工作

已经提出了许多研究来检测PPG信号中的运动伪影。

提取各种时域和频域特征以分类是否  
信号是否干净。然后将噪声段从进一步分析中排除[6]。  
然而，这些方法不能产生连续的PPG信号或提供可靠的PPG信号。

估计某些健康相关的参数，如心率变异性。

提出了信号成分分析方法来改善PPG信号

质量。这些方法将噪声PPG信号分解成噪声分量，  
基于数学算法的清洁组件。其次，噪声成分  
并且该方法仅用干净的分量重建PPG

由算法提供以改善信号质量[7]–[11]。

基于时间序列的方法也被应用于PPG信号重建。这些  
方法将PPG信号视为时间序列数据，并用  
在失真的PPG信号之前的干净信号。然后，训练好的模型预测  
基于先前的干净PPG信号的后续数据点来执行  
PPG信号的重建[12]。然而，这些方法无法重建  
低SNR值的信号。这些方法的重建结果是

还高度依赖于进行中的信号的质量。

此外，基于深度学习的方法最近被应用于重建  
信号。这些模型经过训练以产生干净的PPG信号作为输出[13]，  
[14]第10段。然而，模型仅针对某些类型的噪声开发。

因此，我们认为，一个强大的PPG信号重建方法是重新–  
要求在没有关于PPG信号的先验知识的情况下再生失真的PPG信号。  
噪声，例如噪声的类型、噪声水平或长度。

## 1.1 Research questions

This study, therefore, intends to focus on the following two research questions in motion artifacts removal in PPG signals.

1. Can the distorted PPG signals be reconstructed accurately, especially when SNRs are low?
2. Is the information in the distorted signal and the proceeding points enough to reconstruct the PPG signal?

One of the important issues in reconstructing noisy PPG signals is to deal with signals with low SNR. The waveform of such signals at high noise levels is largely corrupted. Hence, no useful information can be extracted from the fiducial points such as peaks and valleys to reconstruct clean PPG.

Another issue is that real-world motion artifacts can be caused by various types of activities in daily life. Without any other signal as a reference for motion artifacts, the motion artifacts in the noisy PPG signals do not have a certain representative feature, which makes it hard to be distinguished from clean signals. The only available information is the proceeding PPG data points and the distorted segment itself.

Therefore, we focus on the solutions to these two research questions in this study.

## 1.2 Contributions

In this thesis, we propose a deep convolutional GAN-based method to reconstruct noisy PPG signals distorted by motion artifacts. The proposed method leverages the information from both the noisy segment itself and its proceeding signals. The PPG data used in the study is collected by smartwatches. The model is trained with clean PPG signals and tested with PPG signals at different noise levels. Our method is evaluated by the noisy dataset generated by real-world motion artifacts

## 1.1 研究问题

因此，本研究拟集中探讨以下两个研究问题：

PPG信号中的运动伪影去除。

- 1.失真的PPG信号能否准确重建，特别是在SNR较低时？
- 2.失真信号中的信息和前进点是否足以重建PPG信号？

重建有噪PPG信号的重要问题之一是处理

低SNR信号。这种信号在高噪声水平下的波形在很大程度上是损坏.因此，不能从基准点提取有用的信息

例如峰和谷以重建干净的PPG。

另一个问题是，真实世界的运动伪影可以由各种类型的

日常生活中的活动。在没有任何其他信号作为运动伪影的参考的情况下，噪声PPG信号中的运动伪影不具有特定的代表性特征，这使得它很难与干净的信号区分开来。唯一的办法—能够获得的信息是进行中的PPG数据点和失真的段本身。

因此，本研究主要针对这两个研究问题进行探讨。

## 1.2 贡献

在这篇论文中，我们提出了一种基于深度卷积GAN的方法来重建由运动伪影失真的噪声PPG信号。所提出的方法利用来自噪声段本身及其后续信号的信息。的研究中使用的PPG数据由智能手表收集。训练模型用干净的PPG信号，并在不同的噪声水平下用PPG信号进行测试。我们该方法通过由真实世界运动伪影产生的噪声数据集进行评估

with different noise duration and SNRs. Finally, we compare the proposed method with the other three state-of-the-art methods by extracting types of errors that represent the reconstruction error of heart rate and heart rate variability. The major contributions of the thesis can be summarized as follows:

1. A GAN-based method is proposed to reconstruct noisy PPG signals distorted by real-world motion artifacts using the information within the signal and proceeding points.
2. A test dataset containing distorted PPG signals with different noise lengths at noise levels with SNR values ranging from -25 dB to 30 dB is generated to evaluate the performance of the proposed method, compared to the existing three state-of-the-art methods.
3. Two metrics representing the reconstruction error of HR and HRV are extracted to evaluate the performance of proposed method, compared to three existing state-of-the-art methods.

This thesis is related to the accepted publication [15].

### 1.3 Thesis content summary

The rest of the thesis is organized as follows. Chapter 3 reviews the related work on PPG noise cancellation. Chapter 2 introduces the background of PPG and the used model. Chapter 4 provides the details of the collection, participant recruitment, and the wearable device for the dataset used in this study. The data processing, model architecture, and the reconstruction method is presented in Chapter 5. Chapter 6 presents the implementation of the other three state-of-art methods to compare with our proposed method. The results and discussion of the signal reconstruction from all the methods are introduced in 7. Chapter 8 is the conclusion.

## 2 Background

In this chapter, we introduce the PPG and GAN.

### 2.1 Photoplethysmography

Photoplethysmography (PPG) is a non-invasive optical technique that reflects the change of blood flow by measuring the amount of light absorption or reflection [16]. When the heart beats, the blood flow in the vessels changes correspondingly. The tissue on the blood vessels has different light absorption or reflectivity rate for the same wavelength with or without blood flows. The technique uses a light emitter and a light sensor to detect the light change caused by cardiovascular activity on the skin.

A typical PPG waveform is shown in Figure 2.1. One cycle of a typical PPG waveform includes systolic peak, dicrotic notch, and diastolic peak. The rising edge of the waveform reflects the systole, and the amplitude of the systolic peak is related to stroke volume [17]. The falling edge of the waveform is the diastole and wave reflections. The dicrotic notch is caused by the closure of heart valves and the reverse flow of blood, which is commonly seen in subjects with healthy heart valves [18].

The PPG signals can be easily collected using various wearable devices, including smart rings and smartwatches. As it is easy to implement with low cost, PPG has been frequently used in different health monitoring tasks. The cyclic change of the PPG waveform is able to measure various physiological parameters, such as

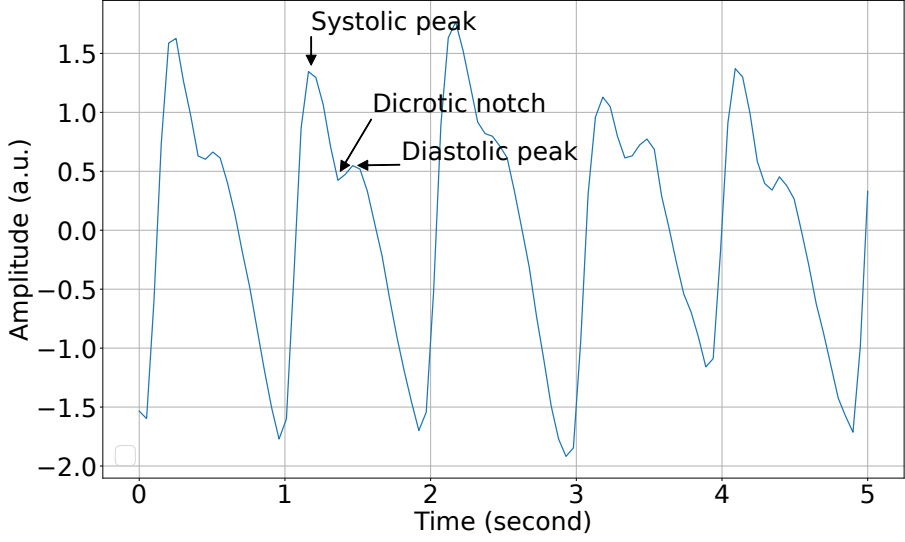


Figure 2.1: Typical waveform of PPG signals.

heart rate (HR), respiration rate [19], heart rate variability (HRV)[20], blood oxygen saturation [21], blood pressure [22] and ankle pressure [23].

### 2.1.1 Noise in Photoplethysmography

The raw PPG signals are usually noisy. The noises are mainly caused by the environment, measuring devices, and body movements of participants. We describe three types of noise, including white noise, baseline wander and motion artifacts, which are commonly seen in PPG signals.

**White noise** White noise is the type of noise with a uniform distribution. In other words, the white noise has a zero mean and standard deviation of 1 [24].

**Baseline wander** Baseline wander is a low-frequency artifact usually caused by subjects' movements, such as respiration. The baseline wander drifts PPG signals baseline up or down over time [25].

**Motion artifact** The motion artifact (MA) is the noise caused by the movement of subjects. Although the PPG signals are widely used in daily monitoring devices, the signal is vulnerable to noises caused by participants' daily activities such as running, waving hands, and finger tapping. Such artifacts corrupt the PPG signals, thus leading to inaccurate estimation for the health-related parameters.

Figure 2.2 shows an example of a 10-second clean PPG signal and a PPG signal corrupted by motion artifact. Figure 2.2 (a) and (c) are the waveforms, and Figure 2.2 (b) and (d) illustrate the corresponding power spectral density (PSD). The PSD is the power of the signal at the corresponding frequency. As indicated in Figure 2.2(b), the frequency with the largest power in the clean PPG signal is 1.5 Hz, which corresponds to the HR. However, the HR frequency in Figure 2.2(d) is not clear due to the MAs. Therefore, the MAs cannot be removed by frequency-based filters, because the frequencies of clean signals and artifacts overlap.

### 2.1.2 Heart rate variability

Heart rate variability (HRV) refers to the change between the successive heartbeat [26]. It is caused by the interaction between the brain and heart, which is regulated by the non-linear activity of the autonomic nervous system (ANS) [27]. The HRV is able to reflect neurocardiac health. Previous studies have proved that HRV is correlated with stress, panic, and worry [28].

The root mean square of successive differences between normal heartbeats (RMSSD) is one of the important HRV parameters, which reflects the differences between successive heartbeat interval. It can estimate HRV mediated by vagal activities [27]. The reduced RMSSD level is highly correlated with the risk of sudden unexplained death in epilepsy [29].

Many studies have been carried out to monitor the daily HRV of participants. Due to the simplicity and low cost, PPG-based wearable devices are used in such

运动伪影运动伪影 (MA) 是由运动引起的噪声的主题。尽管PPG信号广泛用于日常监测设备中，讯号容易受到参加者日常活动所产生的噪音影响，例如跑步，挥手，和手指敲击。这样的伪影破坏PPG信号，

从而导致对健康相关参数的不准确估计。

图2.2示出了10秒干净PPG信号和PPG信号的示例。

nal被运动伪影损坏。图2.2 (a) 和 (c) 是波形，图2.2 (B) 和 (d) 显示了相应的功率谱密度 (PSD) 。PSD是信号在相应频率下的功率。指出图2.2 (B)，干净PPG信号中功率最大的频率为1.5然而，图2.2 (d) 中的HR频率不是由于马的明确。因此，MA不能通过基于频率的

滤波器，因为干净信号和伪影的频率重叠。

### 2.1.2 心率变异性

心率变异性 (HRV) 是指连续心跳之间的变化 [26]第10段。它是由大脑和心脏之间的相互作用引起的，自主神经系统 (ANS) 的非线性活动[27]。的HRV能够反映神经心脏的健康状况。以往的研究已经证明，心率变异性

与压力、恐慌和担忧相关[28]。

正常心跳之间连续差值的均方根 (RMSSD)

是心率变异性的重要参数之一，它反映了心率变异性的差异，连续心跳间隔。它可以估计迷走神经活动介导的HRV [27]。RMSSD水平降低与不明原因的突发性心脏病风险高度相关。

癫痫病[29]。

已经进行了许多研究来监测参与者的日常HRV。

由于简单性和低成本，基于PPG的可穿戴设备被用于这种应用中。

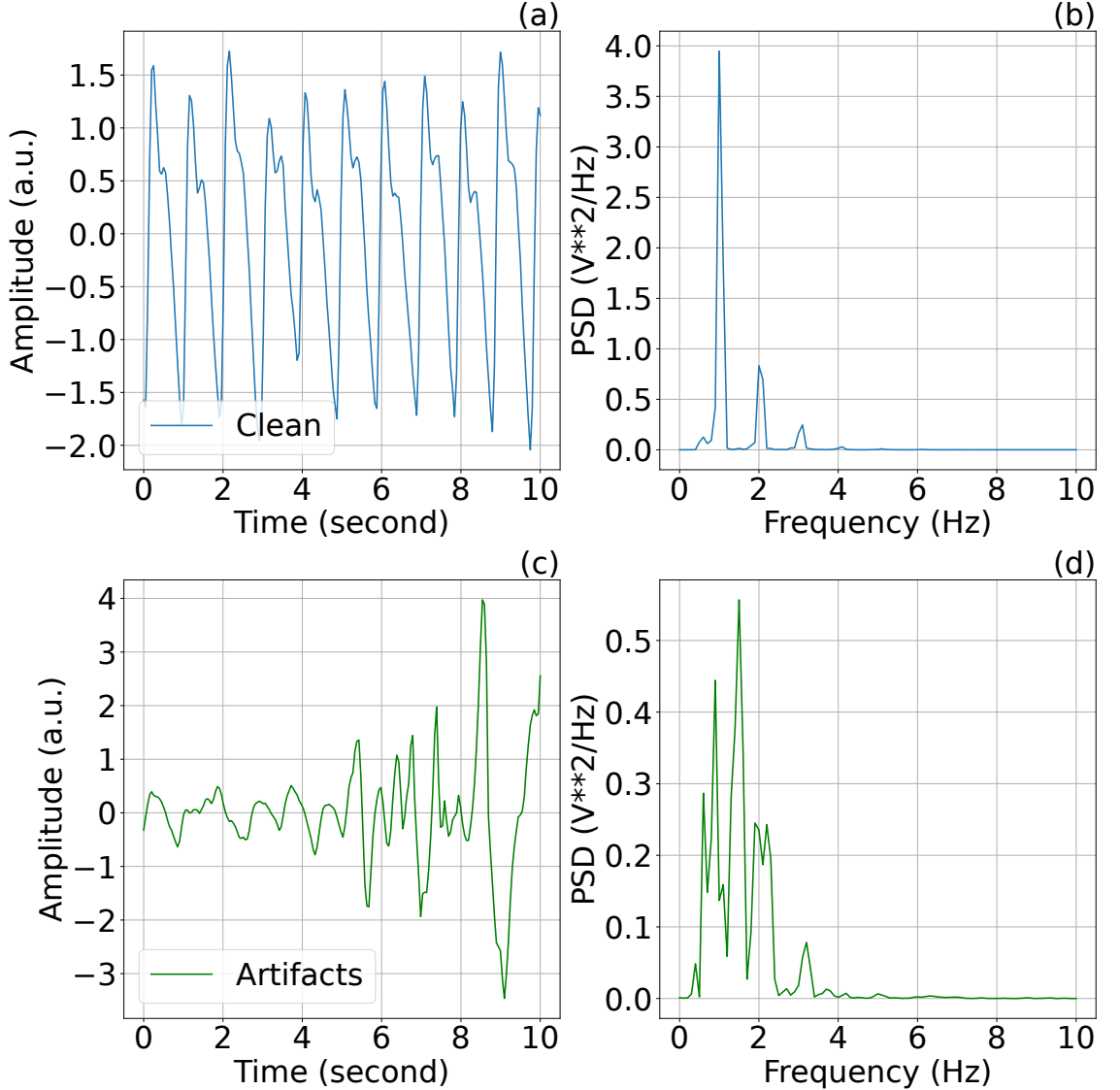


Figure 2.2: Waveform and power spectral density from 10-second PPG segment and artifact. The clean PPG and artifacts are in blue and green. (a) Clean PPG waveform, (b) clean PPG PSD, (c) motion artifact waveform, and (d) motion artifact PSD.

health-monitoring studies [30]–[32]. It is also easy to extract different HRV parameters from the PPG waveform. Therefore, the quality of PPG signals has a large effect on HRV parameters.

## 2.2 Generative adversarial network

The Generative adversarial network (GAN) is a network structure proposed by Goodfellow et al. to generate synthetic data [33]. Figure 2.3 illustrates the standard structure of GAN. The model consists of two sub networks, i.e., a generator and a discriminator. The generator learns the distribution of the input data and reconstructs the input. The discriminator classifies whether the data is original or generated by the generator. The two sub networks compete with each other during training until the difference between the original and generated data is minimized. Therefore, GAN can be used to generate and reconstruct the data. Different studies have applied such feature to de-noise images in computer vision tasks. [34], [35].

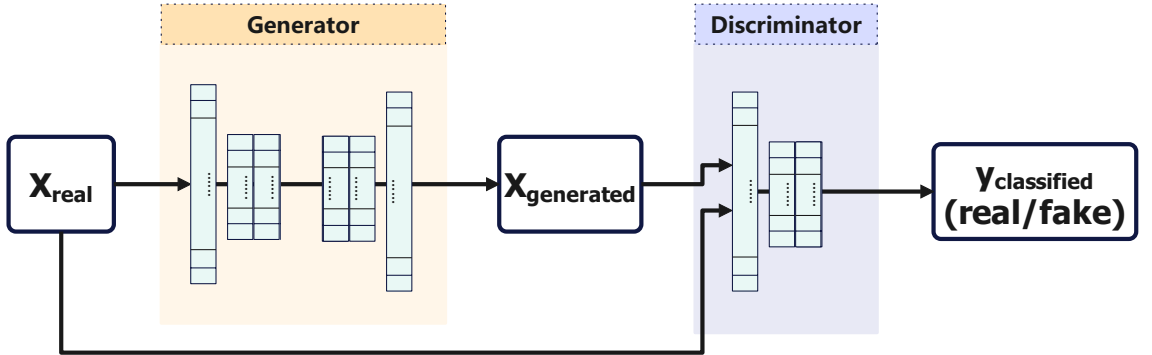


Figure 2.3: The architecture of Generative Adversarial Network

### 2.2.1 Deep Convolutional Generative Adversarial Network

Although GAN can maximize the likelihood by the design of competition between generator and discriminator, the training of GAN is often unstable, which results in nonsensical synthesized data [36]–[38]. The deep convolutional generative adversarial network (DC-GAN) is proposed to solve the problem [39]. DC-GAN is a GAN-based neural network with modified convolutional structure. Compared to

## 2.2 生成对抗网络

生成式对抗网络 (GAN) 是一种网络结构, Goodfellow等人生合成数据[33]。图2.3显示了标准的 GAN的标准结构。该模型由两个子网络组成, 即, 发电机和一个判别器。生成器学习输入数据的分布, 重建输入。数据库将数据分类为原始数据还是由发电机产生。两个子网在运行期间相互竞争, 训练, 直到原始数据和生成数据之间的差异最小化。因此, GAN可以用来生成和重建数据。不同研究

已经将这种特征应用于计算机视觉任务中的去噪图像。[34], [35].

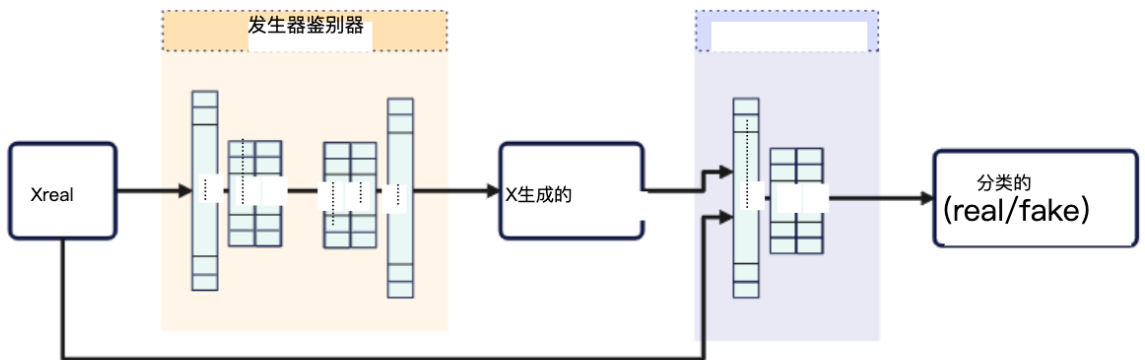


图2.3生成对抗网络的架构

### 2.2.1 深度卷积生成对抗网络

虽然GAN可以通过设计竞争来最大化可能性, 由于GAN的生成器和训练器的不同, GAN的训练往往是不稳定的, 这导致无意义的合成数据[36]–[38]。深度卷积生成广告–对抗网络 (DC–GAN) 被提出来解决这个问题[39]。DC–GAN是一种基于GAN的神经网络, 具有改进的卷积结构。相比

the initial GAN, the DC-GAN adopted three latest changes in convolutional neural networks:

- Using stride convolutional layers to downsample the data instead of max pooling.
- Excluding fully-connected hidden layers in deep network architecture.
- Using Batch Normalization between layers.

The DC-GAN architecture has been proved to be more stable and effective in learning the representation of data [39]. Compared to GAN, DC-GAN is more used to infer data based on contextual information, such as image colorization [40] or inpainting corrupted images [41].

## 3 Related work

Noises distort the waveform of PPG signals, making it difficult to extract accurate health-related parameters for variable-based analysis. Methods to reduce the effect of noise are needed. However, PPG de-noising is a challenging task, especially with high noise level and long noise duration. In this chapter, we describe previous studies dealing with the MAs in PPG signals. To tackle the problem, previous studies can be divided into 2 categories: (1) signal quality assessment methods, which give a classification result of whether a PPG segment is clean or not, and (2) noise removal methods, which remove the noise component and produce de-noised signals.

### 3.1 Quality assessment methods

The quality assessment methods classify the PPG signals as noisy or clean by extracting various features in the time or frequency domain. For instance, in the study from [6], the authors calculated the statistic values, including kurtosis, skewness, and standard deviation of each segment, and detected the motion artifacts by the statistic threshold set from clean signals. Likewise, in [42], other features such as variation in approximate entropy, Shannon entropy, and spectral entropy are extracted to further classify the signal as clean or not by the elliptical envelope algorithm.

Recently, deep-learning-based anomaly detection methods are also applied to assess the PPG signal quality. In deep learning-based methods, the model itself acts

# 3相关工作

噪声使PPG信号的波形失真，使得难以准确提取PPG信号。

用于基于变量的分析的健康相关参数。减少影响的方法

噪音是必要的。然而，PPG去噪是一项具有挑战性的任务，尤其是在  
噪声强度高、噪声持续时间长。在本章中，我们描述了以前的研究  
处理PPG信号中的MA。为了解决这个问题，以前的研究可以  
分为两大类：(1) 信号质量评估方法，它给予  
PPG段是否干净的分类结果，以及 (2) 噪声去除

方法，其去除噪声分量并产生去噪信号。

## 3.1 质量评价方法

质量评估方法将PPG信号分类为有噪声的或干净的，

在时域或频域中跟踪各种特征。例如在

研究[6]，作者计算了统计值，包括峰度，偏度，  
ness和标准差，并检测出运动伪影

通过从干净信号设置的统计阈值，[42]第42话其他人  
例如近似熵、香农熵和谱熵变化

以进一步通过椭圆包络将信号分类为干净或不干净

### 算法

最近，基于深度学习的异常检测方法也被应用于as-  
评估PPG信号质量。在基于深度学习的方法中，

as the feature extractor and consequently relieves the work of feature engineering. The study conducted by [43] proposed a 1-dimensional convolution neural network to detect whether each 5-second PPG signal segment was distorted by motion artifacts. The PPG signals were blindly sectioned to 5-second segments regardless of any peak or valley information. Then the segments were normalized and fed into the 13-layer 1-D convolutional neural network (CNN) model to output the "clean" or "artifact" labels. Similarly, in [44], the authors implemented a bi-directional recurrent neural network-based auto-encoder to detect and remove motion artifacts in an unsupervised manner. The methods mentioned above can accurately evaluate the PPG signal quality. However, such methods only differentiated the PPG signals as clean or noisy, but did not improve the signal quality.

## 3.2 Noise removal methods

Classifying the signal as good or bad is insufficient to obtain the noise-free PPG signal, as excluding the noisy part in the signal would cause loss of collected data. Therefore, in addition to the signal quality assessment methods, many studies are proposed to eliminate the noise components in signals by analyzing different time and frequency features in reference and PPG signals.

### 3.2.1 Reference-signal-based method

Reference-signal-based methods use another reference signal which is recorded simultaneously as the PPG signals to provide information about either noise or clean PPG. Based on different design of data collection, the collected simultaneous signal can either be the reference of noise or clean PPG signals. The authors in [7][8] designed adaptive filters with accelerometers and gyroscopes signals as references of noise to filter out the motion artifacts in noisy PPG signals. Masinelli et al. used

作为特征提取器，从而减轻了特征工程的工作。  
[43]进行的研究提出了一种一维卷积神经网络  
检测每个5秒PPG信号段是否因运动而失真，  
时间。PPG信号盲切为5秒段，无论  
任何峰或谷信息。然后将片段标准化并送入  
13层1-D卷积神经网络（CNN）模型输出“干净”的  
或“人工制品”标签。同样，在[44]中，作者实现了双向重定向，  
用于检测和去除运动伪影的基于当前神经网络的自动编码器  
在无人监督的情况下。上述方法可以准确地评价  
PPG信号质量。然而，这样的方法仅区分PPG信号

干净或嘈杂，但没有改善信号质量。

## 3.2 噪声消除方法

将信号分类为好或坏不足以获得无噪声PPG  
因此，如果排除信号中的噪声部分，将导致收集到的数据丢失。  
因此，除了信号质量评估方法之外，许多研究都是  
提出了通过分析不同时刻的信号来消除信号中的噪声成分

以及参考和PPG信号中的频率特征。

### 3.2.1 参考信号法

基于参考信号的方法使用另一个参考信号，该参考信号被记录为  
PPG信号提供关于噪声或清洁的信息  
PPG。基于不同的数据采集设计，  
可以是噪声或干净PPG信号的参考。作者[7][8]  
设计了以加速度计和陀螺仪信号为参考的自适应滤波器，  
噪声，以滤除噪声PPG信号中的运动伪影。Masinelli等人使用

the Electrocardiogram (ECG) signals as a reference of ground true HR to remove motion artifacts by spectral analysis [45]. Despite the improved HR estimation, these reference signal-based methods still suffer from the limitations of the inaccurate detection of reference sensors. Moreover, extra sensors such as accelerator and ECG sensors are needed for the research, which makes the setup more complicated.

### 3.2.2 Signal-component-analysis methods

Signal components analysis methods are applied to reduce the noise in PPG signals. These methods decompose the noisy signal into noise and clean components, and then remove the noise component in the signal to obtain the reconstructed clean signal. In [9], the noisy PPG signals were first decomposed into a sum of Intrinsic Mode Function (IMF) by Empirical Mode Decomposition(EMD) to improve the signal quality and then reduce the noise by Discrete Wavelet Transform (DWT). In [10] , the authors set the upper and lower envelope boundaries to minimize the MAs in the signals. However, these methods fail to reconstruct the signals when the noise level is high.

### 3.2.3 Time-series methods

Time-series methods are applied to estimate clean PPG signals while the signal is noisy. These methods take the predeciudal samples into account during reconstruction since the physiological activities are time-causal processes. In [12], the combination of a Kalman filter and Auto-regressive (AR) model was introduced to predict the value on the time  $t + 1$  using the values on and before time  $t$ , hence avoiding the motion artifacts caused by sudden subjects' movements. In [46], the authors used the fiducial points such as peak, foot, diastolic peak, and diastolic notch from a previous clean PPG segment to reconstruct a new one by cubic spline interpolation. However, these methods highly rely on the amount and quality of

将心电图 (ECG) 信号作为接地真实HR的参考，  
频谱分析的运动伪影[45]。尽管改进了HR估计，  
这些基于参考信号的方法仍然受到INACCU的限制，  
参考传感器的速率检测。此外，额外的传感器，如加速器和  
研究需要ECG传感器，这使得设置更加复杂。

### 3.2.2 信号成分分析法

信号成分分析方法被应用于减少PPG信号中的噪声。  
这些方法将噪声信号分解为噪声和干净分量，  
然后去除信号中的噪声分量以获得重建的干净的  
信号了在[9]中，噪声PPG信号首先被分解为固有的和  
通过经验模态分解 (EMD) 对模态函数 (IMF) 进行改进，  
信号质量，然后通过离散小波变换 (DWT) 去噪。在  
[10]，作者设置了上包络边界和下包络边界，以最小化MA  
在信号中。然而，这些方法不能重建信号时，噪声

水平很高。

### 3.2.3 时间序列方法

时间序列方法被应用于估计干净的PPG信号，而信号  
很吵。这些方法在重建过程中考虑了蜕膜前样本，  
结构，因为生理活动是时间因果过程。在[12]中，  
结合卡尔曼滤波和自回归 (AR) 模型，  
使用时间t和之前的值预测时间t + 1的值，因此  
避免了由对象的突然运动引起的运动伪影。在[46]中，  
作者使用了基准点，如峰值、足、舒张期峰值和舒张期峰值。  
通过三次样条从先前的干净PPG段中进行凹口以重建新的PPG段  
插值然而，这些方法高度依赖于药物的量和质量。

proceeding data to reconstruct the signal.

### 3.2.4 Deep-learning-based methods

Deep learning models are also developed to reconstruct PPG signals. The study from [13] first transform 1-D PPG signals to its representative 2-D images. Then, a Cycle Generative Adversarial Network (CycleGAN) was trained to de-noise and reconstruct images. Finally, the de-noised image was transformed back to clean PPG signals. Similarly, in [14], a bidirectional recurrent auto-encoder was trained by minimizing the difference between synthesized noisy PPG signals and their original clean signals. Then, the trained model was able to produce clean PPG signals when the input signals were noisy. Although deep learning models have achieved good performance on large datasets, these deep-learning-based methods only considered the noise caused by certain types of movement, such as waving and shaking hands. Moreover, these methods were tested by manually generated noisy PPG dataset. The noisy signals in the test set were synthesized by adding the noises to clean signals, which guaranteed that the noisy segment must contain clean PPG information. Hence, these methods may fail when clean PPG signals are faded in the corrupted signals in real life.

The methods using either quality assessment or noise removal methods are insufficient to eliminate the effect of motion artifacts on PPG signals. The mentioned methods are limited to either short-term analysis of signals or certain types of noises caused by specified activities. Consequently, a method to reconstruct the PPG waveform distorted by real-world motion artifacts without any prior knowledge of the noise is needed.

处理数据以重构信号。

### 3.2.4 深度学习方法

Deep learning models are also developed to reconstruct PPG signals. The study

from [13] first transform 1-D PPG signals to its representative 2-D images. Then, a

Cycle Generative Adversarial Network (CycleGAN) was trained to de-noise and re-

construct images. Finally, the de-noised image was transformed back to clean

PPG

signals. Similarly, in [14], a bidirectional recurrent auto-encoder was trained by

minimizing the difference between synthesized noisy PPG signals and their original

clean signals. Then, the trained model was able to produce clean PPG signals

when

the input signals were noisy. Although deep learning models have achieved good

performance on large datasets, these deep-learning-based methods only

考虑了在真实生活中。

the 使用质量评估功能对噪声消除方法的方法在提高，such as waving and shaking hands.

足以消除运动伪影对PPG信号的影响。上述

方法限于信号的短期分析或某些类型的噪声 manully generated noisy PPG dataset.

由特定活动引起的。因此，重建PPG的方法

在没有任何先验知识的情况下，由真实世界运动伪影失真的波形

The noisy signals in the test set were synthesized by adding the noises to clean sig-

噪音是需要的。噪声段必须包含干净的PPG信息。

因此，当干净的PPG信号在损坏的PPG信号中衰减时，这些方法可能失败。

## 4 Dataset

In this chapter, we introduce the dataset used to train, validate and test the model in this thesis.

The PPG data used in this thesis is a part of a health monitoring study conducted by the Health Technology Group at the University of Turku [47]. The PPG data was collected in Southwest Finland for one month, from July to August 2019. The participants were monitored without any limitation of activities, which allows to collect real-world signals in daily life.

There are 46 participants included in the study. The participants were asked to wear the wearable device on their non-dominant hands 24 hours for 7 days. The recruited participants meet the following requirements:

- Being able to use the wearable device for 24 hours.
- No cardiovascular diseases.
- No symptoms of other diseases during monitoring.
- No restricted physical activities.

Table 4.1 summarizes the background information of all the participants in the study [48].

The wearable device used in the study is a Samsung Gear Sport smartwatch [49]. The size of each smartwatch is  $44.6 \times 42.9 \times 11.6\text{mm}$  in height, width, and depth with a 30.2 mm main display. The watch is embedded with Wi-Fi at 802.11 b/g/n

## 4数据集

在本章中，我们将介绍用于训练、验证和测试模型的数据集  
本论文

本文中使用的PPG数据是健康监测研究的一部分，  
由图尔库大学的健康技术小组进行[47]。PPG数据  
从2019年7月到8月，在芬兰西南部收集了一个月。的  
对参与者的监测没有任何活动限制，这使得

收集日常生活中的真实信号。

共有46名参与者参加了这项研究。参与者被要求  
将可穿戴设备佩戴在他们的非惯用手上24小时，持续7天。的  
招募的参与者符合以下要求：

- 能够24小时使用可穿戴设备。
- 无心血管疾病。
- 监测期间无其他疾病症状。
- 没有限制的身体活动。

表4.1总结了研究中所有参与者的背景信息

48.

研究中使用的可穿戴设备是三星Gear Sport智能手表[49]。  
每个智能手表的尺寸为44.6 × 42.9 × 11.6mm，高，宽，深  
30.2 mm主显示屏手表内置Wi-Fi，802.11 b/g/n

Table 4.1: Background information of participants

Parameters	Values	Values
Age, years, mean (SD)		32.5 (6.6)
BMI, mean (SD)		25.4 (5.2)
	Almost daily	8
Exercise	A few times a week	13
	Once a week or fewer	6
	Primary school	1
Education level	High school	6
	College	6
	University	14
	Working	22
Employment status	Student	1
	Unemployed	3
	Other	1

2.4GHz and Bluetooth v4.2. It is water resistant with the pressure of 5 atmospheres or 50 meters under water. The internal memory of the smartwatch is 0.75 GB of random-access memory (RAM), and 4 GB of read-only memory (ROM). The watch is programmed by the Tizen operating system and utilizes sensors, including accelerator, gyroscope, and PPG sensor.

With our customized data collection application, 16-minute continuous PPG and accelerator/gyroscope signals are collected every half an hour at sampling frequency of 20 Hz. The first minute of the collected signals is removed because the time is for device calibration. The setup enables the battery life of the smartwatches to be longer than 24 hours.

The internal memory of the smartwatches is sufficient for storing the collected

data. The collected data is first stored in the watch's internal storage. After the monitoring, the data is sent to our cloud service for storage.

数据收集的数据首先存储在手表的内部存储器中。后  
监控后，数据会被发送到我们的云服务进行存储。

# 5 Proposed method

In this chapter, we introduce our GAN-based proposed method, including the model architecture, loss functions, training process, and reconstruction method with trained model. We also describe the preparation of training, validation, and test PPG datasets, which are used for model training, hyperparameter selection, and evaluation of the method performance, respectively.

## 5.1 Proposed model architecture

In our study, we develop a deep convolutional GAN-based model to reconstruct the noisy signals distorted by MAs. Previous studies showed that GAN is a powerful approach to de-noise images[34], [50]. We apply such a feature to our study to train a model by clean PPG signals and then use the trained model to denoise PPG signals distorted by MAs.

Our GAN-based model consists of two sub networks: a generator and a discriminator. The generator learns to generate synthesized clean PPG signals from their previous data points, while the discriminator learns to distinguish whether the signals are original input or synthesized by the generator. The two sub-networks compete with each other during training, and consequently the model learns how to synthesize clean PPG signals by the information from previous data.

Inspired by [51], we adopt a similar structure to GANomaly, which uses an Autoencoder architecture for the generator and an encoder architecture for the discrim-

# 5建议方法

在本章中，我们介绍了我们提出的基于GAN的方法，包括模型结构、损失函数、训练过程和具有训练的模型。我们还描述了训练、验证和测试PPG的准备数据集，用于模型训练、超参数选择和评估，方法的性能，分别。

## 5.1 拟议模型架构

在我们的研究中，我们开发了一个基于深度卷积GAN的模型来重建被MA扭曲的噪声信号。以前的研究表明，GAN是一种强大的图像去噪方法[34], [50]。我们将这样的特点应用到我们的研究中，通过干净的PPG信号训练模型，然后使用经训练的模型对PPG进行降噪被MA扭曲的信号。

我们的基于GAN的模型由两个子网络组成：生成器和DIS。罪犯发生器学习生成合成的干净PPG信号，他们以前的数据点，而机器人学习区分是否信号是原始输入或由发生器合成。两个子网在训练过程中相互竞争，因此模型学习如何

通过来自先前数据的信息合成干净的PPG信号。

受[51]的启发，我们采用了与GANomaly类似的结构，它使用了自动用于生成器的编码器架构和用于区分器的编码器架构。

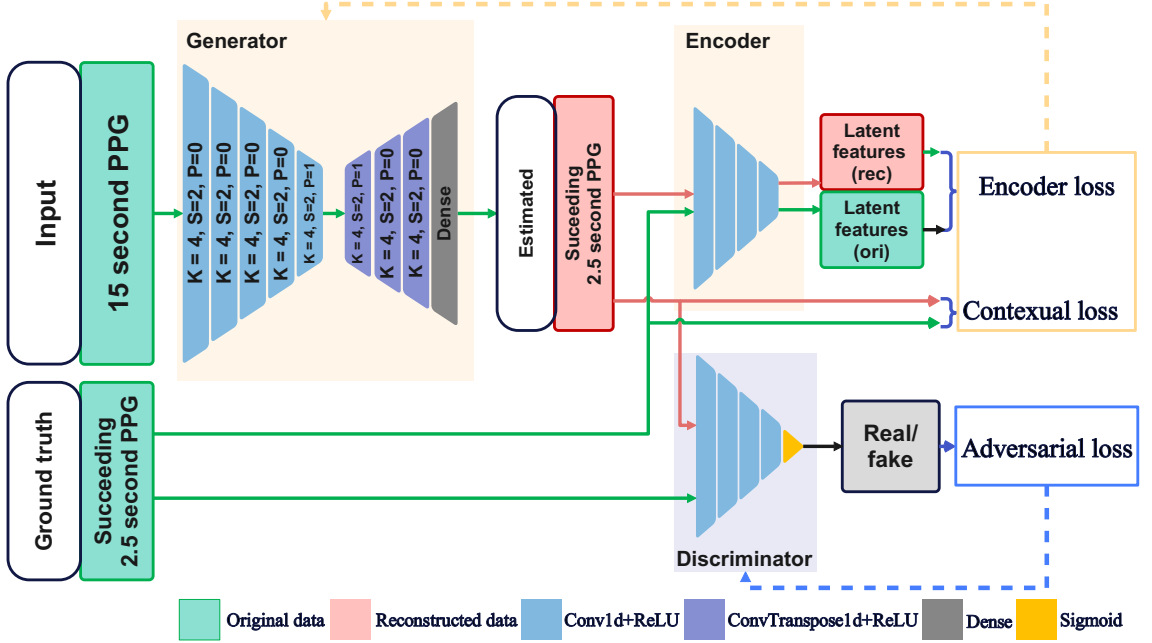


Figure 5.1: The architecture of proposed model. K, S, and P represent the kernel size, stride and padding parameters in convolutional layers respectively

inator. The deep convolutional layers are modified and applied to our model. The architecture of our proposed model is illustrated by Figure 5.1. In each epoch, the model takes 15-second clean PPG signal as input, and then the generator generates its succeeding 2.5 second PPG signal as output. The original succeeding 2.5-second PPG signal is the ground truth. The generator is optimized by minimizing the difference between the estimated succeeding PPG and its ground truth. The discriminator is updated by minimizing the classification error of whether the signal is the original ground truth or estimated by the generator. The K, S, and P in Figure 5.1 represent the kernel size, stride, and padding parameters in convolutional layers, respectively.

**Generator** The generator follows an Auto-encoder structure, i.e., an encoder and a decoder. The generator is trained to generate synthetic succeeding clean signals.

The encoder stacks 5 1D-convolutional layers to compress the PPG input to its representative features in latent space. The decoder stacks 3 transposed 1D-convolution layers and flattens its output by one dense layer to re-generate the PPG signal by the bottle-neck features.

**Encoder** The generator is then followed by another encoder. The encoder acts as a feature extraction part of the generator, which stacks 4 1D-convolution layers to downscale both the estimated signal from the generator and the real PPG signal to find their representative features in latent space.

**Discriminator** The discriminator, aiming to distinguish whether the signal is real or synthesized by the generator, uses the same encoder architecture to compress both reconstructed signals and original input to their corresponding representative features. Then, the Sigmoid layer classifies the features to values "1" or "0", representing the true and fake label.

### 5.1.1 Loss functions

To optimize each sub-network in the pipeline, we use the same three loss functions i.e., the encoder loss, contextual loss, and adversarial loss, as in [51] to optimize the model during training.

**Encoder loss** The encoder loss  $L_{enc}$  is the difference between the representative features compressed from synthesized and real PPG signals by the generator encoder mentioned in Section 5.1. The loss is calculated as:

$$J(fg, fo) = \frac{1}{256} \sum_{i=1}^{256} |fg_i - fo_i|^2 \quad (5.1)$$

where  $fg$  and  $fo$  are the latent features of generated and original PPG signal, respectively, and  $i$  is the index in a batch of samples with a size of 256. The value is backpropagated to update the generator in each iteration.

**Contextual loss** The contextual loss  $L_{con}$  is the difference between the original and the estimated succeeding signal from the generator in 5.1. The loss is calculated as:

$$J(sg, so) = \frac{1}{256} \sum_{i=1}^{256} |sg_i - so_i| \quad (5.2)$$

where  $sg$  and  $so$  are the generated signal and its original ground truth, respectively. The value is also backpropagated to update the generator each iteration.

**Adversarial loss** The adversarial loss is the standard discriminator loss. Binary cross-entropy is used as the loss function to calculate the difference between the actual and classification labels (i.e., real/fake) obtained by the discriminator. The value is backpropagated to optimize the discriminator each iteration.

In this model, except for the last layer of the discriminator which uses Sigmoid to give a binary output, all the other activation functions are Rectified Linear Units (ReLU). The batch normalization is performed between layers with dropout rate of 0.5 to avoid overfitting. The weights for networks are randomly initialized, and Adam is chosen as the optimizer.

### 5.1.2 Reconstruction method

In this thesis, we propose a sliding window method to reconstruct the noisy PPG signals with the trained model. As the real-world distorted PPG signals are not guaranteed to contain clean PPG signals, our proposed method uses a sliding window reconstruction method to leverage the information from both noisy signals and its proceeding clean signals.

Figure 5.2 indicates the reconstruction process of proposed method. A sliding window with a fixed length is used to select input and feed the signals to the generator. The first iteration starts at only clean signal before the distorted part. The generator takes the window of input and gives a prediction of succeeding data points.

语境缺失语境缺失是指原文与原文之间的差异，  
以及来自5.1中的发生器的估计的后续信号。损失是计算出来的

as:

$$J(SG, SO) = \frac{1}{256} \sum_{i=1}^{256} |SG_i - SO_i| \quad (5.2)$$

其中SG和SO分别是所生成的信号及其原始的地面实况。

该值也被反向传播以在每次迭代中更新生成器。

对抗性损失对抗性损失是标准的可预见损失。二进制  
交叉熵被用作损失函数来计算  
实际和分类标签（即，真实的/伪造的）。的

值被反向传播以优化每次迭代的时间。

在这个模型中，除了最后一层使用Sigmoid之外，  
为了给予二进制输出，所有其他激活函数都是整流线性单元  
(ReLU) .在层与层之间进行批量归一化，并具有丢失率为0.5，以避免过度拟合。网络的权重被随机初始化，

亚当被选为优化器。

### 5.1.2 重建方法

在这篇论文中，我们提出了一种滑动窗口的方法来重建噪声PPG  
信号与训练模型。由于真实世界的失真PPG信号不是  
为了保证包含干净的PPG信号，我们提出的方法使用滑动窗口  
利用来自噪声信号及其

发出干净的信号

图5.2显示了所提出的方法的重建过程。滑动  
具有固定长度的窗口用于选择输入并将信号馈送到生成器，  
发电机第一次迭代仅在失真部分之前的干净信号处开始。的  
generator获取输入的窗口，并给出后续数据点的预测。

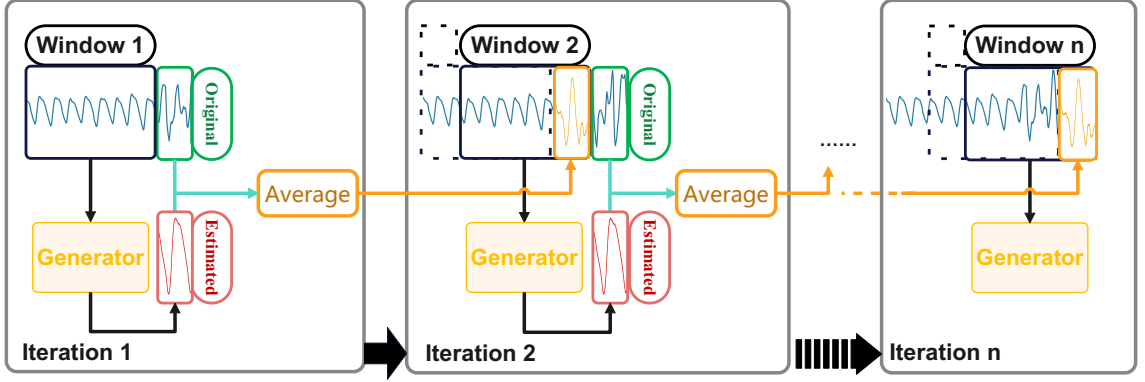


Figure 5.2: The reconstruction process of proposed method

Then the signal is updated by averaging the prediction and the original noise. In the next iteration, the window moves forward with a step, and repeats the process of making a prediction, updating the signal by average value, and moving the window to feed updated signals as input to the trained model. The iterations continues until the window sweeps to the end of the segment.

In our case, the sliding window length is 15 seconds, and the shift size of each step is 2.5 seconds to ensure each prediction at least contains one cardiovascular cycle.

## 5.2 Model training

In this section, we represent the training process of our proposed GAN-based model. The model is only trained with clean PPG signals. Thus the model only learns the distribution of clean PPG signals during training, and the trained parameters are not suitable for generating other signals than clean PPG signals. For example, if the input contains clean PPG and other noise at the same time, and the generator encoder compresses both clean PPG and noise to their representative bottleneck features, the trained generator decoder with its parametrization, can not reconstruct

the noise from the bottleneck feature of noise. Therefore, training with only clean signals enables the model to produce clean PPG signals from the noisy segment.

The model calculates the three types of loss mentioned in Section 5.1.1 and back-propagates them to optimize the generator and discriminator of the model during training. The model performing best on the validation set is selected to reconstruct noisy signal in the testing phase. Note that for the reconstruction method in this thesis, z-score standardization is applied to each PPG segment before feeding it into models.

### 5.2.1 Training and validation data preparation

We preprocess the raw PPG signals before feeding the data into our proposed model. Figure 5.3 is the block diagram, which illustrates all the steps of the preparation for the training and validation dataset. We introduce each preprocessing step shown in Figure 5.3 in the remainder of this section.

### 5.2.2 Segmentation and filtering

We use the PPG data collected in the study described in Chapter 4 to train and validate the model. The dataset contains 15-minute raw PPG signals from 46 participants, and the data from 37 of them form the training and validation dataset.

We first section the 15-minute raw PPG signals into 30-second segments to keep consistent with the input size of our signal quality assessment method. Then, we implement a 4-order high-pass Butterworth filter with a cutoff frequency of 0.5 Hz to remove baseline wander. Figure 5.4 indicates one of the filtering results after the high-pass Butterworth filter. Figure 5.4 (a) is one of the 30-second segment before filtering, while Figure 5.4 (b) is the segment after filtering. As indicated in Figure 5.4, the baseline of the raw PPG signal drifts up at 16 seconds, while after applying the high-pass filter, the baseline becomes stable throughout the 30-second segment.

噪声的瓶颈特性。因此，只有干净的训练信号使模型能够从噪声段产生干净的PPG信号。

该模型计算了第5.1.1节中提到的三种类型的损失，传播它们，以优化模型的生成器和模型，训练选择在验证集上表现最好的模型进行重建测试阶段的噪声信号。注意，对于本实施例中的重建方法，在这篇论文中，z分数标准化在将其馈送到每个PPG段之前应用于每个PPG段。

## 模型

### 5.2.1 培训和验证数据准备

我们在将数据馈送到我们提出的模型之前对原始PPG信号进行预处理。图5.3是框图，它说明了准备的所有步骤，训练和验证数据集。我们将介绍

图5.3在本节的其余部分。

### 5.2.2 分割和滤波

我们使用第4章中描述的研究中收集的PPG数据来训练和验证模型。该数据集包含来自46个部分的15分钟原始PPG信号，其中37个人的数据形成了训练和验证数据集。

我们首先将15分钟的原始PPG信号分成30秒的片段，与我们的信号质量评估方法的输入大小一致。然后我们实现截止频率为0.5 Hz 4阶高通巴特沃思滤波器以消除基线漂移。图5.4显示了一个过滤后的结果。高通巴特沃思滤波器。图5.4 (a) 是之前的30秒片段之一图5.4 (B) 是滤波后的线段。如图所示，5.4，原始PPG信号的基线在16秒时向上漂移，而在应用通过高通滤波器，基线在整个30秒段内变得稳定。

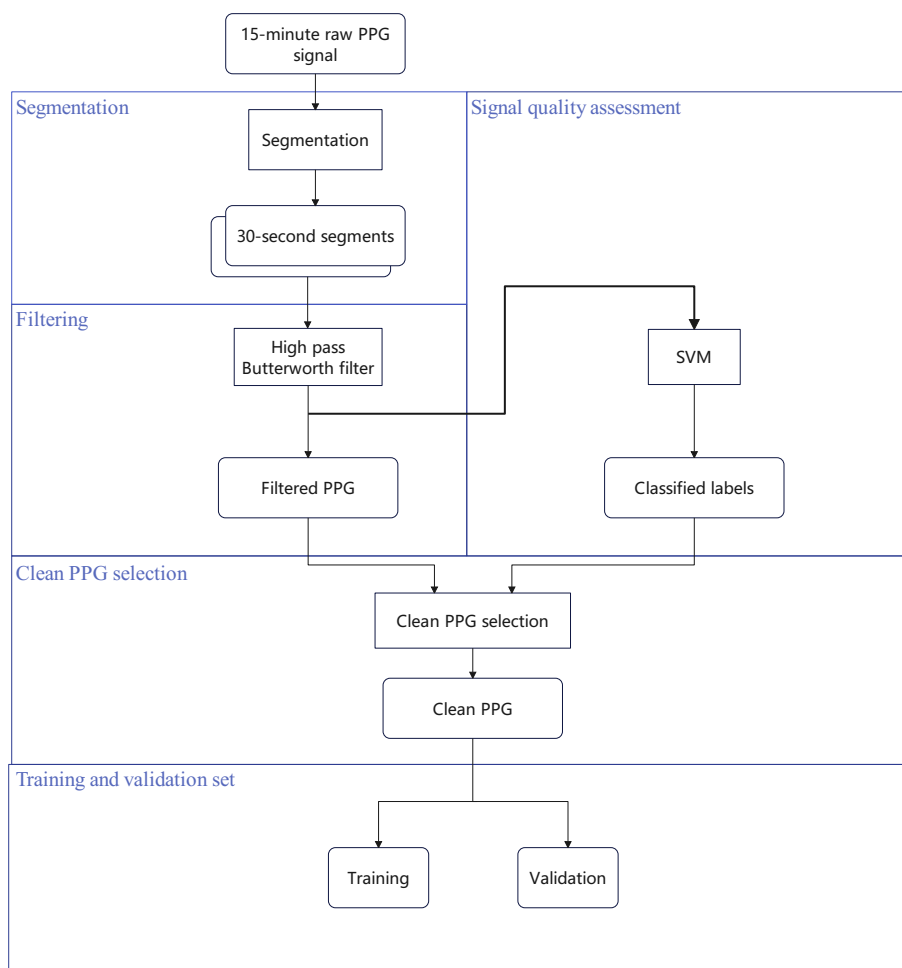


Figure 5.3: Block diagram of training data preparation

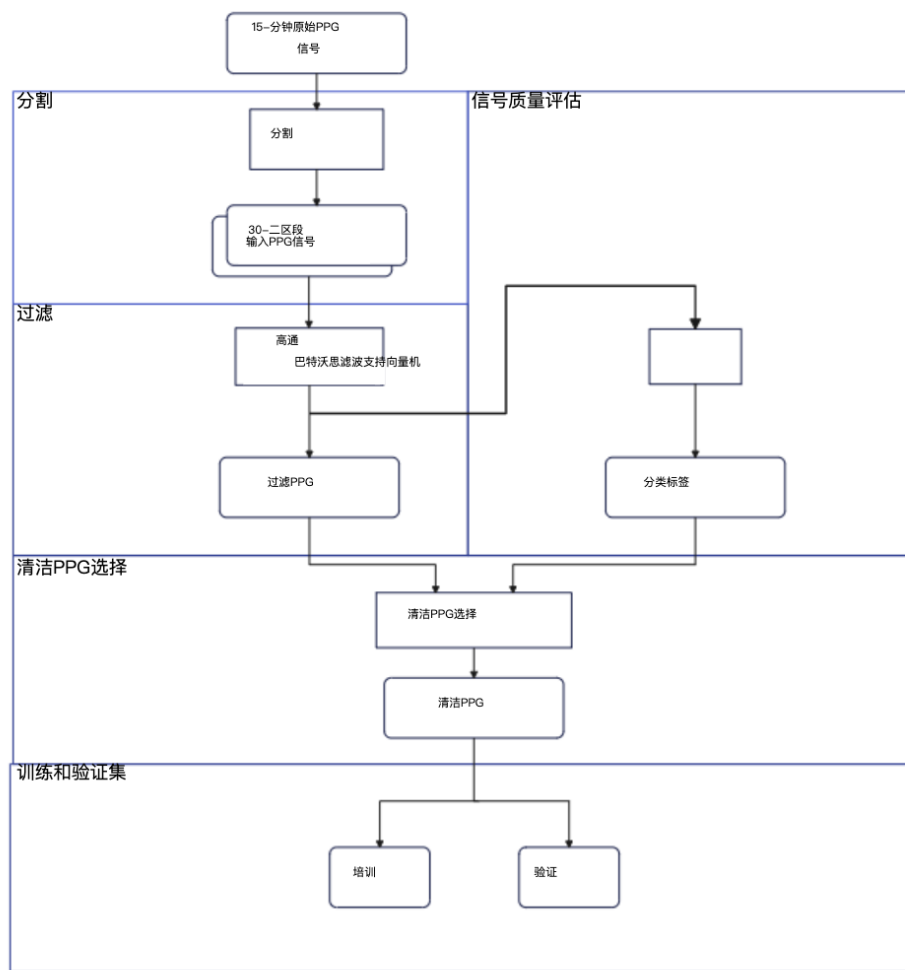


图5.3：训练数据准备框图

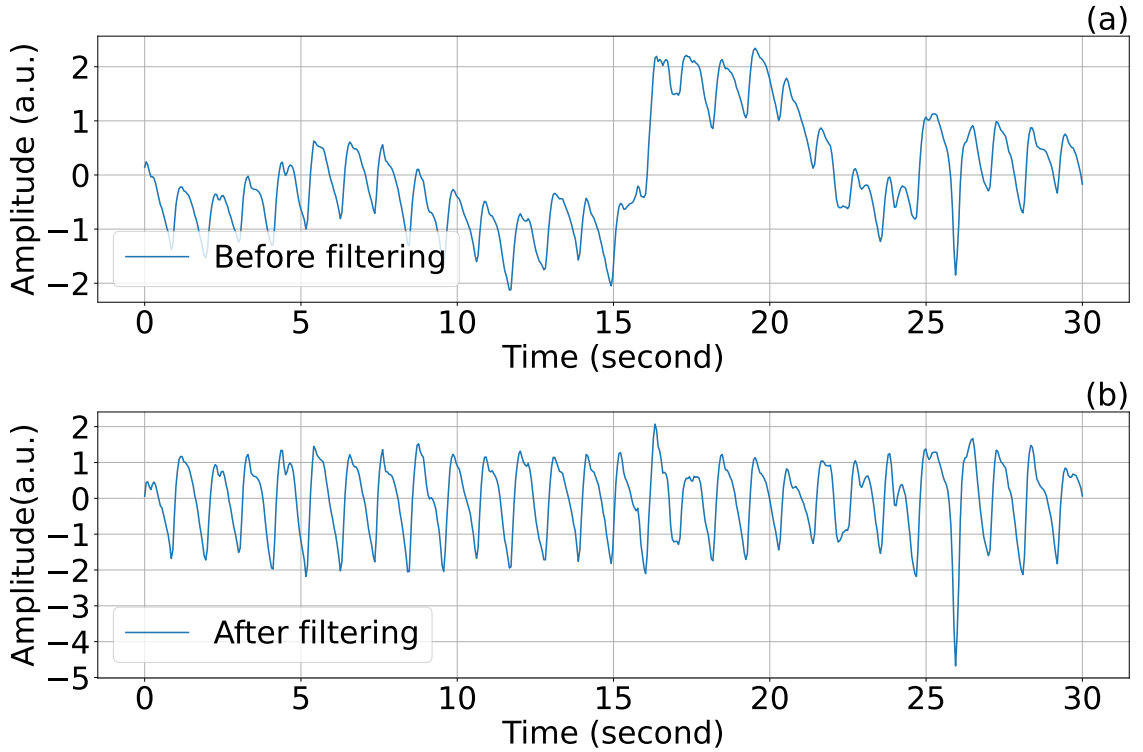


Figure 5.4: PPG signal (a) before filtering, and (b) after filtering

The filter can remove the unrelated low-frequency components and baseline wander.

### 5.2.3 Signal quality assessment

We used a Support Vector Machine (SVM) to assess the PPG signal quality in this thesis. The assessment technique takes 30-second PPG signal as input, and produces a classification result of whether the segment is clean or noisy. The assessment method is from [42], which extracts five features from the PPG waveform, including spectral entropy, Shannon entropy, approximate entropy, kurtosis, and skewness from each 30-second PPG. Then these features are fed into an SVM to classify the clean signals and noise.

Figure 5.5 indicates one of the classification results from SVM. (a) is one of the 30-second segments classified as clean, while (b) as noisy by the SVM. The SVM

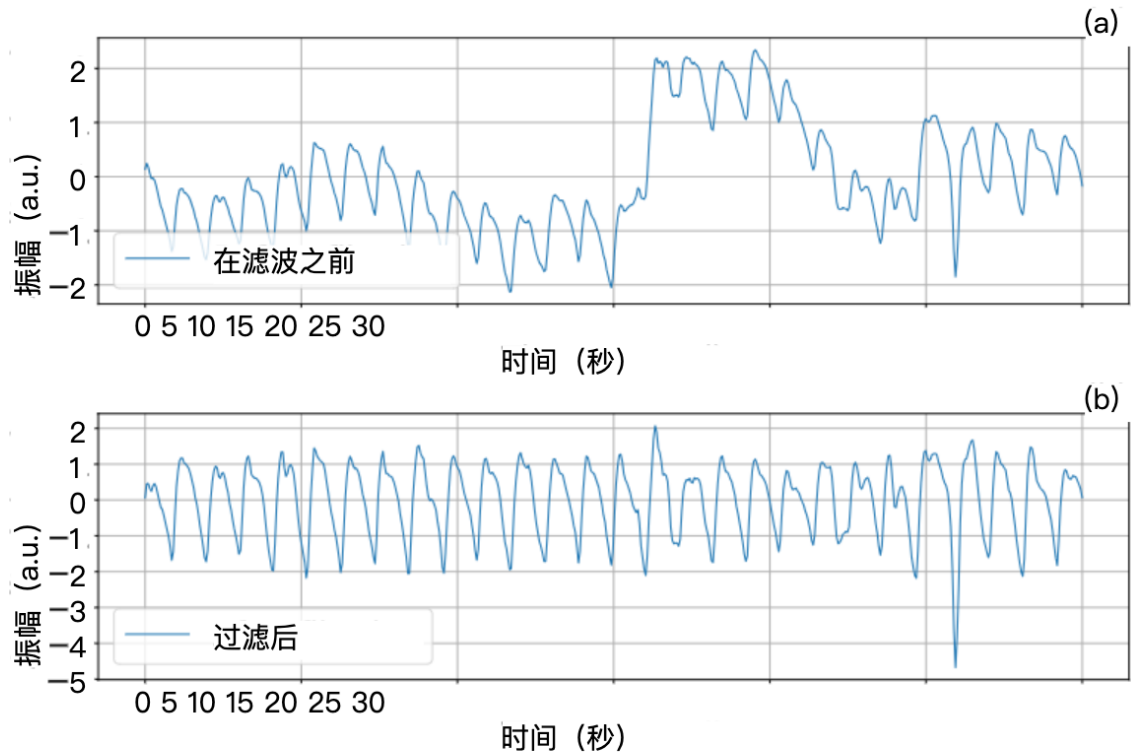


图5.4：PPG信号 (a) 滤波前， (b) 滤波后

该滤波器能滤除不相关的低频分量和基线漂移。

### 5.2.3 信号质量评估

我们使用支持向量机（SVM）来评估PPG信号质量，论文评估技术采用30秒PPG信号作为输入，并产生该片段是干净的还是有噪音的分类结果。评估方法来自[42]，其从PPG波形中提取五个特征，包括谱熵、Shannon熵、近似熵、峰度和偏度每30秒的PPG。然后将这些特征输入到SVM中，

干净的信号和噪音。

图5.5显示了SVM的一个分类结果。(a)是其中一30-第二段被SVM分类为干净，而(B)被SVM分类为有噪音。支持向量机

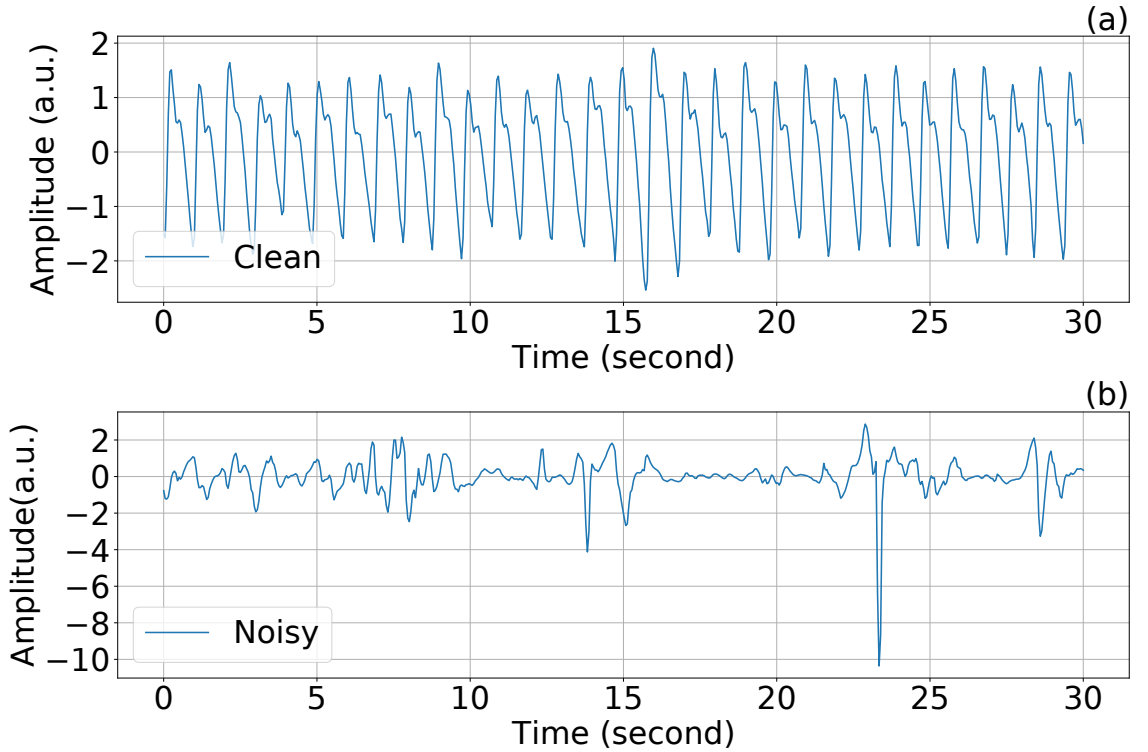


Figure 5.5: PPG signal classified as (a) clean segment, and (b) noisy segment by SVM.

can effectively assess the quality of PPG signals.

Finally, we used the classified labels to select only clean PPG signals from all the filtered 30-second signals. The obtained clean PPG signals are used as the data for the training and validation set.

The clean PPG data from 27 participants of the study is used for training, and the clean PPG from the other 10 participants forms the validation dataset. In total, 61117 30-second clean PPG segments are used to train the model, and 19661 segments for the validation set to select hyperparameters for the model.

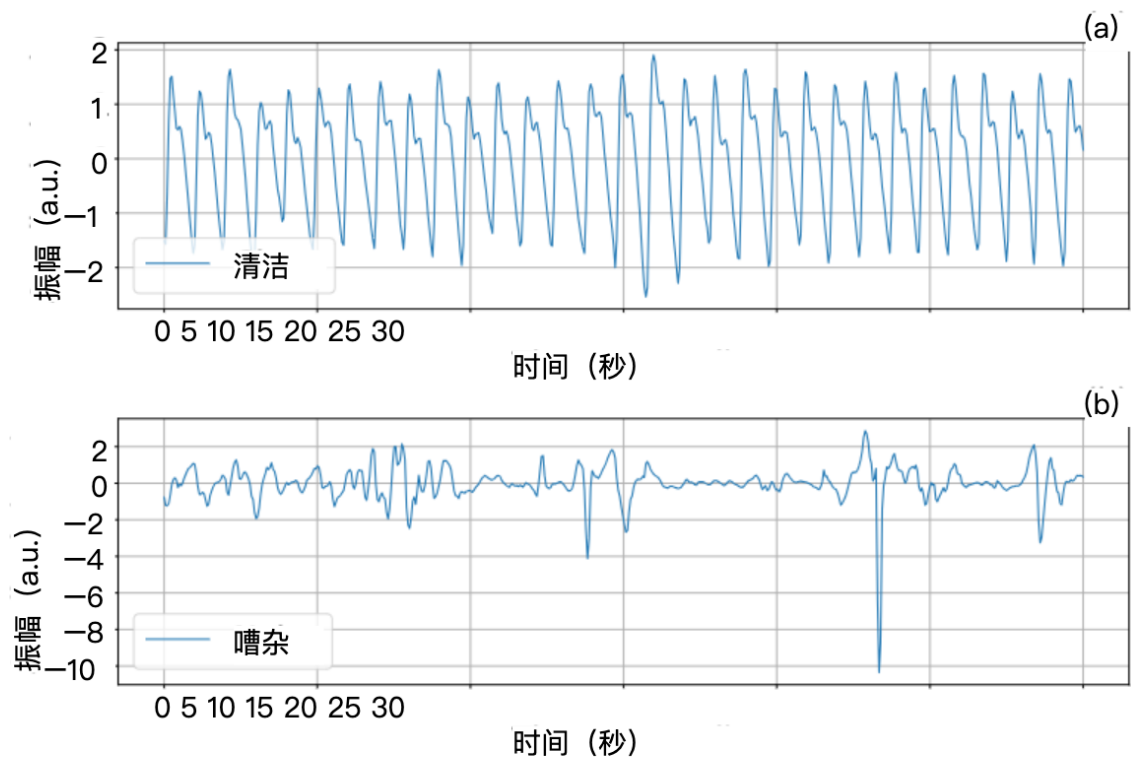


图5.5：PPG信号分类为 (a) 干净段和 (B) 噪声段，  
SVM.

可以有效地评估PPG信号的质量。

最后，我们使用分类标签从所有PPG信号中仅选择干净的PPG信号。  
过滤后的30秒信号将获得的干净PPG信号用作数据  
用于训练和验证集。

来自研究的27名参与者的干净PPG数据用于训练，  
来自其他10个参与者的干净PPG形成验证数据集。在  
总共有61117个30秒干净PPG片段用于训练模型，19661个30秒干净PPG片段用于训练模  
型。  
段来为模型选择超参数。

## 5.3 Test data preparation

We synthesize a test dataset containing noisy PPG signals distorted by real-world MAs. The test dataset is generated to evaluate the method’s performance on different noise levels and noise lengths. In this section, we introduce the preparation of the test dataset used in the study.

The steps of preparing the test dataset are shown in Figure 5.6. The preprocessing steps are similar to the preparation of the training and validation dataset. The raw PPG signals are first sectioned into 30-second segments. Then, the sectioned segments are filtered by a high-pass filter with cut-off frequency of 0.5 Hz to remove baseline wander. The same signal quality assessment method is used to produce the clean or noisy label for 30-second PPG segments. The classified clean and noisy segments are put into our noisy signal generation function to synthesize noisy PPG signals with required noise levels.

### 5.3.1 Noisy signal generation

The PPG data from the remaining 9 participants is used to synthesize the noisy PPG test set at different noise levels and duration. A noisy signal generation method is used in this thesis to synthesize the noisy test dataset. The noisy signals with different SNR values are needed for evaluating the reconstruction results from methods. The noisy signals are generated by the clean data and MAs mentioned in Section 5.2.3

In the thesis, we used a generate function to integrate clean signals and MAs at different noise levels. The noisy generation process follows the Algorithm 5.3.1. The explicit steps are introduced as follows.

**Clean PPG signal selection:** Randomly select a clean 30-second segment from the 9 individuals ( $S$ ).

**Noise selection:** Randomly select a noise segment ( $N$ ) from the MA dataset from

## 5.3 测试数据准备

我们合成了一个测试数据集，其中包含被真实世界扭曲的噪声PPG信号。文学硕士生成测试数据集，以评估该方法在不同情况下的性能。输入噪声电平和噪声长度。在本节中，我们将介绍

研究中使用的测试数据集。

准备测试数据集的步骤如图5.6所示。预处理-

测试步骤类似于训练和验证数据集的准备。的原始PPG信号首先被分成30秒的片段。然后，段由截止频率为0.5 Hz的高通滤波器滤波，以去除基线漂移使用相同的信号质量评估方法来产生30秒PPG片段的干净或嘈杂标签。分类干净和嘈杂将分段放入我们的噪声信号生成函数中以合成噪声PPG

具有所需噪声水平的信号。

### 5.3.1 噪声信号产生

来自其余9个参与者的PPG数据用于合成噪声PPG测试设置在不同的噪音水平和持续时间。一种噪声信号产生方法，用于合成噪声测试数据集。不同的噪音信号-需要输入SNR值来评估方法的重建结果。噪声信号由第节中提到的干净数据和MA生成5.2.3在论文中，我们使用生成函数来整合干净的信号和MA，不同的噪音水平。噪声生成过程遵循算法5.3.1。的

具体步骤介绍如下。

干净的PPG信号选择：随机选择一个干净的30秒段，9个人 (S)

噪声选择：从MA数据集中随机选择噪声段 (N) ，

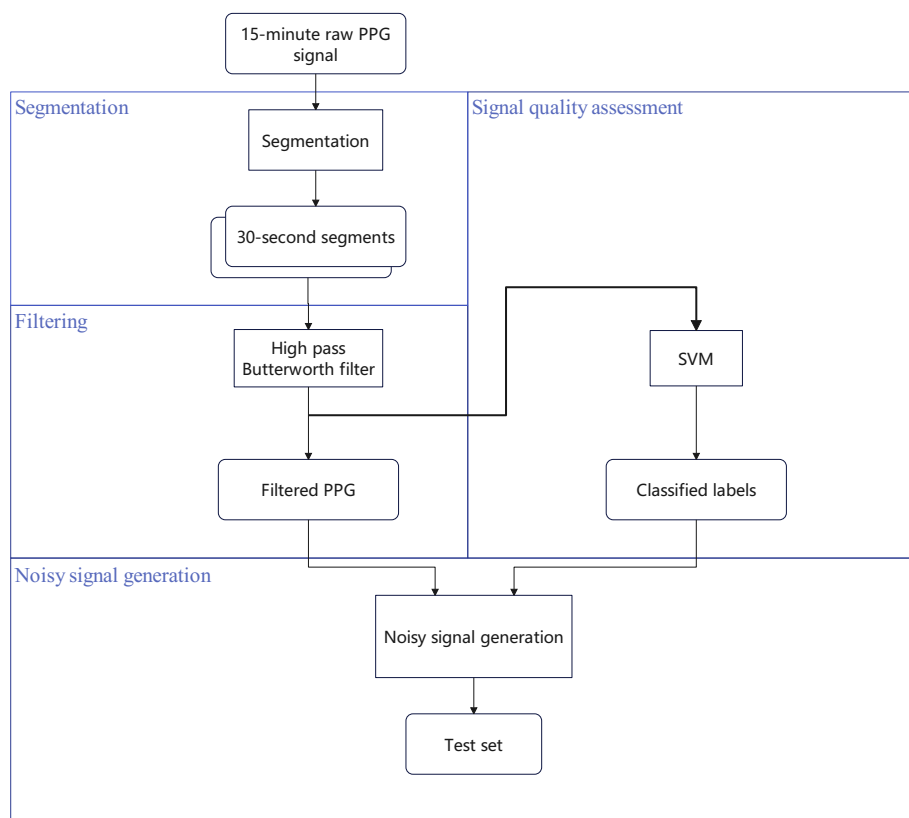


Figure 5.6: Block diagram of test data preparation

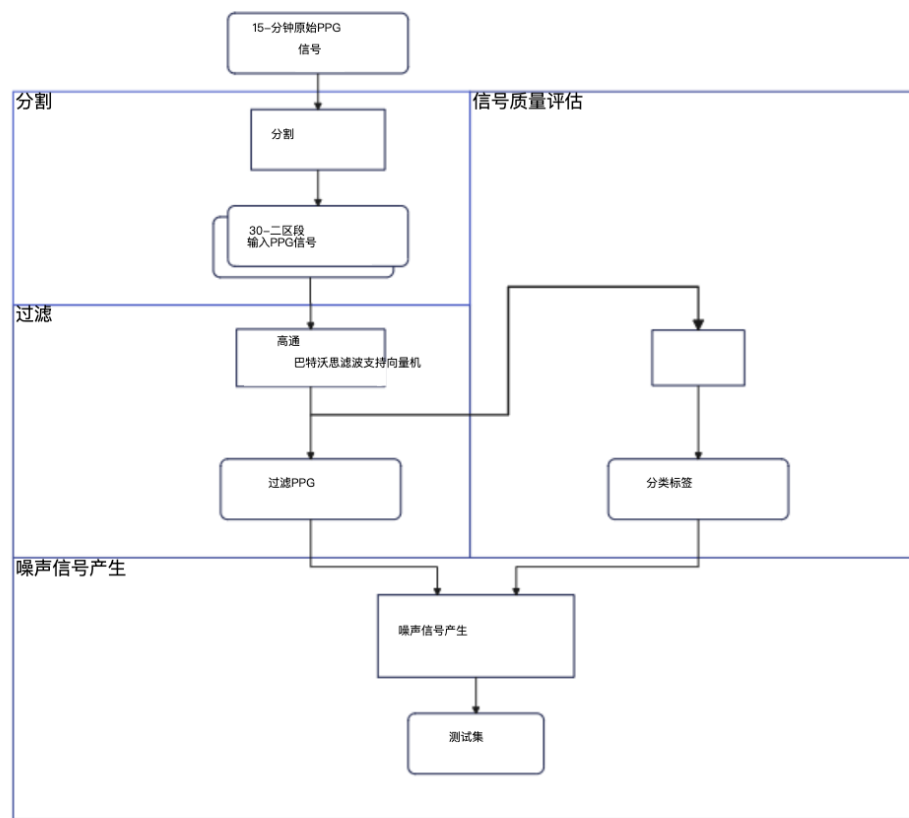


图5.6：测试数据准备框图

---

**Listing 1** The generator function

---

**Initialize:**

```

win_size ← window size
batch_size ← number of batch size
while  $j < \text{batch\_size}$  do
     $S \leftarrow$  a window of the clean PPG signal is chosen randomly
     $N \leftarrow$  select a noise frame randomly
     $w_N \leftarrow$  a random number with uniform distribution (0,16)
     $X \leftarrow S + w_N N$ 
    SNR ← calculate the SNR
     $j += 1$ 
end while

```

---

the 9 individuals. The MA dataset contains MAs with three noise lengths, including 5-second, 10-second, and 15-second motion artifacts. The noise segments are selected accordingly with these three different lengths.

**Noisy PPG generation:** A noisy PPG signal is calculated by a weighted arithmetic mean:

$$X = w_S S + w_N N \quad (5.3)$$

where  $w_S$  and  $w_N$  are the weights of the clean signals and noise, respectively. In this thesis,  $w_S$  equals to 1, while  $w_N$  is a random generated number which follows a uniform distribution ranging from 0 to 16. Note that we select a window corresponding to the noise length (i.e. 5-second, 10-second, and 15-second) at the end of each segment to add noises.

**SNR extraction:** We then calculate the SNR values for each generated noisy PPG signal using the following Equation 5.4:

$$SNR = 10 \log \frac{P_{Signal}}{P_{Noise}} \quad (5.4)$$

---

清单1生成器函数

---

初始化：

```

win_size ← 窗口大小
batch_size ← 批量数量
while j < batch_size do
    S ← 随机选择干净PPG信号的窗口
    N ← 随机选择一个噪声帧
    w ← 均匀分布的随机数 (0, 16)
    X ← S + wN
    SNR ← 计算SNR
    j += 1
end while

```

---

9个人。MA数据集包含具有三种噪声长度的MA，包括5秒、10秒和15秒运动伪影。选择噪声段

这三种不同的长度。

噪声PPG生成：通过加权的arithmetic来计算噪声PPG信号。

平均值：

$$X = wS + wN \quad (5.3)$$

其中Wand分别是干净信号和噪声的权重。在本文中，w等于1，而w是一个随机生成的数，从0到16的均匀分布。请注意，我们选择一个窗口对应—响应于结束时的噪声长度（即5秒、10秒和15秒），

每一段都要加上噪音。

SNR提取：然后计算每个生成的噪声PPG的SNR值

使用下面的等式5.4来计算信号：

$$SNR = 10 \log \frac{P}{P} \quad (5.4)$$

where  $P_{Signal}$  is the power of clean signal, and  $P_{Noise}$  is the power of the selected motion artifacts.

The generated noisy 5-second, 10-second, and 15-second PPG signals with SNRs ranging from -25 dB to 30 dB are used as the data for the test set. In total, the generate function in Section 5.3.1 generates 16384 30-second segments for each noise length.

其中， $P$ 是干净信号的功率，并且 $P$ 是所选信号的功率。

运动伪影。

所生成的具有SNR的噪声5秒、10秒和15秒PPG信号

范围从-25 dB到30 dB的数据用作测试集的数据。总的来说，  
第5.3.1节中的generate函数为每个噪声生成16384个30秒片段

长度

## 6 State-of-the-art methods

This chapter introduces the state-of-the-art PPG reconstruction methods that we use as baseline. Three PPG noise removal methods are selected in this thesis. All the baseline methods do not need any reference signals to keep consistent with our proposed method, and each of them is selected to represent the corresponding method category, including a time time-series, a signal decomposition, and another deep-learning based method mentioned in Chapter 3. The time-series method uses the proceeding samples to predict the distorted part of the signal, where we select the combination of Kalman filter and AR model proposed in [12] to represent the method of this category. The signal decomposition methods analyze the noise and clean PPG components in the noisy signal, and only exclude the noise component to reduce the effect of motion artifacts in corrupted signals. In this regard, we select the EMD and DWT method proposed in [9] as a representation of reconstruction methods in this category. Deep-learning based method develop different models to reconstruct PPG signals. Other than our proposed GAN-based method, we select the Bidirectional Long Short-Term Memory (LSTM) method proposed in [14] to represent the performance of the deep-learning models with other network architecture, which only focus on certain types of noises.

## 6最先进的方法

本章介绍了最先进的PPG重建方法，我们用作基线。本文选取了三种PPG去噪方法。所有基线方法不需要任何参考信号来保持一致，我们提出的方法，他们中的每一个都被选择来代表相应的方法类别，包括时间时间序列、信号分解和其他第三章中提到的基于深度学习的方法。时间序列方法使用进行的样本来预测信号的失真部分，其中我们选择卡尔曼滤波器和AR模型的组合[12]中提出的代表这一类的方法。信号分解方法分析了噪声，清除噪声信号中的PPG分量，仅排除噪声分量以减少被破坏的信号中的运动伪影的影响。为此，我们选择在[9]中提出的EMD和DWT方法作为重建的表示这一类的方法。基于深度学习的方法开发不同的模型，重建PPG信号。除了我们提出的基于GAN的方法，我们选择双向长短期记忆（LSTM）方法在[14]中提出，以表示重新评估深度学习模型与其他网络架构的性能，

只关注某些类型的噪音。

## 6.1 Kalman filter and Auto regression model

We select the Kalman filter and AR model from [12]. The method uses the signals before noise as training data to predict the succeeding data. The Kalman filter and AR model is selected as the state-of-the-art method to represent the time-series method.

The Kalman filter is a filter that leverages the observation from the past to estimate unknown variables. The estimation is calculated by providing solutions with the least-squares method [52]. The Kalman filter in the selected method is used to update the coefficients for the AR model.

The Auto regressive (AR) model is a prediction method on time-series data, which holds the assumption that the variable of interest is linearly correlated with its past values. It predicts the value of the variable on time  $t$  by values of the variable in the past from time 0 to time  $t - 1$  [53]. The AR model in the selected method is implemented to predict the succeeding PPG data points. The combination of Kalman filter and AR model works together to optimize the prediction over time by all the data before the current time.

In our case, the parameters for the Kalman filter follow the same values in [12], that is, the noise covariance matrix of is a normal distribution with the values of mean and standard deviation equaling to 0 and 0.2, respectively. The order  $p$  for the AR model is obtained by AIC criterion.

## 6.2 Empirical Mode Decomposition and Discrete Wavelet Transform

The method that combines EMD and DWT to reconstruct PPG signals is from [9]. The EMD and DWT method is chosen to represent the signal decomposition method for PPG signal reconstruction.

## 6.1 卡尔曼滤波和自回归模型

我们从[12]中选择卡尔曼滤波器和AR模型。该方法使用信号在噪声之前作为训练数据来预测后续数据。卡尔曼滤波器并选择AR模型作为时间序列的最新表示方法

法

卡尔曼滤波器是一种利用过去的观测结果

估计未知变量。通过提供解决方案来计算估计值用最小二乘法[52]。所选方法中的卡尔曼滤波器为

用于更新AR模型的系数。

自回归（AR）模型是一种时间序列数据的预测方法，

它假设感兴趣的变量与以下变量线性相关：

过去的价值观。它通过变量的值来预测变量在时间t的值

从时间0到时间t-1 [53]。所选方法中的AR模型

用于预测后续PPG数据点。的组合

卡尔曼滤波器和AR模型一起工作，通过以下方式优化随时间的预测：

当前时间之前的所有数据。

在我们的情况下，卡尔曼滤波器的参数遵循[12]中的相同值，

也就是说，的噪声协方差矩阵是具有以下值的正态分布：

平均值和标准差分别等于0和0.2。p的顺序

采用AIC准则建立了AR模型。

## 6.2 经验模态分解与离散小波

### 变换

结合EMD和DWT来重建PPG信号的方法来自[9]。

选择EMD和DWT方法作为信号分解方法

PPG信号重建。

The EMD is a signal decomposition method for non-stationary signals. The method decomposes the signal into a set of components, namely Intrinsic Mode Function (IMF) [54], which only have one zero between successive extrema and a zero local mean. In the selected state-of-the-art method, the EMD first decomposes the signal to different levels of IMF components. Then the most relevant component is chosen to improve the signal quality.

The DWT is also a signal decomposition method that maps the signal in time domain to frequency domain [55]. A mother wavelet is used to decompose the signal into a set of high-frequency and low-frequency wavelets. At each level, the signals are filtered by high-pass and low-pass filters to obtain the detail coefficients (i.e. the high-frequency coefficients) and the approximation coefficients (i.e. the low-frequency coefficients). The signals are then reconstructed by a linear combination of the wavelet functions weighted by this set of wavelet coefficients. In the selected method, the DWT takes the output component from the EMD, and then uses the output IMF as input of DWT to further reduce the noise.

Same parameters in [9] are used in this thesis, that is, to choose the first IMF from EMD as the input for DWT and use Daubechies 4 with decomposition level of 5 as the mother wavelet for DWT.

## 6.3 Bidirectional Long Short-Term Memory Auto-encoder

The bidirectional recurrent denoising auto-encoder (BRDAE) is selected from [14]. It represents the state of the art of other deep-learning based methods.

The bidirectional recurrent neural network (RNN) is a deep-learning based method commonly used in tasks dealing with sequential data. Compared with the feed-forward network, RNN considers the time dependencies between the previous and

6.3 双向长短期存储器自动编码器33 EMD是一种用于非平稳信号的信号分解方法。的方法将信号分解为一组分量，即固有模式函数 (IMF) [54]，在连续的极值之间只有一个零，零局部均值在所选的最先进的方法中，EMD首先分解不同级别的IMF成员。那么最相关的部分

以提高信号质量。

小波变换也是一种信号分解方法，它将信号映射到时间上频率域[55]。利用母小波对信号进行分解分成一组高频和低频小波。在每一级，信号被高通和低通滤波器滤波以获得细节系数（即，高频系数）和近似系数（即，低频系数）。频率系数）。然后通过线性组合来重构信号由这组小波系数加权的小波函数。在所选择的方法，DWT从EMD获取输出分量，然后使用

输出IMF作为小波变换的输入，进一步降低噪声。

本文采用了与文献[9]相同的参数，即选取第一个IMF作为DWT的输入，并使用Daubechies 4，分解级别为5作为小波变换的母小波。

## 6.3 双向长短期记忆 编码器

双向递归去噪自动编码器 (BRDAE) 选自[14]。

它代表了其他基于深度学习的方法的最新技术水平。

双向递归神经网络 (RNN) 是一种基于深度学习的方法通常用于处理顺序数据的任务。与饲料相比-前向网络，RNN考虑前一个和后一个之间的时间依赖性。

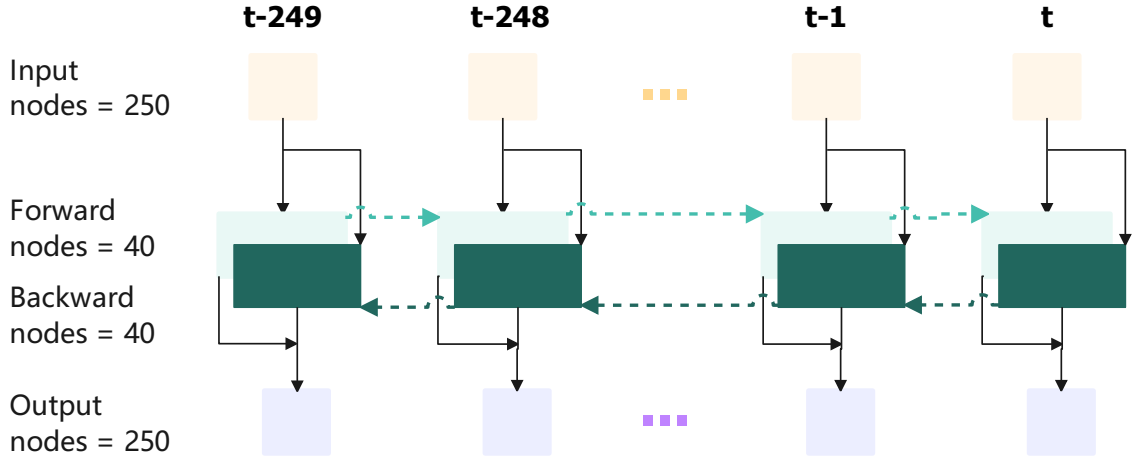


Figure 6.1: The architecture of Bidirectional LSTM method

current hidden state. Therefore, the RNN is able to store the history information of data. In the selected method, a bidirectional Long Short-Term Memory (LSTM) layer is applied to the Auto-Encoder model to extract time dependencies in PPG signals.

We follow the same BRDAE architecture in [14] (see Figure 6.1). The model takes 250 nodes as input and uses a 40-node bidirectional LSTM layer as hidden layer. The bottleneck feature is then reconstructed to an output size of 250 nodes again. The root mean square error between reconstructed signal and true values is calculated and backpropagated to the model as the loss of each training epoch. Adam is selected as the optimizer with a learning rate of 0.001.

The training data for the model is augmented by three types of noise, including white noise, slope noise, and saturation noise. They are randomly added to the clean PPG signal to train the model.

The white noise is the random noise with zero mean and normal distribution described in Chapter 2.1.1. The noisy signal with white noise  $X^{white}$  can be synthesized using the following equation:

### 6.3 双向长短时记忆自动编码器34路输入

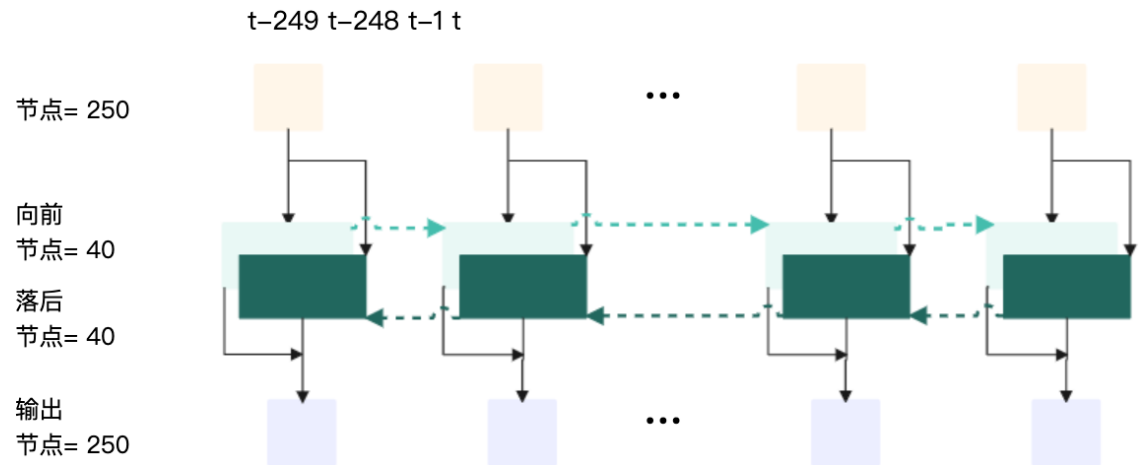


图6.1：双向LSTM方法的架构

当前隐藏状态因此，RNN能够存储历史信息的数据。在选择的方法中，双向长短期记忆（LSTM）层应用于自动编码器模型，以提取PPG中的时间依赖性

信号。

我们遵循[14]中相同的BRDAE架构（见图6.1）。模型以250个节点作为输入，并使用40个节点的双向LSTM层作为隐藏层。然后将瓶颈要素重构为250个结点的输出大小再重建信号与真实值之间的均方根误差计算并反向传播到模型作为每个训练时期的损失。

Adam被选为学习率为0.001的优化器。

模型的训练数据由三种类型的噪声增强，包括白色噪声、斜率噪声和饱和噪声。它们被随机添加到清洁PPG信号以训练模型。

白色噪声是具有零均值和正态分布的随机噪声。在第2.1.1章中描述。可以合成带有白色噪声的带噪信号使用以下等式：

$$X_i^{white} = S_i + \frac{1}{3} \cdot N(0, 1) \quad (6.1)$$

where,  $S_i$  is the  $i^{th}$  sample of the original clean signal, and  $N(0, 1)$  indicates the normally distributed white noise with mean and standard deviation equaling to 0 and 1, respectively. Figure 6.2 shows an example of the synthesized noisy PPG signal with white noise (in orange), and its clean ground truth (in blue).

The slope noise is the noise that causes sloping shift to the baseline of signals. The noisy signal with slope noise  $X_i^{slope}$  can be synthesized using the following equation:

$$X_i^{slope} = S_i + \frac{4}{N} \cdot i \cdot U(-1, 1) \quad (6.2)$$

where  $S_i$  is the  $i^{th}$  sample of the original clean signal, and  $i$  is the index of the sample.  $N$  is the total sample number in the signal segment.  $U(-1, 1)$  represents a random number that follows a uniform distribution between -1 and 1. 4 is considered as the highest slope for the synthesized signal, which is the same value from [14].

The saturation noise represents the distorted PPG signals below or above the analog-to-digital conversion (ADC) range during measurement. The noisy signal with saturation noise  $X_i^{saturation}$  can be synthesized using the following equation:

$$\begin{aligned} X_i^{saturation} &= 0 \text{ or } 1, & \text{if } x_1 \leq i \leq x_2 \\ X_i^{saturation} &= S_i, & \text{otherwise} \end{aligned} \quad (6.3)$$

where  $x_1$  is the starting index of the saturation noise, which is a random number selected from a uniform distribution between 0 and total sample number  $N$ .  $x_2$  is the end index of the saturation noise, which is dependent on the value of  $x_1$ . The  $x_1$  and  $x_2$  should meet the requirement that  $x_2 - x_1 \leq 20\% \cdot N$  because the maximum duration of saturation noise should be less than 20% of the total signal noise. The 20% value is chosen to keep consistent with the training details in [14].

### 6.3 双向长短期记忆自动编码器 35 X

$$x_i = S + \frac{1}{3} \cdot N(0, 1) \quad (6.1)$$

其中， $S$ 是原始干净信号的isample，并且 $N(0, 1)$ 指示正态分布的白色噪声，平均值和标准差等于0和1，分别。图6.2所示为合成噪声PPG的示例

带有白色噪声的信号（橙子）及其干净的地面上实况（蓝色）。

斜坡噪声是使信号向基线倾斜移动的噪声。

具有斜率噪声 $X$ 的噪声信号可以使用以下公式合成：

方程式：

$$X_i = S + \frac{4}{N} \cdot i \cdot U(-1, 1) \quad (6.2)$$

其中， $S$ 是原始干净信号的isample， $i$ 是样本的索引。 $N$ 是信号段中的总样本数。 $U(-1, 1)$ 表示一个随机数在-1和1之间均匀分布的数。4被认为是

合成信号的最高斜率，与[14]中的值相同。

饱和噪声表示低于或高于预定阈值的失真PPG信号。

测量期间的模数转换（ADC）范围。有噪信号

具有饱和噪声的 $X$ 可以使用以下等式合成：

$$\begin{aligned} X_i &= 0 \text{ 或 } 1, \text{ 如果 } x \leq i \leq x \\ X_i &= S, \text{ 否则} \end{aligned} \quad (6.3)$$

其中， $x_i$ 是饱和噪声的起始索引，是一个随机数从0和总样本数 $N$ 之间的均匀分布中选择。 $X_i$ 是饱和噪声的结束指数，取决于 $x$ 的值。的 $x$ 和 $x$ 应满足 $x - x_i \leq 20\% \cdot N$ 的要求，因为最大饱和噪声的持续时间应小于总信号噪声的20%。的

选择20%的值是为了与[14]中的训练细节保持一致。

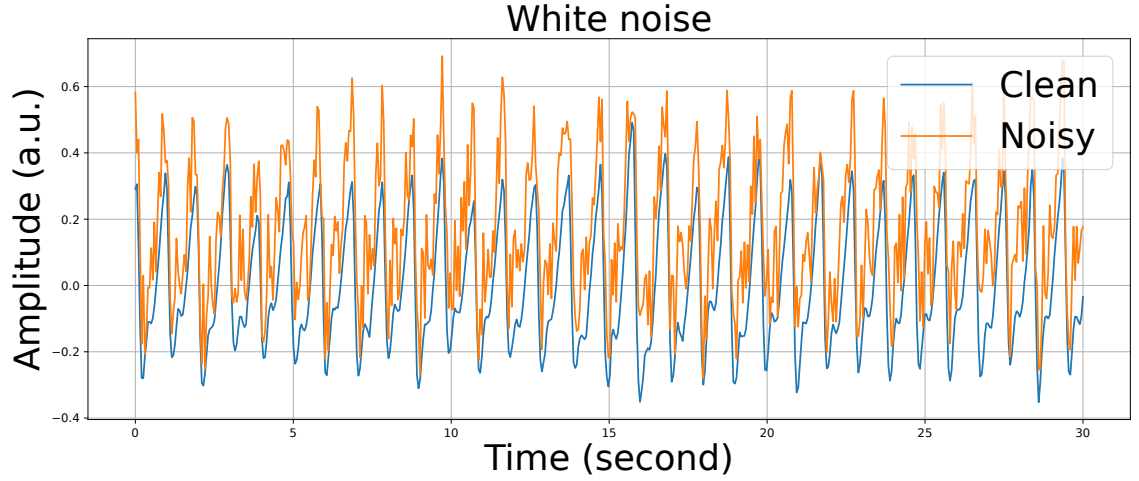


Figure 6.2: An example of synthesized PPG signal with white noise (orange) and ground truth (blue)

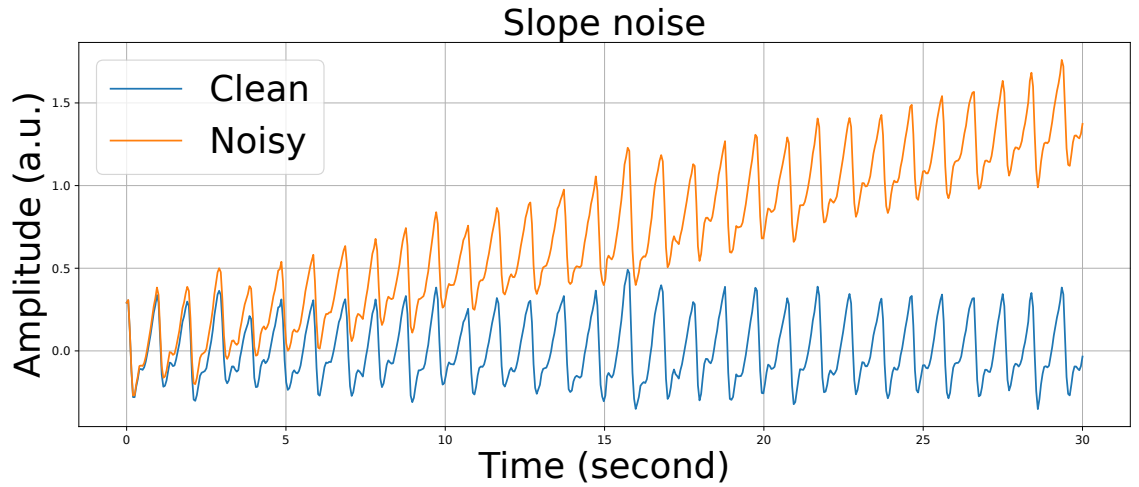


Figure 6.3: An example of synthesized PPG signal with slope noise (orange) and ground truth (blue)

The model is trained by minimizing the differences between the synthesized noisy signal and its original clean signal. In testing, the final trained model takes the noisy signals as input and then outputs the reconstructed clean signal.

### 6.3 双向长短时记忆自动编码器

36 0 5 10 15 20 25 30 时间 (秒)

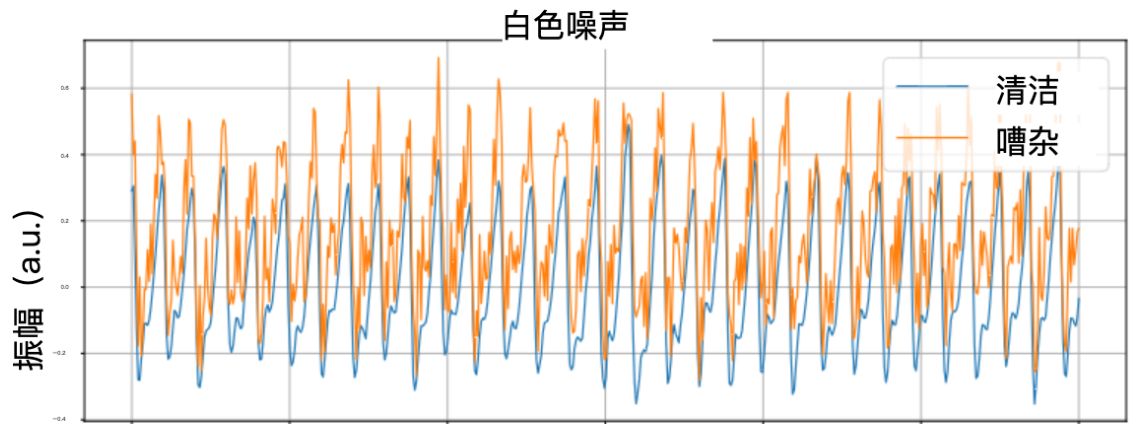


图6.2：具有白色噪声（橙子）和  
地面实况（蓝色）

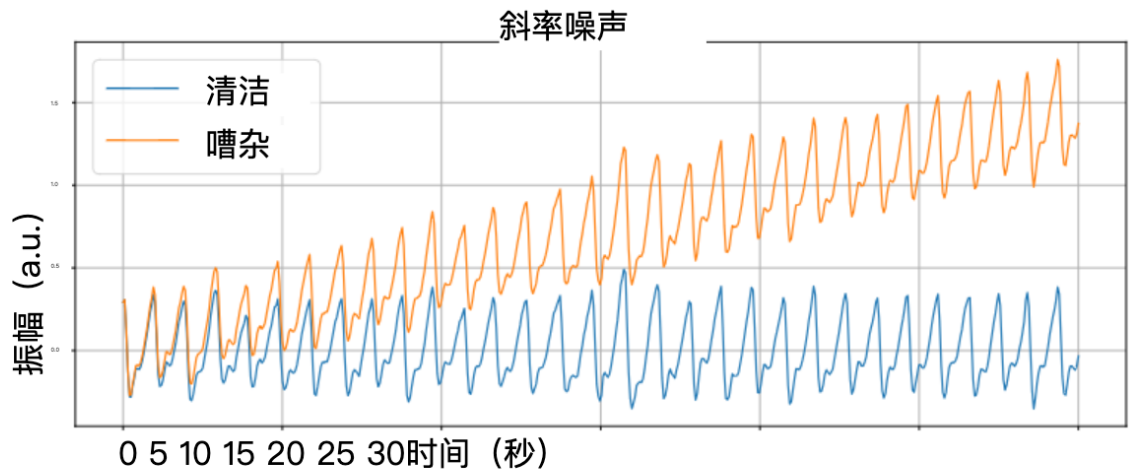


图6.3：具有斜率噪声（橙子）的合成PPG信号示例，  
地面实况（蓝色）

通过最小化合成噪声之间的差异来训练模型。

信号和其原始干净信号。在测试中，最终的训练模型将噪声  
信号作为输入，然后输出重构的干净信号。

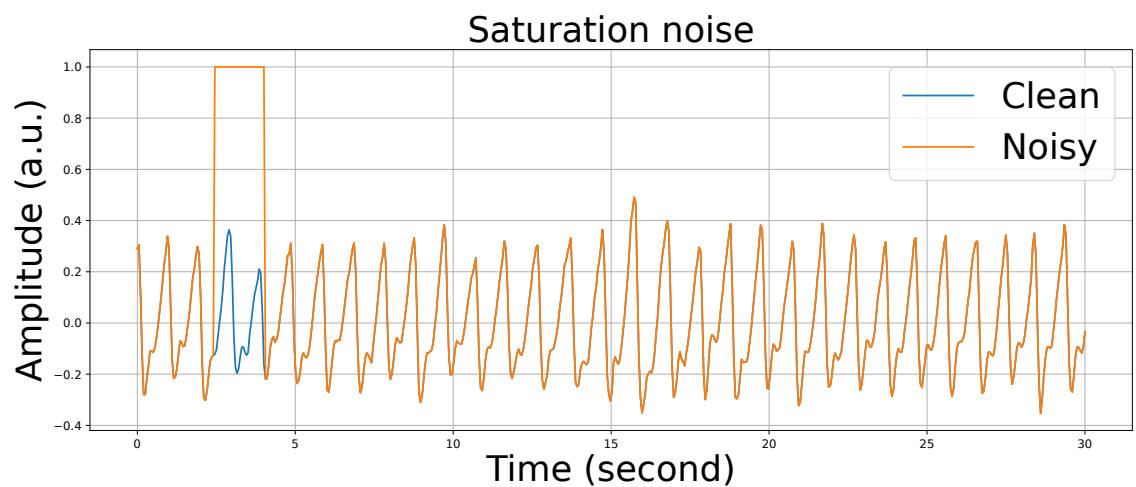


Figure 6.4: An example of synthesized PPG signal with saturation noise (orange) and ground truth (blue)

### 6.3 双向长短时记忆自动编码器

37 0 5 10 15 20 25 30 时间 (秒)

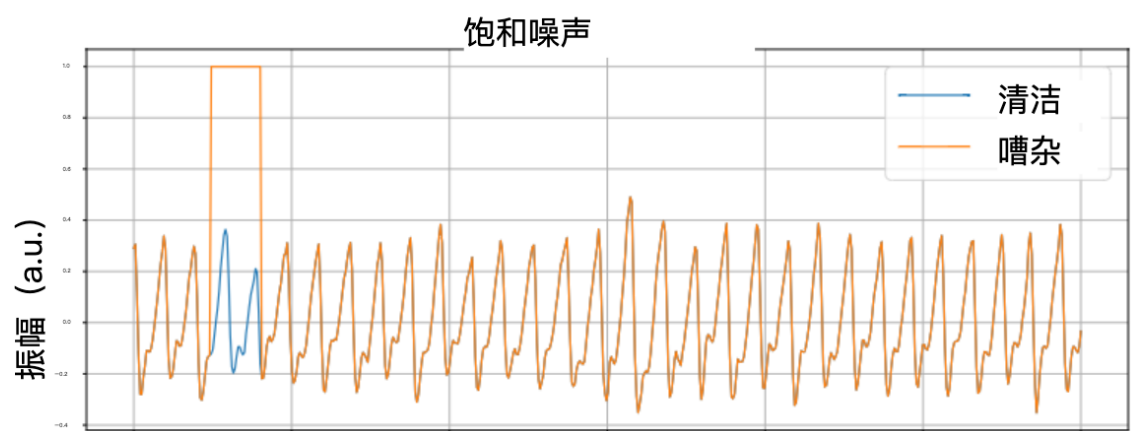


图6.4：具有饱和噪声的合成PPG信号示例（橙子）

Ground Truth (蓝色)

# 7 Results and discussion

In this chapter, we present the reconstruction results obtained by the proposed and the selected three state-of-the-art methods. All the methods are evaluated by the test dataset obtained in Section 5.3.1, which contains noisy PPG signals distorted by 5-second, 10-second, and 15-second real-world motion artifacts. In each noise length group, the SNR values of the signals range from -25 dB to 30 dB.

We introduce the two metrics, i.e., the maximum peak-to-peak error and the RMSSD error, which are used to evaluate the method performance.

## 7.1 Setup

The proposed method and the Bidirectional LSTM method are implemented by PyTorch [56]. The Kalman and AR methods are implemented by pykalman [57], statsmodel [58] package. The EMD and DWT method uses pyEMD [59], and PyWavelets [60] package in Python.

In the thesis, the training process of the proposed method runs 1000 epochs in total, and a batch size of 256 is used for each epoch. The Bidirectional LSTM method runs 2000 epochs for training with a batch size of 250 samples, which is the same as the process proposed in [14]. For both the proposed and Bidirectional LSTM method, the model that performs best on the validation set is chosen as the final model for testing.

For experiments from all the methods, we used a Linux machine with AMD

# 7结果与讨论

在本章中，我们提出的重建结果所获得的建议和所选的三种最先进的方法。所有方法都由第5.3.1节中获得的测试数据集，其中包含失真的噪声PPG信号5秒、10秒和15秒真实世界运动伪影。在每一个噪音

长度组中，信号的SNR值范围为–25 dB至30 dB。

我们引入两个度量，即，最大峰间误差和RMSSD误差，用于评估方法性能。

## 7.1 设置

所提出的方法和双向LSTM方法通过以下方式实现：PyTorch [56]。卡尔曼和AR方法由pykalman [57]实现，statsmodel [58]包。EMD和DWT方法使用pyEMD [59]和Py。

Python中的Wavelet [60]包。

在本文中，所提出的方法的训练过程运行1000个epoch总共，并且每个时期使用256的批量大小。双向LSTM方法运行2000个epoch进行训练，批量大小为250个样本，与[14]中提出的方法相同。对于建议和双向LSTM方法中，选择在验证集上表现最好的模型作为

最终模型进行测试。

对于来自所有方法的实验，我们使用具有AMD的Linux机器

Ryzen Threadripper 2920x 12-Core processor, NVIDIA TITAN RTX GPU (24 GB memory), and 126 GB RAM.

## 7.2 Performance evaluation

In this section, we introduce the two metrics used for the evaluation of method performance. Two types of errors: maximum peak-to-peak error and RMSSD error, are extracted from original and reconstructed signals, which represent the HR and HRV errors respectively, to evaluate the reconstruction results.

### 7.2.1 Maximum peak-to-peak error

The peaks in the original signal and the reconstructed signals are first paired in time order. The pair with the maximum distance from each other is the maximum peak-to-peak error. The maximum peak-to-peak error is used to estimate the heart rate error between the reconstructed and original signals. The error is calculated as:

$$Error_{peak-to-peak} = \max(|Peaks_{reconstructed} - Peaks_{original}|) \quad (7.1)$$

### 7.2.2 RMSSD error

The root mean square of the successive peak interval difference (RMSSD) is an important HRV parameter[61]. The RMSSD error is used to estimate the HRV error between the reconstructed and original signals. The RMSSD error between reconstructed signal and ground truth is calculated as:

$$Error_{RMSSD} = |RMSSD_{reconstructed} - RMSSD_{original}| \quad (7.2)$$

锐龙 Threadripper 2920 x 12核处理器, NVIDIA TITAN RTX GPU (24 GB 内存) 和126 GB RAM。

## 7.2 绩效评价

在本节中, 我们将介绍用于评估方法的两个指标  
性能两种类型的误差: 最大峰间误差和RMSSD误差,  
从原始信号和重建信号中提取, 其表示HR,

心率变异性误差, 以评价重建结果。

### 7.2.1 最大峰间误差

原始信号和重构信号中的峰值首先在  
时间顺序彼此距离最大的一对是最大的  
峰间误差最大峰–峰误差用于估计心脏  
重构信号和原始信号之间的速率误差。误差计算如下:

$$10. \text{ Maximum } (|P_{eaksreconstructed} - P_{eaksoriginal}|) \quad (7.1)$$

### 7.2.2 RMSSD错误

连续峰值间隔差 (RMSSD) 的均方根是  
重要的HRV参数[61]。RMSSD误差用于估计HRV  
重建信号和原始信号之间的误差。之间的RMSSD误差

重建信号和地面实况计算为:

$$\text{错误RM SSD} = |RM\ SSD_{Reconstructed} - RM\ SSD_{original}| \quad (7.2)$$

## 7.3 Reconstruction results

The model performance is evaluated by three lengths of noise, including 5-second, 10-second, and 15-second. The three types of noise duration represent PPG signal distorted by short to long MAs. The reconstruction errors, including maximum peak-to-peak and RMSSD error of signals at different noise levels and lengths of noise, are presented in this section.

An example of the reconstructed PPG waveform distorted by 5-second noise at a high noise level (i.e. SNR = -8.093 dB) is illustrated in Figure 7.1. The blue, orange and red lines represent the ground truth, synthesized noisy signal, and the reconstructed signal respectively. As shown in Figure 7.1 (b), our proposed method performs the best at reconstructing PPG peaks and waveforms compared to the ground truth in blue.

### 7.3.1 5-second noise

The noisy signals distorted by 5-second noise reflect the impact of short-term MA on PPG signals. The performance of all the methods on PPG signals distorted by 5-second noise in different SNR groups is indicated in Figure 7.2. Figure 7.2 (a) shows the maximum peak-to-peak error, and Figure 7.2 (b) is the RMSSD error. The Kalman and AR, EMD and DWT, bidirectional LSTM, and the proposed method are indicated by blue, yellow, green and red lines, respectively. The quantitative values are shown in Table 7.1.

As indicated in Figure 7.2 (a), our method outperforms other baseline methods in all SNR groups with the lowest peak-to-peak error. For example, when SNR is at -25 dB, the maximum peak-to-peak error from the proposed method is 0.689 seconds, while the error from Kalman and AR method is 2.948 seconds, the EMD and DWT is 1.131 seconds, and the Bidirectional LSTM is 1.053 seconds. This indicates that the proposed method is able to estimate reliable HR with PPG distorted by 5-second

## 7.3 重建结果

模型性能通过三种长度的噪声来评估，包括5秒，10秒和15秒。三种类型的噪声持续时间代表PPG信号由短到长的MA扭曲。重建误差，包括最大在不同噪声水平和长度下信号的峰峰值和RMSSD误差

噪声，在本节中介绍。

由5秒噪声失真的重建PPG波形的示例，

图7.1中示出了高噪声电平（即 $\text{SNR} = -8.093 \text{ dB}$ ）。蓝色的，橙子线和红色线表示地面实况、合成噪声信号，分别重建信号。如图7.1 (B) 所示，我们提出的方法在重建PPG峰值和波形方面表现最佳，

蓝色的ground truth

### 7.3.1 5-第二噪声

被5秒噪声扭曲的噪声信号反映了短期MA的影响PPG信号。所有方法在PPG信号上的性能被5-不同SNR组中的第二噪声如图7.2所示。图7.2 (a) 显示最大峰间误差，图7.2 (B) 是RMSSD误差。的卡尔曼和AR，EMD和DWT，双向LSTM，以及所提出的方法分别用蓝、黄、绿色和红线表示。定量

数值见表7.1。

如图7.2 (a) 所示，我们的方法优于其他基线方法，具有最低峰峰值误差的所有SNR组。例如，当 $\text{SNR}$ 为 $-25 \text{ dB}$ ，所提出的方法的最大峰-峰误差为0.689秒，而Kalman和AR方法的误差为2.948秒，是1.131秒，双向LSTM是1.053秒。这表明所提出的方法能够估计PPG失真5秒的可靠HR

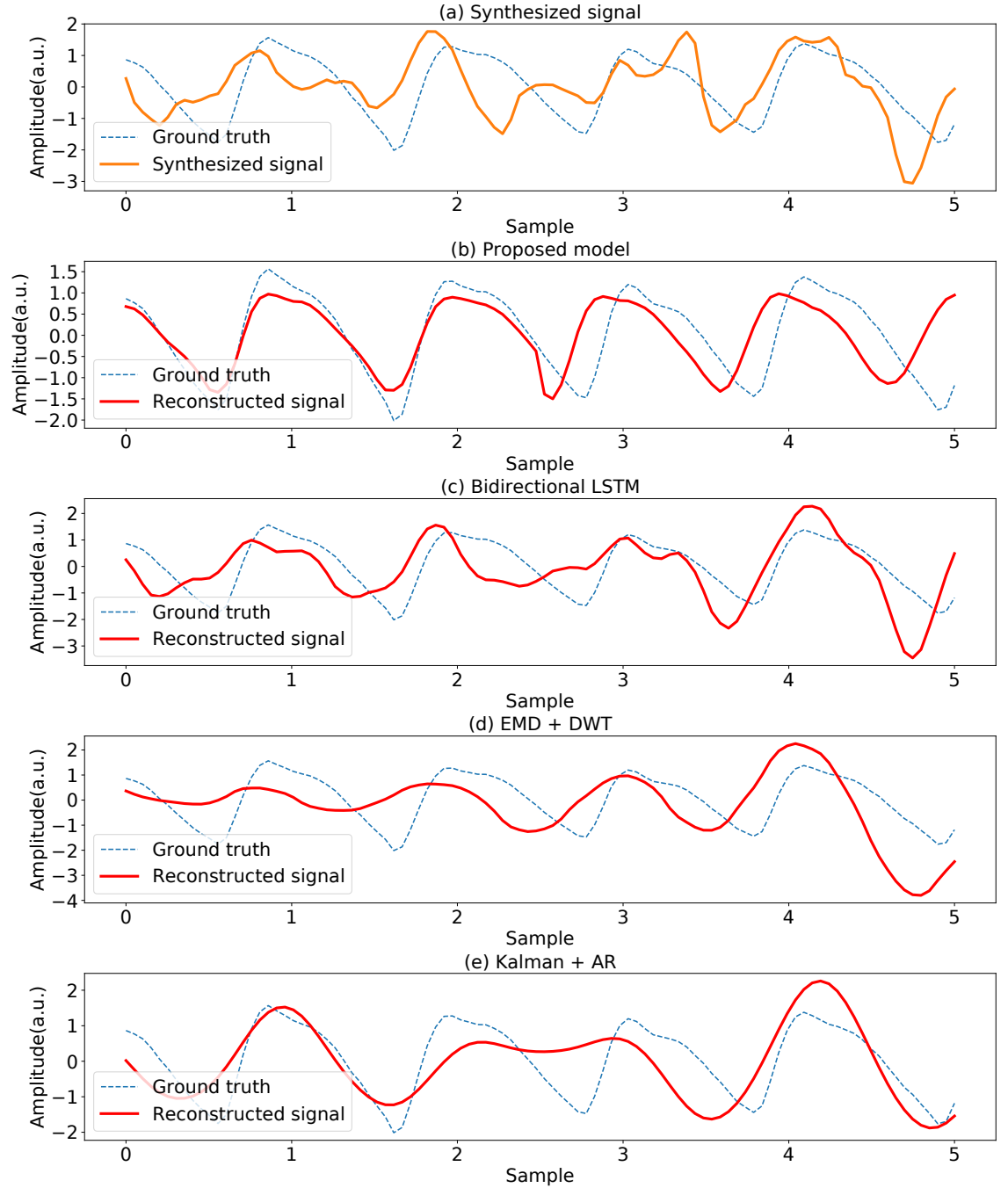


Figure 7.1: Reconstruction results from proposed method and baseline methods (SNR=-8.09 dB). Blue dotted line is the clean ground truth.(a) Synthesized signal, (b) Proposed method, (c) Bidirectional LSTM, (d) EMD and DWT, and (e) Kalman and AR.

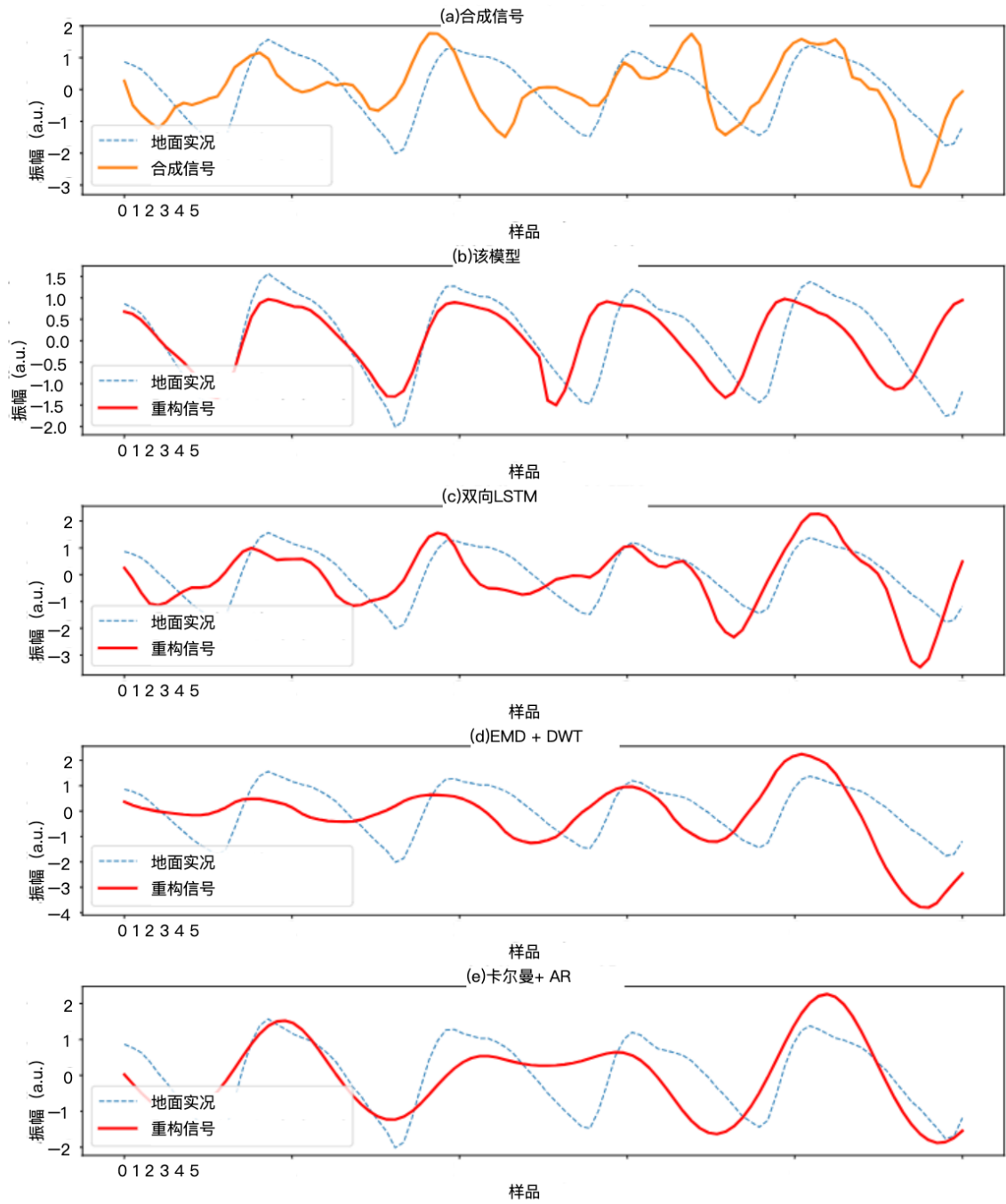


图7.1：建议方法和基线方法的重建结果

(SNR=−8.09 dB)。蓝色虚线是干净的地面真相。(a)合成信号, (b)提出的方法, (c) 双向LSTM, (d) EMD和DWT, 以及 (e) 卡尔曼和AR。

**Table 7.1: Performance of all methods on 5-second noise**

SNR (dB)	Proposed method		Kalman + AR		EMD + DWT		Bidirectional LSTM	
	P-to-P	RMSSD	P-to-P	RMSSD	P-to-P	RMSSD	P-to-P	RMSSD
-25	0.689	0.021	2.948	0.109	1.131	1.526	1.053	0.045
-20	0.599	0.018	2.045	0.080	1.090	1.095	1.052	0.045
-15	0.533	0.014	1.672	0.061	1.083	0.687	0.997	0.043
-10	0.407	0.011	1.342	0.041	1.046	0.442	0.926	0.038
-5	0.312	0.009	1.200	0.033	0.939	0.256	0.828	0.034
0	0.264	0.007	1.155	0.030	0.835	0.200	0.691	0.028
5	0.220	0.006	1.142	0.029	0.691	0.147	0.595	0.023
10	0.211	0.006	1.094	0.028	0.613	0.129	0.548	0.020
15	0.224	0.006	1.066	0.026	0.633	0.143	0.515	0.019
20	0.215	0.006	1.098	0.028	0.562	0.134	0.504	0.019
25	0.222	0.006	1.066	0.027	0.599	0.146	0.52	0.019
30	0.212	0.006	1.120	0.027	0.591	0.138	0.489	0.018

表7.1：所有方法对5秒噪声的性能

SNR (dB)	提出的方法Kalman + AR EMD + DWT双向LSTM							
	P-to-P RMSSD	P-to-P RMSSD	P-to-P RMSSD	P-to-P RMSSD	P-to-P RMSSD	P-to-P RMSSD	P-to-P RMSSD	P-to-P RMSSD
-25	0.689	0.021	2.948	0.109	1.131	1.526	1.053	0.045
-20	0.599	0.018	2.045	0.080	1.090	1.095	1.052	0.045
-15	0.533	0.014	1.672	0.061	1.083	0.687	0.997	0.043
-10	0.407	0.011	1.342	0.041	1.046	0.442	0.926	0.038
-5	0.312	0.009	1.200	0.033	0.939	0.256	0.828	0.034
0	0.264	0.007	1.155	0.030	0.835	0.200	0.691	0.028
5	0.220	0.006	1.142	0.029	0.691	0.147	0.595	0.023
10	0.211	0.006	1.094	0.028	0.613	0.129	0.548	0.020
15	0.224	0.006	1.066	0.026	0.633	0.143	0.515	0.019
20	0.215	0.006	1.098	0.028	0.562	0.134	0.504	0.019
25	0.222	0.006	1.066	0.027	0.599	0.146	0.52	0.019
30	0.212	0.006	1.120	0.027	0.591	0.138	0.489	0.018

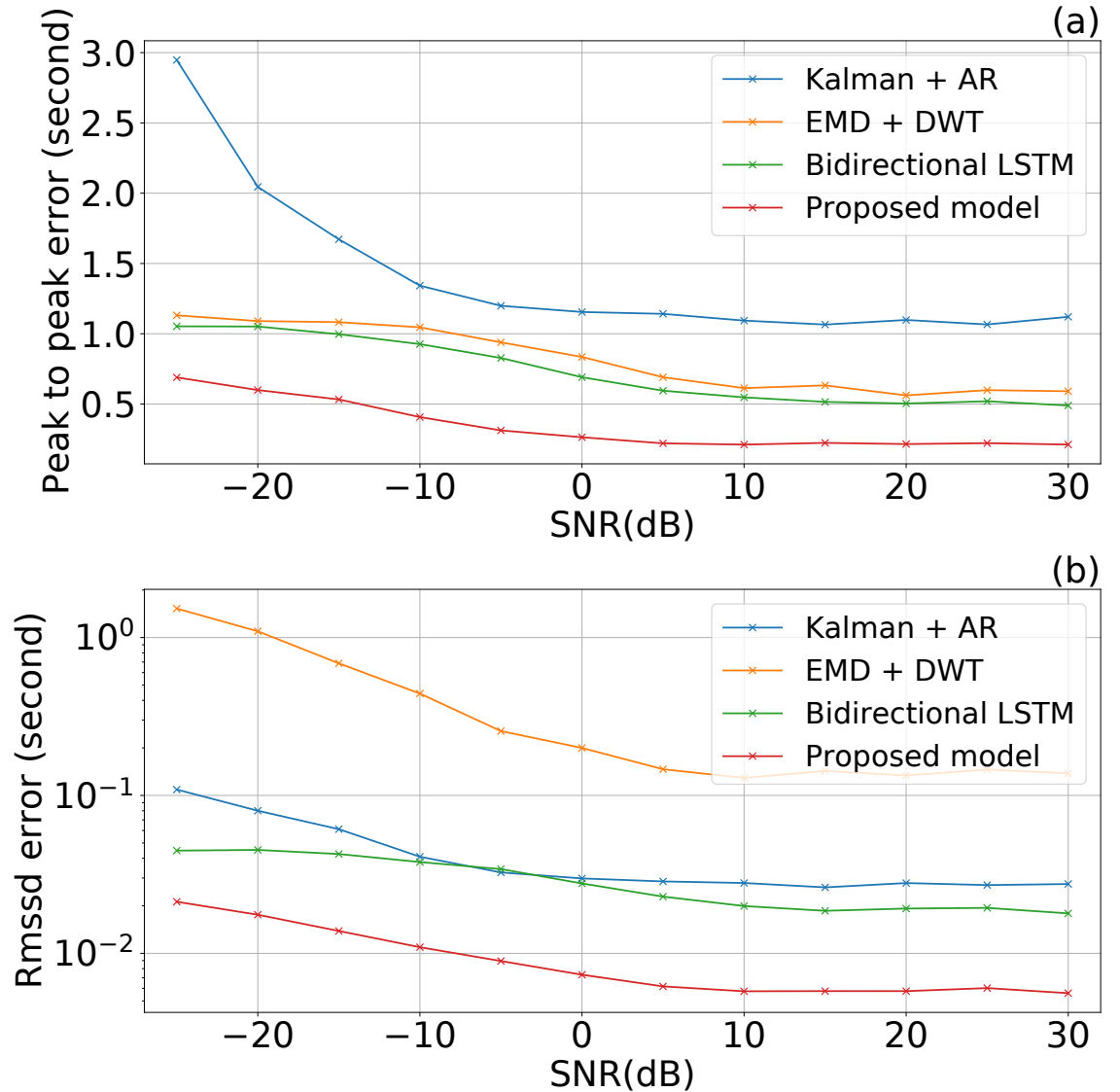


Figure 7.2: Reconstruction errors from all methods with 5-second noise. (a) Maximum peak-to-peak error, and (b) RMSSD error.

noise.

Our method also obtains the lowest RMSSD error at all noise levels. As indicated in Figure 7.2 (b), when SNR is at -25 dB, the RMSSD error from proposed method is 0.021 seconds. However, the error from Kalman and AR method is 0.109 seconds, the EMD and DWT is 1.526 seconds, and the Bidirectional LSTM is 0.045 seconds.

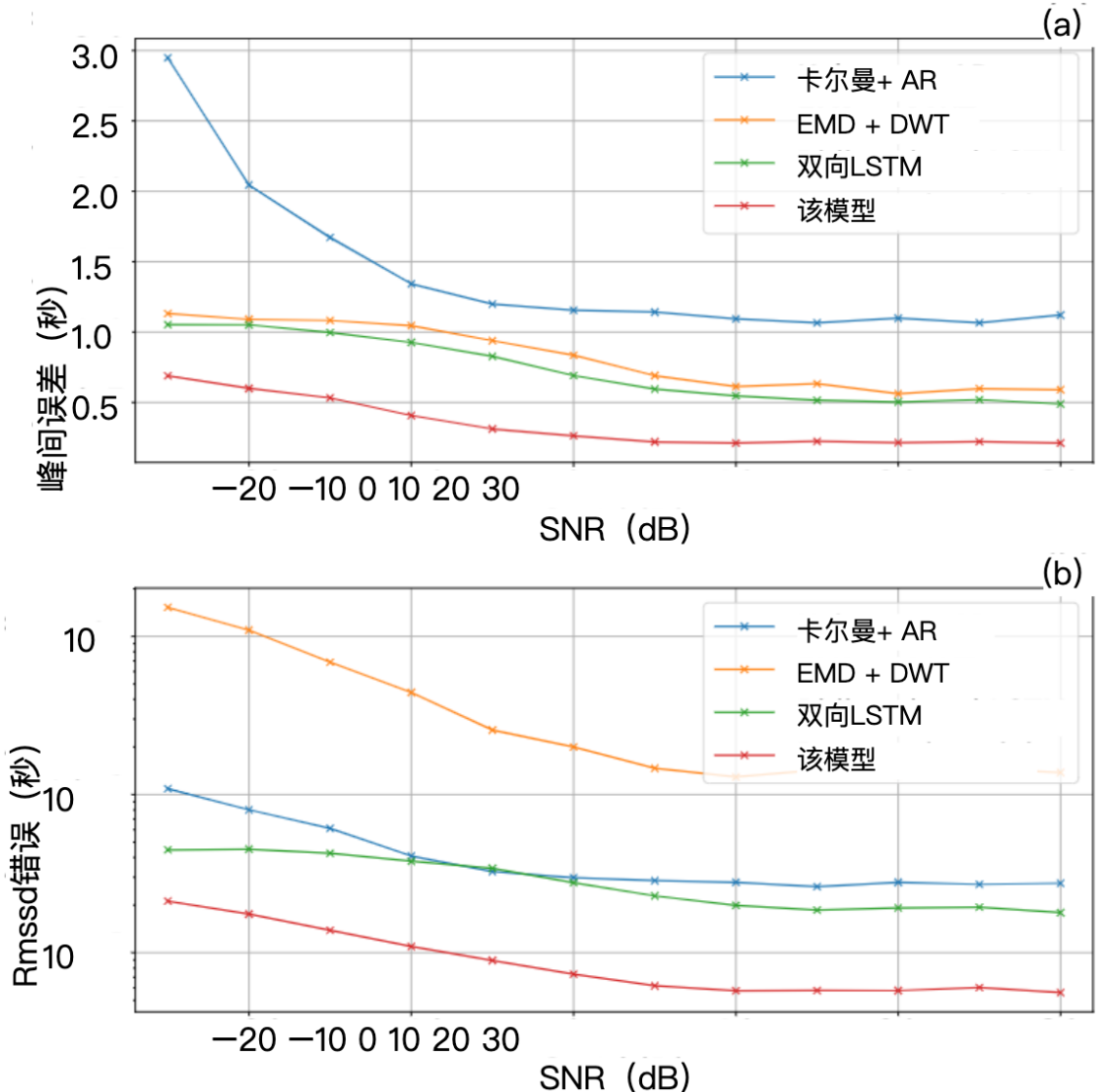


图7.2：所有方法在5秒噪声下的重建误差(a)最大-  
 $\mu$  m峰-峰误差，以及 (B) RMSSD误差。

### 噪声

我们的方法还获得了最低的RMSSD误差在所有的噪声水平。示  
 在图7.2 (B) 中，当SNR为-25 dB时，建议方法的RMSSD误差  
 0.021秒而卡尔曼和AR方法的误差为0.109秒，  
 EMD和DWT是0.1526秒，双向LSTM是0.045秒。

The results show that the proposed method can also produce reliable estimation for HRV with PPG distorted by 5-second noise.

Moreover, the proposed method is more robust to low SNR signals. As shown in Figure 7.2, all methods except Kalman and AR obtain a maximum peak-to-peak error less than 1.0 seconds when the SNR is at 30 dB. However, the errors increase when the SNR values decrease. For instance, when the SNR values drop from 30dB to -25dB, the peak-to-peak error from the proposed method only increases from 0.212 to 0.684 seconds, while such increase is higher in Kalman and AR, EMD and DWT, and Bidirectional LSTM method, with values of 1.120 to 2.948 seconds, 0.591 to 1.131 seconds, and 0.489 to 1.053 seconds, respectively.

Similarly, for RMSSD errors, such increase from the proposed method is still the smallest. When SNR decreases from 30 dB to -25 dB, the RMSSD error from proposed method only increases from 0.006 to 0.021 seconds. However, the EMD and DWT, which has the highest RMSSD error, increases from 0.138 to 1.526 seconds. The RMSSD error increases of Kalman and AR method is 0.027 to 0.109 seconds, and Bidirectional LSTM method is 0.018 to 0.045 seconds.

For signals distorted by short-term MAs, the HRV parameters are more affected than the HR parameters. However, Our method obtains the lowest RMSSD errors in all SNR groups. At the same time, when SNR decreases, the increase of RMSSD error from the proposed method is the smallest. In addition, the proposed method also obtains the lowest peak-to-peak error in all SNR groups. Therefore, our method is robust to high noise level, and can produce reliable reconstruction estimation for both HR and HRV for PPG distorted by short-term MAs.

### 7.3.2 10-second noise

The noisy signals distorted by 10-second noise evaluate the model performance of increased length of MA to PPG signals. The performance of all the methods on PPG

结果表明，该方法也可以产生可靠的估计，  
心率变异性（PPG）被5秒噪声扭曲。

此外，所提出的方法是更强大的低信噪比信号。如图所示

在图7.2中，除了卡尔曼法和AR法之外，所有的方法都能得到最大峰间值  
SNR为30 dB时，误差小于1.0秒。然而，误差增加  
当SNR值降低时。例如，当SNR值从30 dB  
到-25dB，所提出的方法的峰峰值误差仅从  
0.212至0.684秒，而这种增加在卡尔曼和AR、EMD和  
DWT和双向LSTM方法，值为1.120到2.948秒，0.591

1.131秒和0.489至1.053秒。

类似地，对于RMSSD误差，所提出的方法的这种增加仍然是  
最小的当SNR从30 dB降低到-25 dB时，  
所提出的方法仅从0.006增加到0.021秒。然而，EMD和  
RMSSD误差最高的DWT从0.138秒增加到1.526秒。  
卡尔曼和AR方法的RMSSD误差增加为0.027 ~ 0.109秒，

双向LSTM方法的时间为0.018到0.045秒。

对于受短时MA畸变的信号，HRV参数受影响更大  
HR参数。然而，我们的方法获得了最低的RMSSD误差  
在所有SNR组中。同时，当信噪比降低时，  
所提出的方法的误差是最小的。此外，所提出的方法  
在所有SNR组中也获得最低的峰峰值误差。因此，我们的方法  
对高噪声水平是鲁棒，且可以产生可靠的重建估计，

PPG的HR和HRV均被短期MA扭曲。

### 7.3.2 10-第二噪声

由10秒噪声失真的噪声信号评估模型性能，  
MA到PPG信号的长度增加。所有方法在PPG上的性能

**Table 7.2: Performance of all methods on 10-second noise**

SNR (dB)	Proposed method		Kalman + AR		EMD + DWT		Bidirectional LSTM	
	P-to-P	RMSSD	P-to-P	RMSSD	P-to-P	RMSSD	P-to-P	RMSSD
-25	1.352	0.048	4.965	0.282	2.385	2.540	2.041	0.082
-20	1.187	0.039	4.368	0.228	2.340	2.214	1.986	0.080
-15	0.986	0.030	3.413	0.150	2.368	1.687	1.879	0.075
-10	0.790	0.023	2.796	0.098	2.164	0.994	1.816	0.070
-5	0.610	0.017	2.358	0.071	1.897	0.510	1.558	0.059
0	0.448	0.012	2.193	0.060	1.595	0.280	1.239	0.046
5	0.365	0.009	2.159	0.058	1.357	0.186	1.011	0.035
10	0.355	0.009	2.224	0.059	1.209	0.166	0.878	0.030
15	0.319	0.008	2.079	0.055	1.084	0.160	0.804	0.027
20	0.332	0.008	2.150	0.058	1.091	0.162	0.813	0.028
25	0.305	0.008	2.022	0.054	1.070	0.150	0.812	0.027
30	0.350	0.009	2.164	0.059	1.094	0.168	0.796	0.026

signals distorted by 10-second noise in different SNR groups is indicated in Figure 7.3. Figure 7.3 (a) shows the maximum peak-to-peak errors, and Figure 7.3 (b) is the RMSSD errors from all SNR groups. The Kalman and AR, EMD and DWT, bidirectional LSTM and proposed method are indicated by blue, yellow, green and red lines, respectively. The quantitative values are shown in Table 7.2

As indicated in Figure 7.3 (a), the proposed method still performs the best in all SNR groups compared to other baseline methods when PPG signals are distorted by 10-second noise. The peak-to-peak errors from the proposed method are the lowest at all noise levels. For example, when SNR is at -25 dB, the maximum peak-to-peak error from the proposed method is 1.352 seconds, while the error from Kalman and AR method is 4.965 seconds, the EMD and DWT is 2.385 seconds, and the Bidirectional LSTM is 2.041 seconds. This indicates that the proposed method is able to estimate reliable HR with PPG distorted by 10-second noise.

表7.2：所有方法对10秒噪声的性能

SNR (dB)	提出的方法Kalman + AR EMD + DWT双向LSTM							
	P-to-P RMSSD	P-to-P RMSSD	P-to-P RMSSD	P-to-P RMSSD	P-to-P RMSSD	P-to-P RMSSD	P-to-P RMSSD	P-to-P RMSSD
-25	1.352	0.048	4.965	0.282	2.385	2.540	2.041	0.082
-20	1.187	0.039	4.368	0.228	2.340	2.214	1.986	0.080
-15	0.986	0.030	3.413	0.150	2.368	1.687	1.879	0.075
-10	0.790	0.023	2.796	0.098	2.164	0.994	1.816	0.070
-5	0.610	0.017	2.358	0.071	1.897	0.510	1.558	0.059
0	0.448	0.012	2.193	0.060	1.595	0.280	1.239	0.046
5	0.365	0.009	2.159	0.058	1.357	0.186	1.011	0.035
10	0.355	0.009	2.224	0.059	1.209	0.166	0.878	0.030
15	0.319	0.008	2.079	0.055	1.084	0.160	0.804	0.027
20	0.332	0.008	2.150	0.058	1.091	0.162	0.813	0.028
25	0.305	0.008	2.022	0.054	1.070	0.150	0.812	0.027
30	0.350	0.009	2.164	0.059	1.094	0.168	0.796	0.026

在不同SNR组中，10秒噪声导致的信号失真如图所示

7.3.图7.3 (a) 显示了最大峰间误差，图7.3 (B) 为来自所有SNR组的RMSSD错误。卡尔曼和AR，EMD和DWT，双向LSTM和所提出的方法由蓝色、黄色、绿色表示，

红线，分别。定量值见表7.2

如图7.3 (a) 所示，所提出的方法仍然是所有方法中性能最好的当PPG信号失真时，SNR组与其他基线方法相比，10–第二噪音所提出的方法的峰–峰误差是最低的在所有的噪音水平。例如，当SNR为-25 dB时，最大峰–峰值比为-25 dB。所提出的方法的峰值误差为1.352秒，而卡尔曼滤波器的误差为1.352秒。AR方法为4.965秒，EMD和DWT为2.385秒，双向LSTM是2.041秒。这表明，该方法是

能够估计可靠的HR，PPG被10秒噪音扭曲。

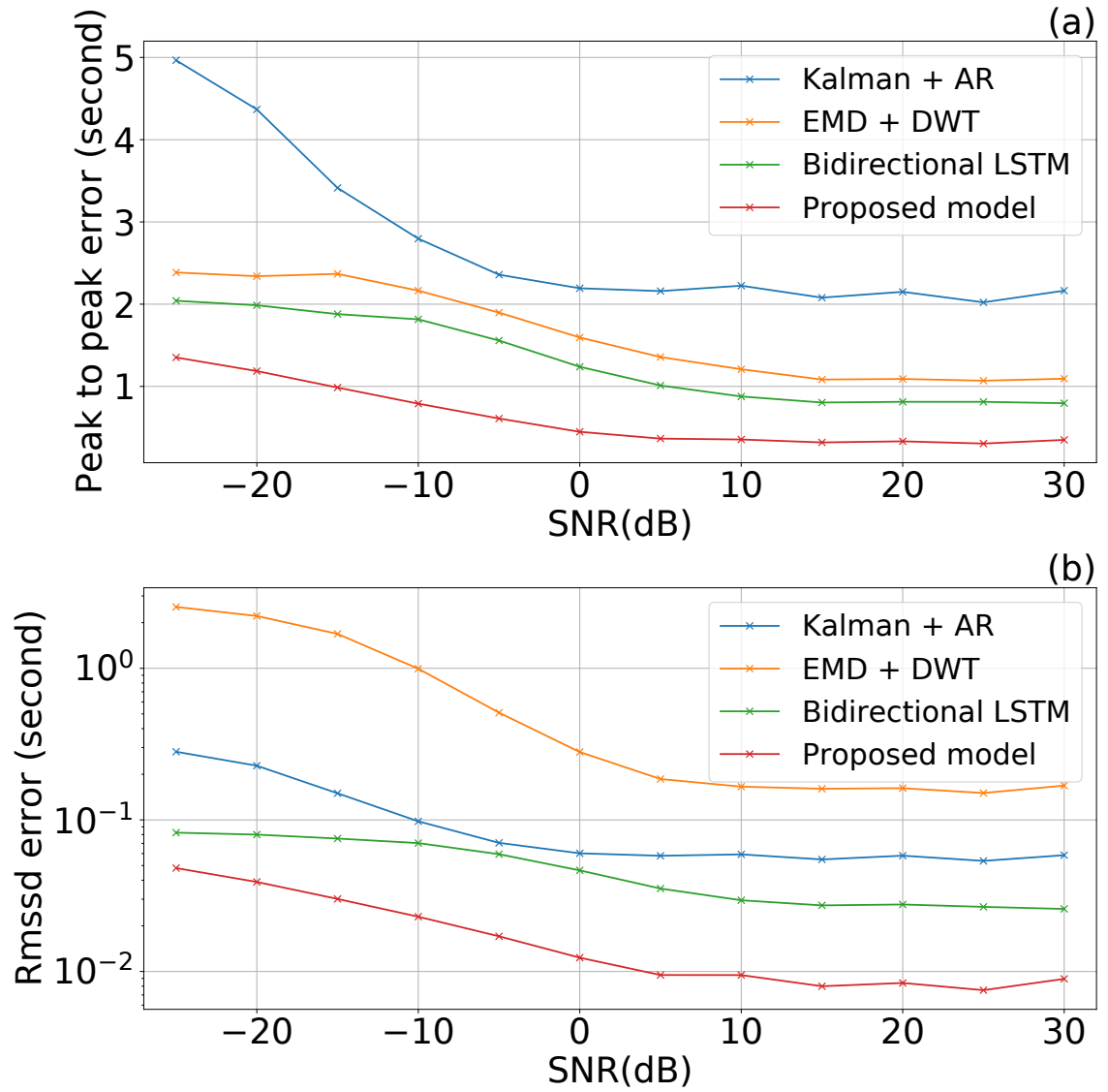


Figure 7.3: Reconstruction errors from all methods with 10-second noise. (a) Maximum peak-to-peak error, and (b) RMSSD error.

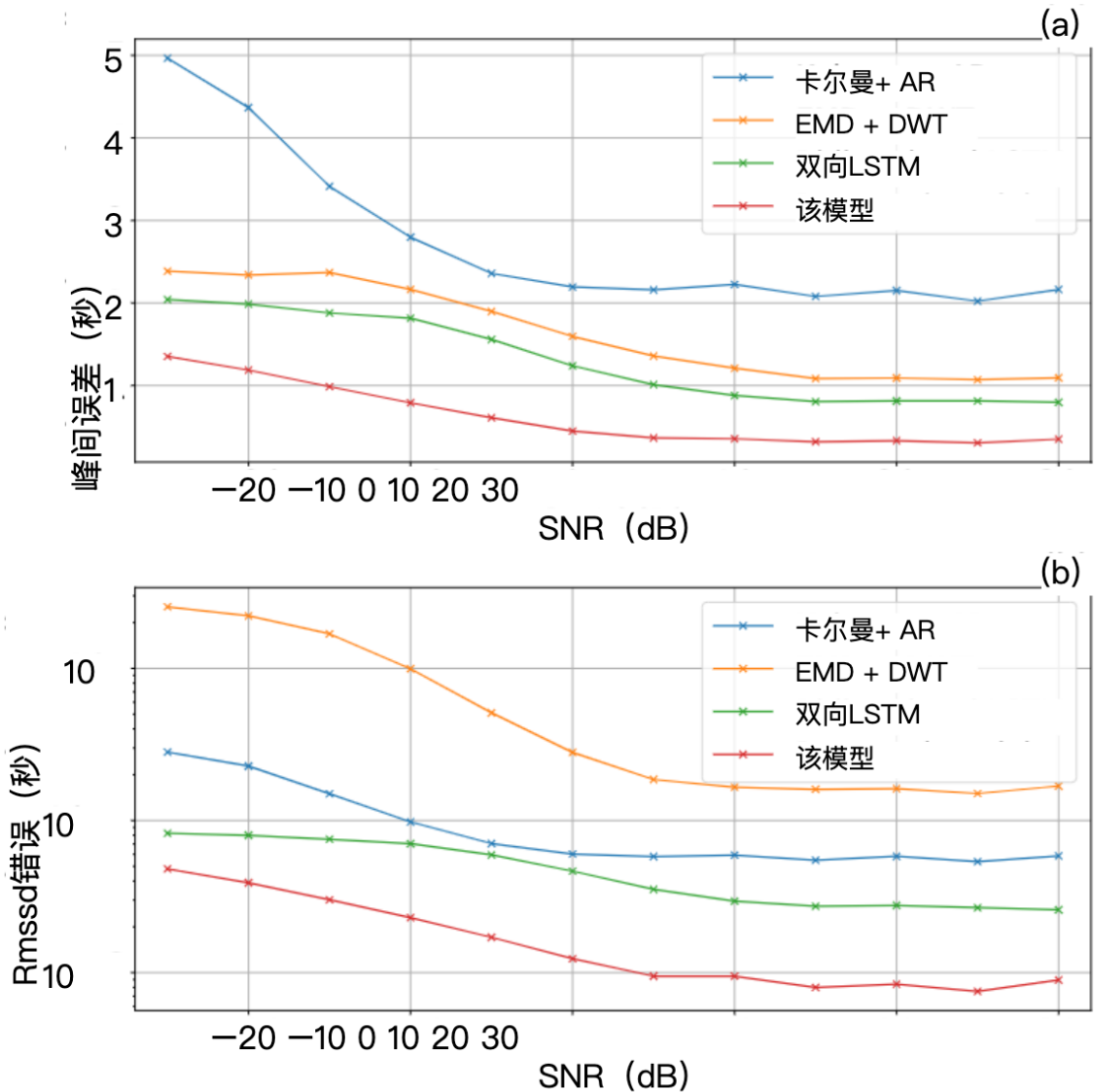


图7.3：所有方法在10秒噪声下的重建误差(a)麦克斯  
最大峰-峰误差，和 (B) RMSSD误差。

The RMSSD errors from our proposed method in 10-second noise case are also the lowest at all noise levels. As indicated in Figure 7.3 (b), when SNR is at -25 dB, the RMSSD error from proposed method is 0.048 seconds. However, the error from Kalman and AR method is 0.282 seconds, the EMD and DWT is 2.540 seconds, and the Bidirectional LSTM is 0.082 seconds. The results show that the proposed method can also produce reliable estimation for HRV with PPG distorted by 10-second noise.

Similar to the 5-second case, the proposed method shows robustness to signals with low SNR values. As shown in Figure 7.3, all methods except Kalman and AR obtain a maximum peak-to-peak error less than 2.0 seconds when the SNR is at 30 dB. However, the errors increase when the SNR values decrease. For instance, when the SNR values drop from 30dB to -25dB, the peak-to-peak error from the proposed method only increases from 0.350 to 1.352 seconds, while such increase is higher in Kalman and AR, EMD and DWT, and Bidirectional LSTM method, with values of 2.164 to 4.965 seconds, 1.094 to 2.385 seconds, and 0.796 to 2.041 seconds, respectively.

For RMSSD errors in 10-second noise length case, such increase from the proposed method is still the smallest. When SNR decreases from 30 dB to -25 dB, the RMSSD error from the proposed method only increases from 0.009 to 0.048 seconds. However, the EMD and DWT increases from 0.168 to 2.540 seconds. The RMSSD error increases of Kalman and AR method is 0.059 to 0.282 seconds, and Bidirectional LSTM method is 0.026 to 0.082 seconds.

When the noise length increases, the effect of noise on both HR and HRV also increases. However, our method still outperforms all state-of-the-art methods with the lowest peak-to-peak and RMSSD errors in all SNR groups. Moreover, when the reconstruction errors increase with the noise level, our method has the smallest increase in the reconstruction error for HR and HRV. Consequently, our method

在10秒噪声情况下，我们提出的方法的RMSSD误差也是在所有噪音级别中最低。如图7.3 (B) 所示，当SNR为-25 dB时，所提出的方法的RMSSD误差为0.048秒。但Kalman和AR方法的误差为0.282秒，EMD和DWT为2.540 Bidirectional LSTM是0.082秒。结果表明该方法也可以对PPG失真的HRV产生可靠的估计

### 10秒噪音

与5秒的情况类似，所提出的方法对信号具有鲁棒性低SNR值。如图7.3所示，除了卡尔曼和AR之外，当SNR为时，获得小于2.0秒的最大峰峰值误差30分贝。然而，当SNR值减小时，误差增大。比如说，当SNR值从30 dB下降到-25dB时，所提出的方法仅从0.350秒增加到1.352秒，而这种增加是在Kalman和AR、EMD和DWT以及Bidirectional LSTM方法中具有较高的性能，2.164至4.965秒、1.094至2.385秒和0.796至2.041秒的值，

分别

对于10秒噪声长度情况下的RMSSD错误，从亲噪声的增加，提出的方法仍然是最小的。当SNR从30 dB降低到-25 dB时，该方法的RMSSD误差仅从0.009增加到0.048秒然而，EMD和DWT从0.168增加到2.540秒。的卡尔曼和AR方法的RMSSD误差增加为0.059 ~ 0.282秒，

双向LSTM方法是0.026到0.082秒。

随着噪声长度的增加，噪声对心率和心率变异性的影响也逐渐减弱，增大然而，我们的方法仍然优于所有最先进的方法，所有SNR组中的最低峰峰值和RMSSD误差。此外，当重建误差随着噪声水平的增加而增加，我们的方法具有最小的HR和HRV的重建误差增加。因此，我们的方法

**Table 7.3: Performance of all methods on 15-second noise**

SNR (dB)	Proposed method		Kalman + AR		EMD + DWT		Bidirectional LSTM	
	P-to-P	RMSSD	P-to-P	RMSSD	P-to-P	RMSSD	P-to-P	RMSSD
-25	1.821	0.067	7.772	0.567	3.647	1.476	2.848	0.112
-20	1.647	0.059	6.479	0.420	3.655	1.441	2.818	0.109
-15	1.374	0.047	5.303	0.290	3.565	1.202	2.774	0.104
-10	1.019	0.031	4.298	0.173	3.320	0.778	2.513	0.094
-5	0.723	0.021	3.502	0.113	2.975	0.480	2.255	0.082
0	0.499	0.013	3.263	0.094	2.425	0.285	1.727	0.063
5	0.389	0.009	3.367	0.094	1.821	0.170	1.400	0.048
10	0.350	0.008	3.190	0.088	1.693	0.163	1.124	0.036
15	0.324	0.007	3.077	0.086	1.437	0.135	1.076	0.035
20	0.328	0.007	3.086	0.086	1.469	0.158	1.042	0.034
25	0.328	0.007	3.298	0.093	1.530	0.153	0.996	0.033
30	0.312	0.007	3.134	0.088	1.543	0.165	0.998	0.031

is still robust to low SNRs when noise length increases, and can produce reliable estimation for HR and HRV in signals distorted by 10-second MAs.

### 7.3.3 15-second noise

The noisy signals distorted by 15-second noise are used to evaluate the model performance of PPG distorted by longer MAs (compared to the MAs evaluated earlier). The performance of all the methods on PPG signals distorted by 15-second noise in different SNR groups is indicated in Figure 7.4. Figure 7.4 (a) shows the maximum peak-to-peak, Figure 7.4 (b) is the RMSSD error. The Kalman and AR, EMD and DWT, bidirectional LSTM and the proposed method are indicated by blue, yellow, green and red lines, respectively. The quantitative values are shown in Table 7.3

As indicated in Figure 7.4 (a), the proposed method outperforms other state-of-the-art methods in all SNR groups when PPG signals are distorted by 15-second

表7.3：所有方法对15秒噪声的性能

SNR (dB)	提出的方法Kalman + AR EMD + DWT双向LSTM							
	P-to-P RMSSD	P-to-P RMSSD	P-to-P RMSSD	P-to-P RMSSD	P-to-P RMSSD	P-to-P RMSSD	P-to-P RMSSD	P-to-P RMSSD
-25	1.821	0.067	7.772	0.567	3.647	1.476	2.848	0.112
-20	1.647	0.059	6.479	0.420	3.655	1.441	2.818	0.109
-15	1.374	0.047	5.303	0.290	3.565	1.202	2.774	0.104
-10	1.019	0.031	4.298	0.173	3.320	0.778	2.513	0.094
-5	0.723	0.021	3.502	0.113	2.975	0.480	2.255	0.082
0	0.499	0.013	3.263	0.094	2.425	0.285	1.727	0.063
5	0.389	0.009	3.367	0.094	1.821	0.170	1.400	0.048
10	0.350	0.008	3.190	0.088	1.693	0.163	1.124	0.036
15	0.324	0.007	3.077	0.086	1.437	0.135	1.076	0.035
20	0.328	0.007	3.086	0.086	1.469	0.158	1.042	0.034
25	0.328	0.007	3.298	0.093	1.530	0.153	0.996	0.033
30	0.312	0.007	3.134	0.088	1.543	0.165	0.998	0.031

当噪声长度增加时，对于低SNR仍然是鲁棒的，并且可以产生可靠的估计10秒MA失真信号中的HR和HRV。

### 7.3.3 15-第二噪声

用15秒噪声失真的噪声信号来评估模型，较长MA导致PPG失真（与之前评价的MA相比）。所有方法对15秒噪声失真的PPG信号的性能，不同的SNR组如图7.4所示。图7.4 (a) 显示了最大值图7.4 (B) 中的峰-峰误差是RMSSD误差。卡尔曼和AR, EMD和DWT、双向LSTM和所提出的方法由蓝色、黄色

分别是绿色和红色线。定量值见表7.3

如图7.4 (a) 所示，所提出的方法优于其他状态-当PPG信号失真15秒时，所有SNR组中的最先进方法

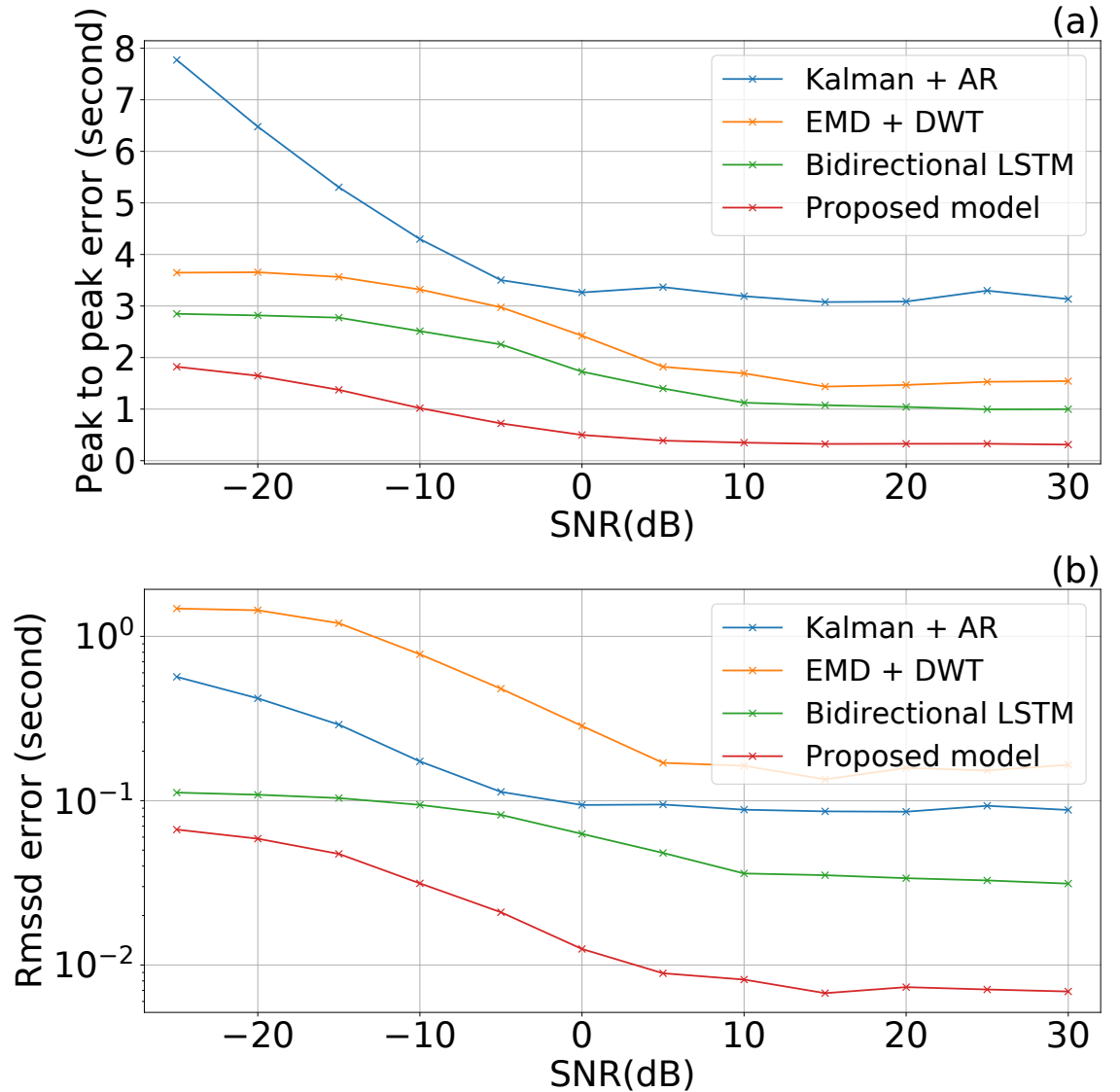


Figure 7.4: Reconstruction errors from all methods with 15-second noise. (a) Maximum peak-to-peak error, and (b) RMSSD error.

noise. Our proposed method achieves the lowest value of peak-to-peak error at all noise levels. For example, when SNR is at -25 dB, the maximum peak-to-peak error from the proposed method is 1.821 seconds, while the error from Kalman and AR method is 7.772 seconds, the EMD and DWT is 3.647 seconds, and the Bidirectional LSTM is 2.848 seconds. This indicates that the proposed method is able to estimate

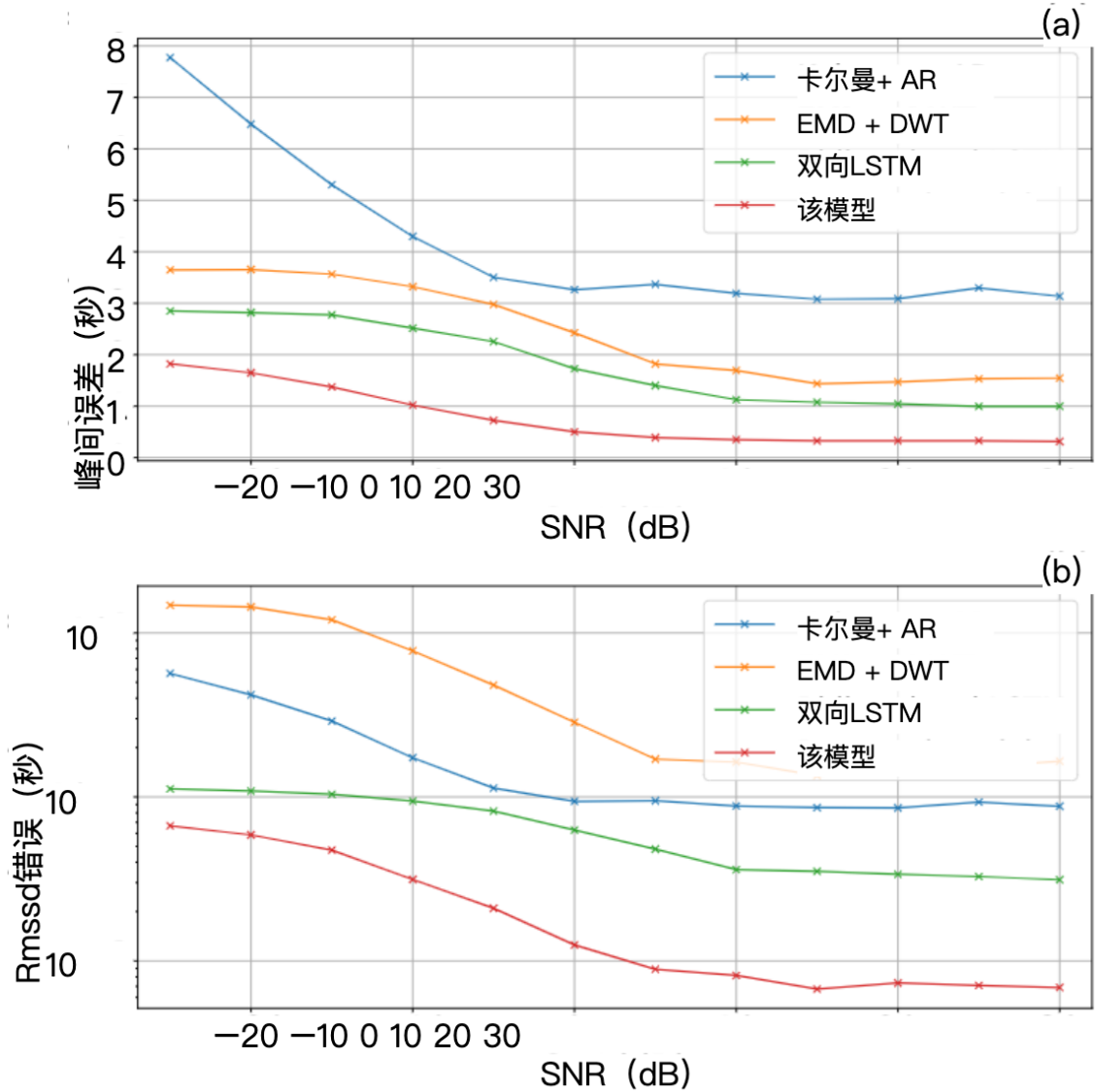


图7.4：所有方法在15秒噪声下的重建误差(a)麦克斯

最大峰-峰误差，和 (B) RMSSD误差。

噪声我们提出的方法达到了最低值的峰峰值误差在所有 noise levels. 例如，当SNR为-25 dB时，该方法的误差为1.821秒，而卡尔曼和AR方法的误差为1.821秒，方法是7.772秒，EMD和DWT是3.647秒，双向 LSTM是2.848秒。这表明所提出的方法能够估计

reliable HR with PPG distorted by 15-second noise.

The proposed method also achieves the lowest value of RMSSD error in all SNR groups. As indicated in Figure 7.4 (b), when SNR is at -25 dB, the RMSSD error from the proposed method is 0.067 seconds, while the error from Kalman and AR method is 0.567 seconds, the EMD and DWT is 1.476 seconds, and the Bidirectional LSTM is 0.112 seconds. This indicates that the proposed method is able to estimate reliable HRV with PPG distorted by 15-second noise.

Similar to previous noise length cases, the proposed method shows robustness to signals with low SNR values. As shown in Figure 7.3, all methods except Kalman and AR obtain a maximum peak-to-peak error less than 2.0 seconds when the SNR is at 30 dB. However, the errors increase when the SNR values decrease. For instance, when the SNR values drop from 30dB to -25dB, the peak-to-peak error from the proposed method only increases from 0.312 to 1.821 seconds, while such increase is higher in Kalman and AR, EMD and DWT, and Bidirectional LSTM method, with values of 3.134 to 7.772 seconds, 1.543 to 3.647 seconds, and 0.998 to 2.848 seconds, respectively.

For RMSSD errors in signals with 15-second noise case, such increase from the proposed method is still the smallest. When SNR decreases from 30 dB to -25 dB, the RMSSD error from the proposed method only increases from 0.007 to 0.067 seconds. However, the EMD and DWT, increases from 0.165 to 1.476 seconds. The RMSSD error increases of Kalman and AR method is 0.088 to 0.567 seconds, and Bidirectional LSTM method is 0.031 to 0.112 seconds.

When the PPG signals are distorted by long MAs, the MAs have a significant impact on both HR and HRV. However, our method still outperforms the baseline methods with the lowest peak-to-peak and RMSSD errors. In addition, when the peak-to-peak and RMSSD errors increase as the SNR values decrease, our method obtains the smallest value for such increase of error in signals distorted by 15-second

可靠的HR, PPG被15秒的噪音扭曲。

该方法还实现了在所有信噪比下RMSSD误差的最小值

组如图7.4 (B) 所示, 当SNR为-25 dB时, RMSSD误差  
该方法的误差为0.067秒, 而卡尔曼和AR方法的误差为0.067秒,  
方法是0.567秒, EMD和DWT是1.476秒, 双向  
LSTM是0.112秒。这表明所提出的方法能够估计

可靠的心率变异性, PPG被15秒的噪音扭曲。

类似于以前的噪声长度的情况下, 所提出的方法显示出鲁棒性,  
低SNR值的信号。如图7.3所示, 除卡尔曼滤波外,  
和AR获得小于2.0秒的最大峰-峰误差,  
在30分贝。然而, 当SNR值减小时, 误差增大。比如说,  
当SNR值从30 dB下降到-25dB时,  
所提出的方法仅从0.312增加到1.821秒, 而这种增加是  
在Kalman和AR、EMD和DWT以及Bidirectional LSTM方法中具有较高的性能,  
3.134至7.772秒、1.543至3.647秒和0.998至2.848秒的值,

分别

对于具有15秒噪声情况的信号中的RMSSD误差,

提出的方法仍然是最小的。当SNR从30 dB降低到-25 dB时,  
该方法的RMSSD误差仅从0.007增加到0.067  
秒然而, EMD和DWT从0.165增加到1.476秒。的  
卡尔曼和AR方法的RMSSD误差增加为0.088 ~ 0.567秒,

双向LSTM方法是0.031到0.112秒。

当PPG信号被长MA失真时, MA具有显著的

影响HR和HRV。然而, 我们的方法仍然优于基线  
具有最低峰间误差和RMSSD误差的方法。此外, 当  
峰峰值和RMSSD误差随着SNR值的降低而增加, 我们的方法  
在失真15秒的信号中获得误差增加的最小值

noise. Therefore, our methods show robustness to high noise level and can produce reliable estimation for both HR and HRV in signals distorted by long MAs.

## 7.4 Impact of Noise Duration

In addition to the robustness of low SNR level discussed above, our method also shows a better performance to longer noise duration for estimating HR and HRV. We take the examples from the highest (30 dB) and lowest (-25 dB) SNR groups to clarify the problem. The maximum peak-to-peak error increases when the noise length increases. With our proposed method, such increase is the smallest compared to all baseline methods.

In -25 dB SNR, the maximum peak-to-peak error from the proposed method increases from 0.689 to 1.821 seconds, when the noise duration increases from 5 seconds to 15 seconds. However, the maximum peak-to-peak error from Kalman and AR method increases from 2.948 to 7.772 seconds, the EMD and DWT increases from 1.131 to 3.647 seconds, and the Bidirectional LSTM increases from 1.053 to 2.848 seconds.

In 30 dB SNR, the maximum peak-to-peak error from the proposed method increases from 0.212 to 0.312 seconds, when the noise duration increases from 5 seconds to 15 seconds. However, the maximum peak-to-peak error from Kalman and AR method increases from 1.120 to 3.134 seconds, the EMD and DWT increases from 0.591 to 1.543 seconds, and the Bidirectional LSTM increases from 0.489 to 0.998 seconds. Therefore, the proposed method is also robust to longer noise length.

噪声因此，我们的方法对高噪声水平具有鲁棒性，并且可以产生可靠的估计HR和HRV的信号失真的长MA。

## 7.4 噪音持续时间的影响

除了上面讨论的低SNR水平的鲁棒性之外，我们的方法还显示出更好的性能，以较长的噪音持续时间估计HR和HRV。我们从最高（30 dB）和最低（-25 dB）SNR组中选取示例来澄清问题。当噪音增大时，长度增加。与我们提出的方法相比，这种增加是最小的。

所有基线方法。

在-25 dB SNR下，所提出的方法的最大峰峰值误差当噪音持续时间从5秒增加到1.821秒时，秒到15秒。然而，来自卡尔曼的最大峰间误差和AR方法从2.948秒增加到7.772秒，EMD和DWT增加从1.131秒增加到3.647秒，双向LSTM从1.053秒增加到2.848秒。在30 dB SNR时，所提出的方法的最大峰峰值误差当噪音持续时间从5秒增加到0.212秒时，秒到15秒。然而，来自卡尔曼的最大峰间误差和AR方法从1.120秒增加到3.134秒，EMD和DWT增加从0.591秒增加到1.543秒，双向LSTM从0.489秒增加到

0.998秒因此，所提出的方法对较长的噪音长度也是鲁棒的。

## 8 Conclusion

In this thesis, we proposed a GAN-based method to reconstruct PPG signals distorted by real-world motion artifacts.

The proposed method was trained with clean PPG signals and reconstructed noisy signals using both current noisy signal, and the prediction based on previous clean PPG samples. The proposed method thus leveraged the temporal information in both current and proceeding data points, and enabled the reconstruction of PPG signals at high noise level. For preparing the training, validation and test dataset, the raw PPG signals were filtered and sectioned into 30-second segments. Then the quality of the signals is assessed to obtain the clean and distorted PPG signals.

A noisy test dataset was generated to evaluate the performance of our proposed and state-of-the-art methods in the literature. The test dataset contained noisy PPG signals corrupted by motion artifacts collected in daily life. The noisy segments in the test dataset were generated at different noise levels and noise duration.

The proposed method was compared with three other state-of-the-art PPG reconstruction methods in the literature, including a time-series, a signal decomposition and a deep-learning based method. All methods were evaluated by extracting two types of errors: maximum peak-to-peak error and RMSSD error, which represent the HR and HRV errors, respectively.

Our method performed the best at all noise levels with different noise lengths and produced the lowest values of the two types of error. The results indicated

## 8结论

在这篇论文中，我们提出了一种基于GAN的方法来重建PPG信号，  
被真实世界的运动伪影所折磨

所提出的方法是用干净的PPG信号训练和重建的  
噪声信号，其使用当前噪声信号和基于先前噪声信号的预测两者。  
清洁PPG样品。因此，所提出的方法利用了时间信息  
在当前和正在进行的数据点，并使PPG的重建  
高噪声水平的信号。为了准备训练、验证和测试数据集，  
过滤原始PPG信号并将其分成30秒的片段。则

评估信号的质量以获得干净的和失真的PPG信号。

一个嘈杂的测试数据集，以评估我们提出的性能  
和最先进的方法。测试数据集包含噪声PPG  
被日常生活中收集的运动伪影破坏的信号。噪音片段，

在不同的噪声水平和噪声持续时间下生成测试数据集。

将所提出的方法与其他三种最先进的PPG重建进行了比较，  
结构方法的文献，包括时间序列，信号分解  
和基于深度学习的方法。所有方法均通过提取两种  
误差类型：最大峰间误差和RMSSD误差，代表

HR和HRV误差。

我们的方法在不同噪声长度的所有噪声水平下表现最好  
并产生两种类型的误差中的最低值。结果表明

that our method was effective to reconstruct noisy PPG signals distorted by real-world motion artifacts with low SNR values and long noise duration. The proposed method could consequently provide reliable estimation for both HR and HRV.

我们的方法可以有效地重建被真实的失真的噪声PPG信号，  
低SNR值和长噪声持续时间的世界运动伪影。拟议

因此，方法可以提供可靠的估计HR和HRV。

# References

- [1] D. Castaneda, A. Esparza, M. Ghamari, C. Soltanpur, and H. Nazeran, "A review on wearable photoplethysmography sensors and their potential future applications in health care", *International journal of biosensors & bioelectronics*, vol. 4, no. 4, p. 195, 2018.
- [2] P. Renevey, R. Delgado-Gonzalo, A. Lemkaddem, *et al.*, "Optical wrist-worn device for sleep monitoring", in *EMBEC & NBC 2017*, Springer, 2017, pp. 615–618.
- [3] C. El-Hajj and P. Kyriacou, "Cuffless blood pressure estimation from ppg signals and its derivatives using deep learning models", *Biomedical Signal Processing and Control*, vol. 70, p. 102984, 2021.
- [4] L. M. Eerikäinen, A. G. Bonomi, F. Schipper, *et al.*, "Comparison between electrocardiogram-and photoplethysmogram-derived features for atrial fibrillation detection in free-living conditions", *Physiological measurement*, vol. 39, no. 8, p. 084001, 2018.
- [5] J. Kim, T. Lee, J. Kim, and H. Ko, "Ambient light cancellation in photoplethysmogram application using alternating sampling and charge redistribution technique", in *2015 37th Annual International Conference of the IEEE Engineering in Medicine and Biology Society (EMBC)*, IEEE, 2015, pp. 6441–6444.

# 参考文献

- [1]D.卡斯塔涅达, A.埃斯帕萨, M. Ghamari, C. Soltanpur和H. Nazeran, "A 可穿戴式光电容积脉搏波传感器的研究进展 应用在医疗保健", 国际生物传感器和生物电子杂志– ICS, 第4卷, 第4期, 第195页, 2018年。
- [2]P. Renevey, R. Delgado-Gonzalo, A. Lemkaddem等人, “光学腕戴式 睡眠监测设备”, EMBEC & NBC 2017, Springer, 2017, 第100页。615– 618.
- [3]C. El-Hajj和P. Kyriacou, “根据ppg sig的无袖带血压估计, nals及其衍生物使用深度学习模型”, 生物医学信号专业, cessing and Control, 第70卷, 第102 984页, 2021年。
- [4]L. m.我的朋友, A. g. Bonomi, F. , 解得, et al.之间的比较 心房颤动的心电图和光电容积描记图衍生特征– 在自由生活条件下的Lation检测”, 生理测量, 第39卷, 第8号, 第084 001页, 2018年。
- [5]J.金, T. Lee, J. Kim, and H. Ko, “照片中的环境光消除– 使用交替采样和电荷重新分配的体积描记图应用, 2015年第37届IEEE国际年会 医学和生物学工程学会 (EMBC) , IEEE, 2015年, 第100页。6441– 6444.

- [6] S. Hanyu and C. Xiaohui, "Motion artifact detection and reduction in ppg signals based on statistics analysis", in *2017 29th Chinese control and decision conference (CCDC)*, IEEE, 2017, pp. 3114–3119.
- [7] D. Jarchi and A. J. Casson, "Estimation of heart rate from foot worn photoplethysmography sensors during fast bike exercise", in *2016 38th Annual International Conference of the IEEE Engineering in Medicine and Biology Society (EMBC)*, IEEE, 2016, pp. 3155–2158.
- [8] A. J. Casson, A. V. Galvez, and D. Jarchi, "Gyroscope vs. accelerometer measurements of motion from wrist ppg during physical exercise", *ICT Express*, vol. 2, no. 4, pp. 175–179, 2016.
- [9] S. D. Tang, Y. S. Goh, M. D. Wong, and Y. E. Lew, "Ppg signal reconstruction using a combination of discrete wavelet transform and empirical mode decomposition", in *2016 6th International Conference on Intelligent and Advanced Systems (ICIAS)*, IEEE, 2016, pp. 1–4.
- [10] H. Yuan, S. F. Memon, T. Newe, E. Lewis, and G. Leen, "Motion artefact minimization from photoplethysmography based non-invasive hemoglobin sensor based on an envelope filtering algorithm", *Measurement*, vol. 115, pp. 288–298, 2018.
- [11] M. R. Ram, K. V. Madhav, E. H. Krishna, N. R. Komalla, K. Sivani, and K. A. Reddy, "Ica-based improved dtcwt technique for ma reduction in ppg signals with restored respiratory information", *IEEE Transactions on Instrumentation and Measurement*, vol. 62, no. 10, pp. 2639–2651, 2013.
- [12] P. Nooralishahi, C. K. Loo, and L. W. Shiung, "Robust remote heart rate estimation from multiple asynchronous noisy channels using autoregressive model with kalman filter", *Biomedical Signal Processing and Control*, vol. 47, pp. 366–379, 2019.

- [6]S. Hanyu和C. Xiaohui, “ppg中的运动伪影检测和减少  
基于统计分析的信号”, 在2017年第29届中国控制与决策  
会议 (CCDC) , IEEE, 2017年, pp. 3114–3119.
- [7]D. Jarchi和A. J. Casson, “从脚穿的照片估计心率”,  
快速自行车运动中的体积描记传感器”, 2016年第38届年会  
IEEE医学与生物工程国际会议  
社会 (EMBC) , IEEE, 2016年, 第。3155–2158.
- [8]A. J. Casson, A. V. Galvez和D. Jarchi, “陀螺仪与加速度计测量–  
体育锻炼期间手腕PPG运动的保证”, ICT Express,  
卷2, 没有4, PP。175—179, 2016。
- [9]S. D.唐, Y. S.吴, M. D. Wong和Y. E. Lew, “Ppg信号重建  
利用离散小波变换和经验模式分解的组合,  
2016第六届智能与先进制造国际会议  
系统 (ICIAS) , IEEE, 2016年, pp. 1–4.
- [10]H. Yuan, S. F. Memon, T. Newe, E. 刘易斯和G. Leen, “运动伪影min–  
基于光电体积描记法无创血红蛋白传感器的最小化  
基于包络滤波算法”, 测量, 第115卷, 第115页。288–298,  
2018.
- [11]M. R. Ram, K. V. Madhav, E. H. Krishna, N. R.科马拉湾Sivani和K. A.  
Reddy, “用于ppg信号中ma减少的基于ICA的改进的dtcwt技术  
具有恢复的呼吸信息”, IEEE仪器交易  
和Measurement, 第62卷, 第10期, 第10页。2639–2651, 2013。
- [12]P. Nooralishahi, C. K. Loo和L. W. Shiung, “稳健的远程心率  
使用自回归的来自多个异步噪声信道的估计  
具有卡尔曼滤波器的模型”, 生物医学信号处理和控制, 第47卷,  
页。366–379, 2019。

- [13] A. H. A. Zargari, S. A. H. Aqajari, H. Khodabandeh, A. M. Rahmani, and F. Kurdahi, "An accurate non-accelerometer-based ppg motion artifact removal technique using cyclegan", *arXiv preprint arXiv:2106.11512*, 2021.
- [14] J. Lee, S. Sun, S. M. Yang, *et al.*, "Bidirectional recurrent auto-encoder for photoplethysmogram denoising", *IEEE journal of biomedical and health informatics*, vol. 23, no. 6, pp. 2375–2385, 2018.
- [15] W. Yuning, A. Iman, K. Kianoosh, M. R. Amir, and L. Pasi, "Ppg signal reconstruction using deep convolutional generative adversarial network", in *International Conference of the IEEE Engineering in Medicine and Biology Society (EMBC)*, IEEE, 2022.
- [16] A. B. Hertzman, "The blood supply of various skin areas as estimated by the photoelectric plethysmograph", *American Journal of Physiology-Legacy Content*, vol. 124, no. 2, pp. 328–340, 1938.
- [17] W. B. Murray and P. A. Foster, "The peripheral pulse wave: Information overlooked", *Journal of clinical monitoring*, vol. 12, no. 5, pp. 365–377, 1996.
- [18] R. Blazek and C. Lee, "Multi-resolution linear model comparison for detection of dicrotic notch and peak in blood volume pulse signals", *Anal Biomed Signals Images*, vol. 20, no. 20, pp. 378–386, 2010.
- [19] K. Nakajima, T. Tamura, and H. Miike, "Monitoring of heart and respiratory rates by photoplethysmography using a digital filtering technique", *Medical engineering & physics*, vol. 18, no. 5, pp. 365–372, 1996.
- [20] J. Allen, "Photoplethysmography and its application in clinical physiological measurement", *Physiological measurement*, vol. 28, no. 3, R1, 2007.
- [21] A. D. Foster, C. Neumann, and E. Rovenstine, "Peripheral circulation during anesthesia, shock and hemorrhage; the digital plethysmograph as a clini-

- [13]一个。H.一个。扎尔加里, S. 一个。H.阿卡贾里, H. 霍达班德, a. 米。拉赫马尼和F. Kurdahi, “一种精确的基于非加速度计的ppg运动伪影去除方法, 技术使用cyclegan”, arXiv预印本arXiv: 2106.11512, 2021。
- [14]J.李, S.孙习M. Yang等人, “双向递归自动编码器光电容积描记图去噪”, IEEE生物医学和健康信息杂志–Matics, vol. 23, no. 6, pp. 2375–2385, 2018年。
- [15]W. Yunning, A. Iman, K. Kianoosh, M. R. Amir和L. Pasi, “Ppg信号使用深度卷积生成对抗网络进行重建”, IEEE医学与生物工程国际会议学会 (EMBC) , IEEE, 2022年。
- [16]A. B. Hertzman, “通过测量皮肤的血液供应, 光电体积描记器”, 美国生理学杂志–遗产124卷, 第2卷, 第124页。328—340, 1938年
- [17]W. B. 默里和P.A. Foster, “外周脉搏波: 信息被忽视”, 《临床监测杂志》, 第12卷, 第5期, pp. 365–377, 1996年。
- [18]R. Blazek和C. Lee, “多分辨率线性模型比较检测的重搏切迹和峰值的血容量脉搏信号”, 分析生物医学信号《图像》, 第20卷, 第20期, 第100页。378–386, 2010。
- [19]K.中岛T. Tamura和H. Miike, “心脏和呼吸系统的监测使用数字滤波技术的光电体积描记法测量心率”, 医学Engineering & Physics, 第18卷, 第5期, 第18 – 19页。365–372, 1996年。
- [20]J.艾伦, “光电体积描记法及其在临床生理学中的应用测量”, 生理测量, 第28卷, 第3期, R1, 2007。
- [21]A. D.福斯特角Neumann和E. Rovenstine, “外周循环dur–麻醉, 休克和出血;数字体积描记器作为临床,

- cal guide”, in *The Journal of the American Society of Anesthesiologists*, The American Society of Anesthesiologists, vol. 6, 1945, pp. 246–257.
- [22] Y. Kurylyak, F. Lamonaca, and D. Grimaldi, ”A neural network-based method for continuous blood pressure estimation from a ppg signal”, in *2013 IEEE International instrumentation and measurement technology conference (I2MTC)*, IEEE, 2013, pp. 280–283.
- [23] B. Jönsson, C. Laurent, M. Eneling, T. Skau, and L.-G. Lindberg, ”Automatic ankle pressure measurements using ppg in ankle-brachial pressure index determination”, *European journal of vascular and endovascular surgery*, vol. 30, no. 4, pp. 395–401, 2005.
- [24] H.-H. Kuo, *White noise distribution theory*. CRC press, 2018.
- [25] M. Blanco-Velasco, B. Weng, and K. E. Barner, ”Ecg signal denoising and baseline wander correction based on the empirical mode decomposition”, *Computers in biology and medicine*, vol. 38, no. 1, pp. 1–13, 2008.
- [26] R. McCraty and F. Shaffer, ”Heart rate variability: New perspectives on physiological mechanisms, assessment of self-regulatory capacity, and health risk”, *Global advances in health and medicine*, vol. 4, no. 1, pp. 46–61, 2015.
- [27] F. Shaffer and J. P. Ginsberg, ”An overview of heart rate variability metrics and norms”, *Frontiers in public health*, p. 258, 2017.
- [28] H.-G. Kim, E.-J. Cheon, D.-S. Bai, Y. H. Lee, and B.-H. Koo, ”Stress and heart rate variability: A meta-analysis and review of the literature”, *Psychiatry investigation*, vol. 15, no. 3, p. 235, 2018.
- [29] C. M. DeGiorgio, P. Miller, S. Meymandi, *et al.*, ”Rmssd, a measure of vagus-mediated heart rate variability, is associated with risk factors for sudep: The sudep-7 inventory”, *Epilepsy & behavior*, vol. 19, no. 1, pp. 78–81, 2010.

calguide”，在美国麻醉医师学会杂志上，  
美国麻醉医师学会，第6卷，1945年，第100页。246–257.

- [22]Y. Kurylyak, F. Lamonaca和D. Grimaldi, “一种基于神经网络的方法用于从ppg信号进行连续血压估计”，在2013年IEEE In-国际仪器仪表和测量技术会议 (I2 MTC) ，  
IEEE，2013年，PP。280–283.
- [23]B. 约翰逊，C. 劳伦，M. 在那里，T. 对不起，L. g. Lindberg 《自动化》  
在踝臂压力指数测定中使用PPG测量踝压力，  
终止”，欧洲血管和血管内手术杂志，第30卷，  
第四，pp. 395—401，2005年。
- [24]H.- H. 郭，白色噪声分布理论。CRC Press, 2018.
- [25]M. 布兰科-贝拉斯科湾Weng和K. E. Barner, “ECG信号去噪和  
基于经验模式分解的基线漂移校正”，Com-  
计算机在生物学和医学中，第38卷，第1期，第110页。2008年1月13日。
- [26]R. McCarry和F. Shaffer, “心率变异性：物理学的新观点—  
生物学机制、自我调节能力评估和健康风险”，  
《全球卫生和医学进展》，第4卷，第1号，第111页。46–61, 2015年。
- [27]F. Shaffer和J. P. Ginsberg, “心率变异性指标概述  
和规范”，公共卫生前沿，第258页，2017年。
- [28]H.- G. Kim, E. J. Cheon, D.- S. Bai, Y. H. 李和B. - H. 古，“压力和  
心率变异性：一项荟萃分析和文献综述”，精神病学  
调查，第15卷，第3期，第235页，2018年。
- [29]C. M. DeGiorgio, P. 米勒, S. Meymandi等人，“Rmssd, 迷走神经的测量—  
介导的心率变异性与sudep的危险因素相关：  
sudep-7 inventory”，Epilepsy & behavior, vol. 19, no. 1, pp. 78–81, 2010年。

- [30] H.-Y. Jan, M.-F. Chen, T.-C. Fu, W.-C. Lin, C.-L. Tsai, and K.-P. Lin, "Evaluation of coherence between ecg and ppg derived parameters on heart rate variability and respiration in healthy volunteers with/without controlled breathing", *Journal of Medical and Biological Engineering*, vol. 39, no. 5, pp. 783–795, 2019.
- [31] C. Hoog Antink, Y. Mai, M. Peltokangas, S. Leonhardt, N. Oksala, and A. Vehkaoja, "Accuracy of heart rate variability estimated with reflective wrist-ppg in elderly vascular patients", *Scientific reports*, vol. 11, no. 1, pp. 1–12, 2021.
- [32] W.-H. Lin, D. Wu, C. Li, H. Zhang, and Y.-T. Zhang, "Comparison of heart rate variability from ppg with that from ecg", in *The international conference on health informatics*, Springer, 2014, pp. 213–215.
- [33] I. Goodfellow, J. Pouget-Abadie, M. Mirza, *et al.*, "Generative adversarial nets", *Advances in neural information processing systems*, vol. 27, 2014.
- [34] Z. Chen, Z. Zeng, H. Shen, X. Zheng, P. Dai, and P. Ouyang, "Dn-gan: Denoising generative adversarial networks for speckle noise reduction in optical coherence tomography images", *Biomedical Signal Processing and Control*, vol. 55, p. 101632, 2020.
- [35] L. D. Tran, S. M. Nguyen, and M. Arai, "Gan-based noise model for denoising real images", in *Proceedings of the Asian Conference on Computer Vision (ACCV)*, Nov. 2020.
- [36] L. Weng, "From gan to wgan", *arXiv preprint arXiv:1904.08994*, 2019.
- [37] J. Zhu, G. Yang, and P. Lio, "How can we make gan perform better in single medical image super-resolution? a lesion focused multi-scale approach", in *2019 IEEE 16th International Symposium on Biomedical Imaging (ISBI 2019)*, IEEE, 2019, pp. 1669–1673.

- [30]H.- Y.扬, M.- F.陈文C.傅, W.- C.林角, 英–地L. Tsai和K.- P. Lin, “Evaluating ECG和PPG导出参数之间的相干性对心率瓦里的影响有/无呼吸控制的健康志愿者的能力和呼吸–ing”, Journal of Medical and Biological Engineering, 第39卷, 第5期, 第100页。783–795, 2019.
- [31]C.胡格·安丁克, Y.麦, M.佩尔托坎加斯, S.莱昂哈特, N.奥沙拉, 还有一个。Vehkaoja, “使用反射手腕估计心率变异性的准确性–老年血管病患者的ppg”, 科学报告, 第11卷, 第1期, 第10页。1–12, 2021.
- [32]W.- H. Lin, L.吴角, 加–地Li, H. Zhang和Y.- T.张, “心的比较心率变异性从ppg与从ecg”, 在国际会议健康信息学, Springer, 2014, pp. 213–215.
- [33]I.作者简介: 李伟杰Mirza等人, “生成性对抗nets”, Advances in neural information processing systems, vol.27, 2014.
- [34]Z.陈, Z.曾, H.沉, X. Zheng, P.Dai, 和P.Ouyang, “Dn–gan: De–cal噪声生成对抗网络用于光学系统中的散斑噪声降低相断层扫描图像”, 生物医学信号处理和控制, 第55卷, 第101 632页, 2020年。
- [35]L. D.特兰, S. M.阮, M. Arai, “Gan基噪声模型用于降噪–ing真实的图像”, 亚洲计算机视觉会议论文集(ACCV) , 2020年11月。
- [36]L. Weng, “From gan to wgan”, arXiv preprint arXiv: 1904.08994, 2019.
- [37]J. Zhu, G.杨, 和P. Lio, “我们如何才能让甘在罪中表现得更好–医学图像超分辨率? 病灶聚焦多尺度方法”, 2019年IEEE第16届国际生物医学成像研讨会 (ISBI) IEEE , 2019 , pp 。1669–1673.

- [38] L. Metz, B. Poole, D. Pfau, and J. Sohl-Dickstein, "Unrolled generative adversarial networks", *arXiv preprint arXiv:1611.02163*, 2016.
- [39] A. Radford, L. Metz, and S. Chintala, "Unsupervised representation learning with deep convolutional generative adversarial networks", *arXiv preprint arXiv:1511.06434*, 2015.
- [40] P. L. Suárez, A. D. Sappa, and B. X. Vintimilla, "Infrared image colorization based on a triplet dcgan architecture", in *Proceedings of the IEEE Conference on Computer Vision and Pattern Recognition Workshops*, 2017, pp. 18–23.
- [41] R. Yeh, C. Chen, T. Y. Lim, M. Hasegawa-Johnson, and M. N. Do, "Semantic image inpainting with perceptual and contextual losses", *arXiv preprint arXiv:1607.07539*, vol. 2, no. 3, 2016.
- [42] A. Mahmoudzadeh, I. Azimi, A. M. Rahmani, and P. Liljeberg, "Lightweight photoplethysmography quality assessment for real-time iot-based health monitoring using unsupervised anomaly detection", *Procedia Computer Science*, vol. 184, pp. 140–147, 2021.
- [43] C.-H. Goh, L. K. Tan, N. H. Lovell, S.-C. Ng, M. P. Tan, and E. Lim, "Robust ppg motion artifact detection using a 1-d convolution neural network", *Computer methods and programs in biomedicine*, vol. 196, p. 105 596, 2020.
- [44] J. Azar, A. Makhoul, R. Couturier, and J. Demerjian, "Deep recurrent neural network-based autoencoder for photoplethysmogram artifacts filtering", *Computers & Electrical Engineering*, vol. 92, p. 107 065, 2021.
- [45] G. Masinelli, F. Dell'Agnola, A. A. Valdés, and D. Atienza, "Spare: A spectral peak recovery algorithm for ppg signals pulswave reconstruction in multimodal wearable devices", *Sensors*, vol. 21, no. 8, p. 2725, 2021.

[38]L. Metz, B. 可怜的, d. 孔雀, 和J. SOLL—Dickstein, “未滚动生成广告—versarial networks”, arXiv preprint arXiv: 1611.02163, 2016.

[39] A. Radford, L. Metz, and S. Chintala, ”Unsupervised representation learning with deep convolutional generative adversarial networks”, arXiv preprint arXiv: 1511.06434, 2015年。

[40]P. L. Suárez, A. D. Sappa和B. X. Vintimilla, “红外图像彩色化  
基于三重dcgan架构”, 在IEEE会议论文集中  
计算机视觉和模式识别研讨会, 2017年, pp. 18–23.

[41]R.是的, C. 陈, T. Y.林, 米。长川约翰逊和M. N.做, “Semantic  
图像修复与感知和上下文损失”, arXiv预印本  
arXiv: 1607.07539, Vol. 2, no. 3, 2016.第2卷, 2016年。

[42]A.马哈茂德扎德岛Azimi, A. M. Rahmani和P. Liljeberg, “轻量级  
基于实时物联网的健康监测的光电体积描记质量评估  
使用无监督的异常检测进行检测”, Procedia Computer Science,  
第184卷, 第184页。140–147, 2021.

[43]C. H.戈湖K.谭, N. H. Lovell, S. C. Ng, M. P. Tan和E.林, “罗-  
使用1-D卷积神经网络的胸围PPG运动伪影检测”,  
生物医学中的计算机方法和程序, 第196卷, 第105 596页, 2020年。

[44]J. Azar, A.马胡尔河Couturier和J. Demerjian, “深层递归神经网络  
基于网络的自动编码器, 用于光电容积描记图伪影过滤”, Com-  
计算机与电气工程, 第92卷, 第107 065页, 2021年。

[45]G. Masinelli, F. Dell'Agnola, A. A. Valdés和D. Atienza, “备用: 一个光谱  
多通道PPG信号的峰值恢复算法  
模态可穿戴设备”, 传感器, 第21卷, 第8期, 第2725页, 2021年。

- [46] P. Ghosal, S. Himavathi, and E. Srinivasan, "Ppg motion artifact reduction using neural network and spline interpolation", in *2020 7th International Conference on Smart Structures and Systems (ICSSS)*, IEEE, 2020, pp. 1–6.
- [47] M. A. Mehrabadi, I. Azimi, F. Sarhaddi, *et al.*, "Sleep tracking of a commercially available smart ring and smartwatch against medical-grade actigraphy in everyday settings: Instrument validation study", *JMIR mHealth and uHealth*, vol. 8, no. 11, e20465, 2020.
- [48] F. Sarhaddi, K. Kazemi, I. Azimi, *et al.*, "A comprehensive accuracy assessment of samsung smartwatch heart rate and heart rate variability", *medRxiv*, 2022. DOI: 10.1101/2022.04.29.22274461. eprint: <https://www.medrxiv.org/content/early/2022/05/01/2022.04.29.22274461.full.pdf>. [Online]. Available: <https://www.medrxiv.org/content/early/2022/05/01/2022.04.29.22274461>.
- [49] *Samsung gear sport*, <https://www.samsung.com/global/galaxy/gear-sport>, Accessed: 2010-09-30.
- [50] L. D. Tran, S. M. Nguyen, and M. Arai, "Gan-based noise model for denoising real images", in *Proceedings of the Asian Conference on Computer Vision*, 2020.
- [51] S. Akcay, A. Atapour-Abarghouei, and T. P. Breckon, "Ganomaly: Semi-supervised anomaly detection via adversarial training", in *Asian conference on computer vision*, Springer, 2018, pp. 622–637.
- [52] G. Welch, G. Bishop, *et al.*, "An introduction to the kalman filter", 1995.
- [53] R. Shibata, "Selection of the order of an autoregressive model by akaike's information criterion", *Biometrika*, vol. 63, no. 1, pp. 117–126, 1976.

[46]P. Ghosal, S. Himavathi和E. Srinivasan, “Ppg运动伪影减少

使用神经网络和样条插值”，在2020年第七届国际会议上，

智能结构和系统（ICSSS），IEEE，2020年，pp。1–6.

[47]M. A.梅赫拉巴迪岛Azimi, F. Sarhaddi等人，“对一个商人的睡眠跟踪

市面上可买到的智能戒指和智能手表，

日常设置：仪器验证研究”，JMIR mHealth和uHealth，

第8卷，第11期，E20465，2020。

[48]F. Sarhaddi, K.卡齐米岛Azimi等人，“全面的准确性评估—

三星智能手表心率和心率变异性的研究”，medRxiv，

2022. doi: 10.1101/2022.04.29.22274461。电子版：

<https://www.medrxiv.org/content/early/2022/05/01/2022.04.29.22274461.full.pdf>。[在一

行]。可用网址：

<https://www.medrxiv.org/content/early/2022/05/01/2022.04.29.22274461>.

[49]三星齿轮运动，<https://www.samsung.com/global/galaxy/gear-sport/>

体育，检索日期：2010–09–30。

[50]L. D.特兰, S. M.阮, M. Arai, “用于去噪的基于Gan的噪声模型

真实的图像”，在亚洲计算机视觉会议论文集上，

2020.

[51]S. Akcay, A. Atapour–Abarghouei和T. P. Brecket, “Ganomaly: Semi–

通过对抗训练进行监督异常检测”，亚洲会议

on 计算机 视觉， Springer， 2018， pp . 622–637.

[52]G. Welch, G. Bishop等人，“卡尔曼滤波器介绍”，1995年。

[53]R.柴田，“赤池自回归模型的阶数选择

信息标准”，《生物统计学》，第63卷，第1期，第113 – 117页。117–126，1976年。

- [54] Z. Wu and N. E. Huang, "A study of the characteristics of white noise using the empirical mode decomposition method", *Proceedings of the Royal Society of London. Series A: Mathematical, Physical and Engineering Sciences*, vol. 460, no. 2046, pp. 1597–1611, 2004.
- [55] I. Daubechies, *Ten lectures on wavelets*. SIAM, 1992.
- [56] A. Paszke, S. Gross, F. Massa, *et al.*, "Pytorch: An imperative style, high-performance deep learning library", *Advances in neural information processing systems*, vol. 32, 2019.
- [57] D. D. et al., *Kalman filter, smoother, and em algorithm for python*, <https://github.com/pykalman/pykalman>, Github Repository, Sep. 2015.
- [58] S. Seabold and J. Perktold, "Statsmodels: Econometric and statistical modeling with python", in *Proceedings of the 9th Python in Science Conference*, Austin, TX, vol. 57, 2010, pp. 10–25 080.
- [59] L. D. et al., *Python implementation of empirical mode decomposition (emd) method*, <https://github.com/laszukdawid/PyEMD>, Github Repository, 2017.
- [60] G. Lee, R. Gommers, F. Waselewski, K. Wohlfahrt, and A. O'Leary, "Pywavelets: A python package for wavelet analysis", *Journal of Open Source Software*, vol. 4, no. 36, p. 1237, 2019.
- [61] F. Shaffer, Z. M. Meehan, and C. L. Zerr, "A critical review of ultra-short-term heart rate variability norms research", *Frontiers in Neuroscience*, vol. 14, 2020.

[54]Z. Wu和N. E. Huang, “利用噪声特性研究白色噪声的特性”，

经验模态分解法”，《皇家医学会学报》，

伦敦。A辑：数学、物理和工程科学，第460卷，

2046, pp. 1597—1611, 2004年。

[55]I. Daubechies, 《Ten Lectures on Wavelets》 SIAM, 1992年。

[56]A.帕斯克河格罗斯, F. 马萨等人, “Pytorch: 命令式风格, 高-

性能深度学习库”, 神经信息处理的进展

系统, 第32卷, 2019年。

[57]D. D. 例如, 卡尔曼滤波器、平滑器和em算法, 用于python, <https://github.com/pykalman/pykalman>, Github Repository, 2015年9月。

[58]S. Seabold和J. Perktold, “Statmodels: 计量经济学和统计模型,

在第九届Python科学会议论文集中,

Austin, TX, vol. 57, 2010, pp. 10–25 080.

[59]L. D. 例如, 经验模式分解 (emd) 的Python实现

方法, <https://github.com/laszukdawid/PyEMD>, Github Repository,

2017.

[60] G. Lee, R. Gommers, F. Waselewski, K. Wohlfahrt, and A. O’Leary, ”Py-  

wavelets: A python package for wavelet analysis”, Journal of Open Source  

软件, 第4卷, 第36卷, 第1237, 2019。

[61] F. Shaffer, Z. M. Meehan, and C. L. Zerr, ”A critical review of ultra-short-  

term heart rate variability norms research”, Frontiers in Neuroscience, vol. 14,

2020.